Hydraulics and Instabilities of Quasi-Geostrophic Zonal Flows

by

Elise Ann Ralph

B.A., University of Chicago (1988),
S.M., MIT-WHOI Joint Program (1991)

Submitted to the Joint Program in Physical Oceanography
in partial fulfillment of the requirements for the degree of

Doctor of Philosophy

at the

MASSACHUSETTS INSTITUTE OF TECHNOLOGY

and the

WOODS HOLE OCEANOGRAPHIC INSTITUTION

September 1994

Author .....
Joint Program in Physical Oceanography
September 2, 1994

Certified by .....
Larry J. Pratt
Associate Scientist
Thesis Supervisor

Accepted by .....
Carl Wunsch
Chairman, Joint Committee for Physical Oceanography

Hydraulics and Instabilities of Quasi-Geostrophic Zonal Flows

by

Elise Ann Ralph

Submitted to the Joint Program in Physical Oceanography
on September 2, 1994, in partial fulfillment of the
requirements for the degree of
Doctor of Philosophy

Abstract

The thesis addresses the applicability of traditional hydraulic theory to an unstable, mid-latitude jet where the only wave present is the Rossby wave modified by shear. While others (Armi 1989, Pratt 1989, Haynes *et al.*1993 and Woods 1993) have examined specific examples of shear flow "hydraulics", my goal was to find general criteria for the types of flows that may exhibit hydraulic behavior. In addition, a goal was to determine whether a hydraulic mechanism could be important if smaller scale shear instabilities were present.

A flow may exhibit hydraulic behavior if there is an alternate steady state with the same functional relationship between potential vorticity and streamfunction. Using theorems for uniqueness and existence of two point boundary value problems, a necessary condition for the existence of multiple states was established. Only certain flows with non-constant, negative $\frac{dQ(\psi)}{d\psi}$ have alternate states.

Using a shooting method for a given transport and a given smooth relationship between potential vorticity and streamfunction, alternate states are found over a range of beta. Multiple solutions arise at a pitchfork bifurcation as a stability parameter is raised above the stability threshold determined by the necessary condition for instability. The center branch of the pitchfork is unstable to the gravest mode, while the two outer branches do not even have discrete modes. Other pitchfork bifurcations occur as higher meridional modes become unstable. Again, the inner branch is unstable to the next gravest mode, while the outer branches do not support this discrete mode. These results place the barotropic instability problem into a large set of nonlinear systems described by bifurcation theory. However, if the eastward transport across the channel is large enough, the normal modes may stabilize and these waves have a phase speed less than the minimum velocity of the flow. In this case, the flow is analogous to sub-critical hydraulic flow.

The establishment of these states and the nature of transitions between them is studied in the context of an initial value problem, solved numerically, in which the zonally uniform jet is forced to adjust to the sudden appearance of an obstacle. The time-dependent adjustment of an initially stable flow exhibits traditional hydraulic

behavior such as control and influence in the far-field. However, if the flow is unstable, the instability dominates the evolution. If the topographic slope renders the flow more unstable than the ambient flow, then the resulting adjustment can be understood as a local instability.

The thesis has established a connection between hydraulic adjustment and the barotropic instability of the flow. Both types of dynamics arise from adjustments among multiple equilibria in an unforced, inviscid fluid.

Thesis Supervisor: Larry J. Pratt
Title: Associate Scientist

Acknowledgments

I would like to first thank my advisor Larry Pratt, whose encouragement and support helped me find my own way of asking and answering questions. Over the years, Larry has provided many useful suggestions which improved the clarity of the ideas and the text in this thesis. I also appreciated the advice of my thesis committee: Glenn Flierl, Nelson Hogg, Joe Pedlosky and Paola Rizzoli. I have enjoyed interacting with all of them. I would like to especially thank Paola for her warmth and enthusiasm and Joe for his encouragement as I gained confidence in my abilities.

I am indebted to Glenn Flierl and Roger Samelson who generously gave me the psuedo-spectral models which were used in this thesis. Glenn was very helpful as I struggled with the numerics, and patient as I struggled through other areas of the thesis. Some of the computations in Chapter 3 were carried out on a machine generously provided by Ralph Stephen. I would like to also thank Tom Bolmer for setting this up for me. Outside of my thesis work, thanks also go to Mike McCartney for giving me the opportunity to go to sea and reminding me that oceanography is fun.

I am very grateful to my extended family whose love and support have sustained me through my years of schooling. Finally, a special thanks to my cheerful husband, Chris Bradley. His presence has added to my life in countless ways, and provided me with the "balance" that enabled me to complete this thesis.

This research was supported by National Science foundation grants OCE 91-15359 and OCE 89-16446, and also by a Department of Defense AASERT grant adminstered under ONR N00014-89-J-1182.

Contents

Chapter 1

Introduction

There are many examples of eastward-flowing jets on the planets, and in particular in the atmosphere and the oceans of the Earth. These currents occasionally split, forming a double-jet structure. In the atmosphere the double jet passes around a persistent, large-amplitude anomaly. This phenomenon is known as blocking and it has received considerable attention because of its importance in determining regional climate. The bifurcation of oceanic jets is not as well documented, although it appears that the Gulf Stream, the Kuroshio and the Antarctic Circumpolar Current split near topographic features. The present chapter contains a short review of the observations and theories of bifurcating geophysical jets followed by an outline of the thesis which is concerned with a theory of bifurcation based on the transitions between distinct zonal flows.

1.1 Observations

One of the earliest observational papers of atmospheric blocking dates back to Rex (1950) who established five criteria which a blocking case must exhibit

- the basic westerly current must split into two branches,
- each branch must transport appreciable mass,
- the double-jet system must extend over 45° of longitude,

- a sharp transition from zonal type flow upstream to meridional flow downstream must be observed across the current split, and
- the pattern must persist with recognizable continuity for at least ten days.

These observations suggest that blocking may be thought of as an abrupt transition between two distinct zonal flows, a narrow flow upstream and a split flow downstream.

A more recent, extensive study of blocking events by Dole, 1982 and Dole and Gordon, 1983 stress several additional observations

- during the onset and decay of the blocking event, several Fourier components of the block amplify and decay simultaneously,
- the final vertical structure of the block is equivalent barotropic, and
- the blocking events are not spatially correlated around the globe.

As Malguzzi and Malanotte-Rizzoli (1984) point out, the first two of these observations are consistent with nonlinear behavior which may cause phase locking and the formation of coherent structures. Other indications of nonlinearity are the formation of closed streamlines observed by Hansen and Chen (1982). Illari and Marshall (1983) and Illari (1984) also note that closed streamlines may occur in blocking events, and stress the role of eddy interactions in the maintenance of the block. The final point by Dole, that the blocking structures are not spatially correlated, suggests that blocking is fundamentally a regional, rather than global process.

The bifurcation of oceanic jets has been observed much less frequently, although it appears that both the Kuroshio and the Gulf Stream may bifurcate, or at least widen, in the presence of topography. In the Kuroshio system, Mizuno and White (1983) use maps of temperature at $300m$ to identify a secondary northern branch of the current in the vicinity of the Shatsky Rise. They also note that during one year (spring 1979 to summer 1980) the bifurcation point moved continuously upstream, to a point $1000km$ west of the Shatsky Rise. In addition, their observations show large amplitude meanders downstream of the Shatsky Rise. In the Gulf Stream system, the Geosat altimeter was used by Kelly (1991) to identify two different regimes,

which are connected by a narrow transition region at the New England Seamount chain. Upstream of the seamounts, the flow is characterized by straight Gulf Stream paths and eastward-propagating meanders. The downstream path is broader, with larger meanders and no consistent propagation direction, i.e. waves may propagate both up- and downstream. In addition, smaller-scale recirculation gyres were located upstream of the transition. A recent numerical investigation (Ezer, 1994) using a primitive equation model of the Gulf Stream region, reproduced these features of the transition. By eliminating the New England Seamount Chain they eliminated the recirculation cells and showed that this transition is indeed due to the topography, and not local atmospheric forcing. In addition, Lee and Cornillon (1994a, 1994b) also observe that long wavelength meanders can propagate upstream. Both sets of observations point to the importance of understanding the abrupt spatial transitions between different zonal flows, and the role of upstream propagating waves in such a transition.

Certainly neither the Gulf Stream system at the New England Seamounts nor the Kuroshio at the Shatsky Rise are typically thought of as forming "split" flows, and so are not truly analogous to the atmospheric block. The Gulf Stream maintains its single jet structure until it reaches the Southeast Newfoundland Rise. It is this region of the ocean that provides the strongest example of a split jet and accordingly a history of the hydrographic measurements in the area is summarized here.

Helland-Hansen (1912) conducted the earliest sections in this area, measuring temperature and salinity to 2000 m. Traveling north along $50^{o}W$ they abruptly passed from the Sargasso Sea to a colder, fresher region; north of this region they returned to a warmer more saline mass, similar to the Sargasso Sea waters. Based on these observations, Helland-Hansen proposed that the Gulf Stream split into two branches, although the branch point could not be well-defined because of the sparseness of the observations. Using the available temperature data, Iselin (1936) constructed a streamline map based on the depth of the 10^{o} isotherm. This map shows the Gulf Stream separating into two branches close to $40^{o}N, 47^{o}W$. The northward branch forms the North Atlantic Current, while the southern, more diffuse branch becomes

the Azores current.

In contrast to the branching current hypothesis, Worthington (1962, 1976) , using data collected during the International Geophysics Year, proposed that the Southeast Newfoundland Rise separates the circulation of the North Atlantic into two anticyclonic gyres. Worthington's scheme is based on the observed distribution of dissolved oxygen, which showed that the water in the northern gyre was $1ml^{-1}/l$ richer in oxygen than the Gulf Stream waters in the same $T - S$ class.

Motivated by the discrepancies between Worthington's two gyre hypothesis and the earlier proposed schemes, Mann (1967) , carried out the first comprehensive sections of the area in the spring of 1963 and 1964. The sections from 1963 made up a synoptic picture of the area. The dynamic topography, referenced to 2000 m, (Figure 1-1) indicates one current rounding the ridge, forming an elongated cyclonic meander, before splitting at $38^{o}N, 44^{o}W$. The 1964 cruise revisited the ridge area and, in a series of sections, observed a similar cyclonic meander pinch together, forming a closed eddy. Although a synoptic map of dynamic topography can not be drawn for the 1964 cruises, the pinch-off may move the splitting point of the current further north to approximately $40^{o}N, 47^{o}W$. Mann also calculated the transports of the two branches relative to 2000 m. The branch turning northward to follow the ridge (the North Atlantic Current) carried approximately 35 Sv, (15 Sv of which came from the slope water), while the southern branch transported 30 Sv, and marked the northern boundary of the 18^{o} water. Mann was also able to resolve a large anticyclonic eddy to the northeast of the branch point.

Clarke *et al.* (1980) carried out a three-ship survey of the region, with better spacing than Mann (1967) in order to reconcile Mann's circulation and Worthington's measured water mass distributions. The dynamic topography (Figure 1-2), referenced to 2000 *db* is similar to Mann's map. The jet passes over the Southeast Newfoundland Rise, forming a low pressure trough over the ridge. This trough is less elongated than the 1963 meander, and a small low pressure cell, located at the same point as Mann's branch point $(39^{o}N, 44^{o}W)$ is present in the 1972 data. The map clearly shows a branching of the dynamic height contours at $40^{o}N, 46^{o}W$. The anticyclonic eddy,

first discovered by Mann, is also apparent. Although differing in detail, the dynamic topography map favors Mann's interpretation of the bifurcation. The authors also proposed that the oxygen distribution in the North Atlantic current observed by Worthington could be consistent with a branching current, if a "reasonable" amount of lateral mixing (a diffusion coefficient of $10^7 cm^2 s^{-1}$) with the northern water was taken into account.

During the spring of 1987, a comprehensive hydrographic survey was carried out in conjunction with satellite-tracked buoys and infrared images by Krauss, *et al.* (1990) in order to analyze the eddy field and the branching of the Gulf Stream. Based on the dynamic topography, they found that the Gulf Stream splits near $40^0 N, 46^0 W$, the same location found by the previous authors. In addition, they found that there was intense eddy activity, and concluded that the splitting is a highly dynamic process.

More recently, Koshlyakov and Sazhina (1994), also observed the Gulf Stream split at $39^o N, 46^o W$, at the tip of a large-amplitude cyclonic meander oriented along the Southeast Newfoundland Rise. In addition to this meander, a large anticyclone was observed northeast of the branch point. A second survey, carried out four weeks later, shows that the cyclonic meander detached, forming a very strong cyclonic meander, with isotherms doming up $800m$ in the main thermocline. This ring is located south of the anticyclonic eddy, forming a dipole structure.

All of the observations from the Gulf Stream splitting region indicate that the jet bifurcates at approximately the same place, at the tip of the Southeast Newfoundland Rise. Thus, the splitting is a permanent feature of the circulation and appears to be due to the interaction of the jet with the topography. Although the splitting has been repeatedly observed, the region has several intense eddies, indicating that the process is highly dynamic.

Because the Antarctic Circumpolar Current is composed of several fronts (Nowlin and Clifford, 1982), it has more freedom to widen and narrow in the presence of topography. Upon examination of the Gordon *et al.* (1986) atlas, Pratt (1989) points out that the Circumpolar current does indeed narrow, by nearly a factor of one-half, downstream of both the Kerguelen Plateau and the Macquarie Ridge. Drake Passage

is another region where transitions between different flows take place. Upstream of Drake Passage the current system is quite broad, while in Drake Passage the flow narrows before abruptly widening downstream of the passage.

1.2 Previous Theories

Because the blocking states are quite long-lasting compared to the synoptic time scale, a number of theories have attempted to identify blocking events and their absence with multiple equilibrium states of the atmosphere. Charney and DeVore (1979) considered a global mechanism by using a highly truncated spectral model in a re-entrant channel. The system is perturbed by topography or by thermal forcing. For a given forcing function, multiple equilibria were found and they may be associated with planetary waves which are resonant on a global scale. The high amplitude states are associated with blocking and the low amplitude equilibria are associated with the unblocked state. A drawback of this model is its reliance on global modes which must propagate around the globe without a significant loss of amplitude. In addition, the global model is not consistent with the regional location of blocking events in the atmosphere and the location of split jets in the ocean.

Pierrehumbert and Malguzzi (1984) also considered multiple equilibria. However, their theory was based on a local mechanism; multiple equilibria were found to exist in a local balance independent of the conditions outside the blocking region. They found that if the inviscid and unforced system has a steady state with closed streamlines (for example, a modon) then the weakly forced and damped system can exhibit both a low amplitude state which is nearly zonal and a high amplitude state with closed streamlines.

Although Pierrehumbert and Malguzzi cited the observational work of Illari (1984) to suggest that eddy activity provided the forcing in their system, they explicitly gave the forcing as a function of the spatial coordinates, rather than letting the dynamics determine the forcing. In contrast, Haines and Marshall (1987) did consider dynamically consistent eddy forcing. A wavemaker was used to introduce eddies

of alternating signs. This forces a disturbance equation in which the disturbance potential vorticity is advected by the mean flow and potential vorticity is gained by disturbances passing through mean potential vorticity gradients. Given the eddy activity determined by this equation, the eddy flux divergence was calculated and explicitly used to force the equation governing the mean flow. They found that nonlinear free modes could readily be excited by the local eddy forcing and a high-amplitude modon structure was formed.

A second class of local equilibrium solutions to the blocking problem has been developed by Malguzzi and Malanotte-Rizzoli (1984). In this case the solutions are weakly nonlinear solutions of the potential vorticity equation and therefore closed streamlines are not present. The potential vorticity is a single-valued function of the stream function. The solutions are long, stationary solitary waves in the zonal flow and the governing equation is the steady Korteweg-deVries equation. More recently, Helfrich and Pedlosky (1993) considered the time-dependent dynamics of these weakly nonlinear solitary waves when the background zonal flow was near the baroclinic stability threshold. If the flow is stable, but only marginally so, the solitary wave is unstable and it may break up into two smaller stable solitary waves or it may implode, forming a narrow and stronger solitary wave. More recent work by the authors (Helfrich and Pedlosky, 1994) on the imploding solitary wave shows that it equilibrates as a finite-amplitude, zonally uniform structure with closed streamlines. This region is connected to the undisturbed up- and downstream flows by narrow meridional jets and thus the equilibrated state represents a transition between two distinct zonal equilibria. The authors suggest that the instability of the solitary wave provides a link between the weakly nonlinear theories of the KdV soliton and the fully nonlinear theories considered by Haines and Marshall (1987).

Theories on the splitting of large scale jets in the ocean are much rarer, probably because documented examples of splitting are rarer in the ocean. One of the earliest papers concerned with a theory of why the Gulf Stream splits is Warren (1969). Noting that the branching occurs in a region where the bottom contours diverge, Warren investigated the effect of diverging isobaths on a fluid in which potential

vorticity is conserved. The flow is assumed to be a rectangular jet which passes over a region where the topographic slope changes slowly in the zonal direction so that up- and downstream have quite different topographies. Because the zonal change in the topographic slope is gradual, the curvature term is neglected in the vorticity equation meaning that the x-dependence is merely parametric, so the velocity profile for a given topography may be found by integrating an ordinary differential equation in y. If the Rossby number is larger than the change in depth across the current, divided by the total depth, then inertia constrains the current to hold together in a single jet. However, if the topographic slope is large enough however, then the flow will follow the bottom contours and split.

Another line of work on splitting jets is based on an analogy with open channel hydraulics. Transitions occur between alternate states which may be either sub- or supercritical with respect to the upstream propagation of long waves. In several similar systems, Benjamin (1966, 1967, 1984) and Pratt (1984a, 1984b) has shown that the supercritical flows support stationary KdV solitary waves. Following Benjamin's method for planetary flows reproduces Malguzzi and Malanotte-Rizzoli's results for the amplitude and length scale of the solitary wave based on the shear of the mean flow. The stationary solitary wave (and the strongly nonlinear wave considered by Haines and Marshall) only exists in a supercritical flow. A subcritical flow supports stationary Rossby waves which will radiate energy away from a coherent structure. Using the weakly nonlinear equation with a small constant to parameterize an energy loss from dissipation, Benjamin was able to show that a transition between two distinct zonal states, from a supercritical one to a subcritical could take place. Benjamin's method can easily be used for the planetary flows considered here, but in light of his highly simplified parameterization of the dissipation and the instability found by Helfrich and Pedlosky, these calculations are not relevant.

The analogy between open channel hydraulics and planetary flows predates even Benjamin's work. Rossby (1950) first suggested that the transition to a split flow may be analogous to a hydraulic jump; however, in planetary flow the abrupt expansion is lateral rather than vertical because of the nature of planetary waves. Such a transition

from supercritical to subcritical flow would be accompanied by energy loss; Woods (1993) estimated the energy loss due to such a transition, and speculated that it would be dissipated through the generation of intense eddies, the scale of which he estimated based on the strength of the jump. In fact, the observations of the lateral jump in width of the Gulf Stream system, accompanied by vigorous eddy activity, are what first motivated me to consider transitions between conjugate zonal flows as a model of bifurcating jets. The additional observations by Kelly (1991) of the Gulf Stream near the New England seamount chain also suggest a hydraulic transition from supercritical flow to subcritical flow. Because this idea motivated the thesis, a full review of later work on planetary scale hydraulics by Armi (1989), Pratt (1989), Woods (1993) and Haynes *et al.* (1993) is given in the next chapter.

1.3 Outline of thesis

The observations and previous theoretical work suggest considering transitions between distinct, steady, zonal flows, i.e. transitions between multiple equilibria and in particular transitions between hydraulic states. An objective of the thesis is to examine the theory of planetary scale hydraulics, not simply to look at the phenomena such a theory produces, but also to explore its strengths and limitations as a conceptual model for understanding the behavior of geophysical zonal jets.

Thus, rather than simply explore a single example of zonal flow are exhibit hydraulic behavior as the previous investigators have done, Chapter 2 establishes a necessary condition for the existence of multiple zonal flows with the same $Q(\psi)$ structure. These multiple states have been interpreted by the previous investigators as alternate hydraulic states. Using a simple $Q(\psi)$ function that satisfies this necessary condition, multiple states are found via a shooting method and their interpretation was investigated by calculating dispersion relationships for the several flows found. The major findings of this chapter are:

- A necessary condition for the existence of multiple equilibria in an inviscid, unforced quasi-geostrophic channel is that $dQ/d\psi$ is negative and bounded from

above by

$$\frac{dQ}{d\psi} < -\left(\frac{\pi}{2L}\right)^2,$$

where $2L$ is the width of the channel.

- Multiple solutions arise at a pitchfork bifurcation as a stability parameter is raised above the stability threshold determined by the necessary condition for instability.

- The center branch of the pitchfork is unstable to the gravest mode, while the two outer branches do not even have discrete modes. Other pitchfork bifurcations occur as higher meridional modes become unstable. Again, the inner branch is unstable to the next gravest mode, while the outer branches do not support this discrete mode.

Chapter 3 is devoted to the time-dependent adjustment of these flows. The numerical experiments were specifically designed to search for hydraulic behavior. Several zonal flows are perturbed by the introduction of topography. If the topographic slope exceeds a value predicted by the steady state theory of chapter 2, the resulting adjustment establishes distinct zonal flows which can be qualitatively understood in terms of local instabilities and hydraulics. Three types of transitions between zonal flows were observed:

- Stable, sub-critical flow adjusts in a similar way to a hydraulic adjustment; up- and downstream influence is established simultaneously.

- If the flow is unstable, the instability dominates the evolution. If the topographic slope renders the flow more unstable than the ambient flow, then the resulting adjustment can be understood as a local instability.

- A narrow, eastward jet, belonging on the outer branch of the solution curve, forms a split flow around the ridge. The transition is localized; no far-field

effects are established. The transition is conservative and bears no resemblance to a hydraulic jump.

In all cases, there is a transition among distinct zonal flows with the same $Q(\psi)$ structure.

Since the majority of the thesis work is carried out for a single layer fluid inside a channel, Chapter 4 is a brief chapter devoted to the existence of multiple states in an unbounded domain. Pairs of multiple solutions are found, but in the simple example explored here both are unstable, suggesting that the equilibration to an alternate zonal flow cannot take place.

The thesis has established a connection between hydraulic adjustment and the barotropic instability of the flow. Both types of dynamics arise from adjustments among multiple equilibria in an unforced, inviscid fluid. These findings are reiterated in Chapter 5, which contains a summary of the thesis and a brief discussion of the strengths and limitations of the conceptual model developed here.

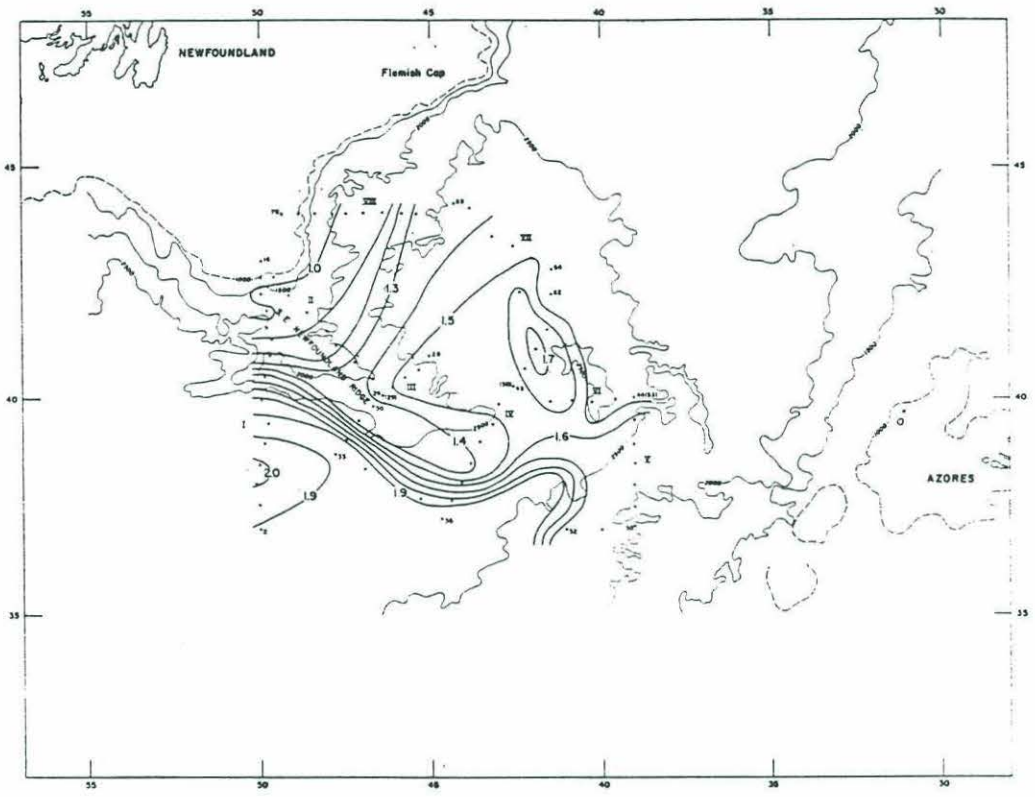

Figure 1-1: Dynamic topography relative to $2000m$, from Mann, 1967.

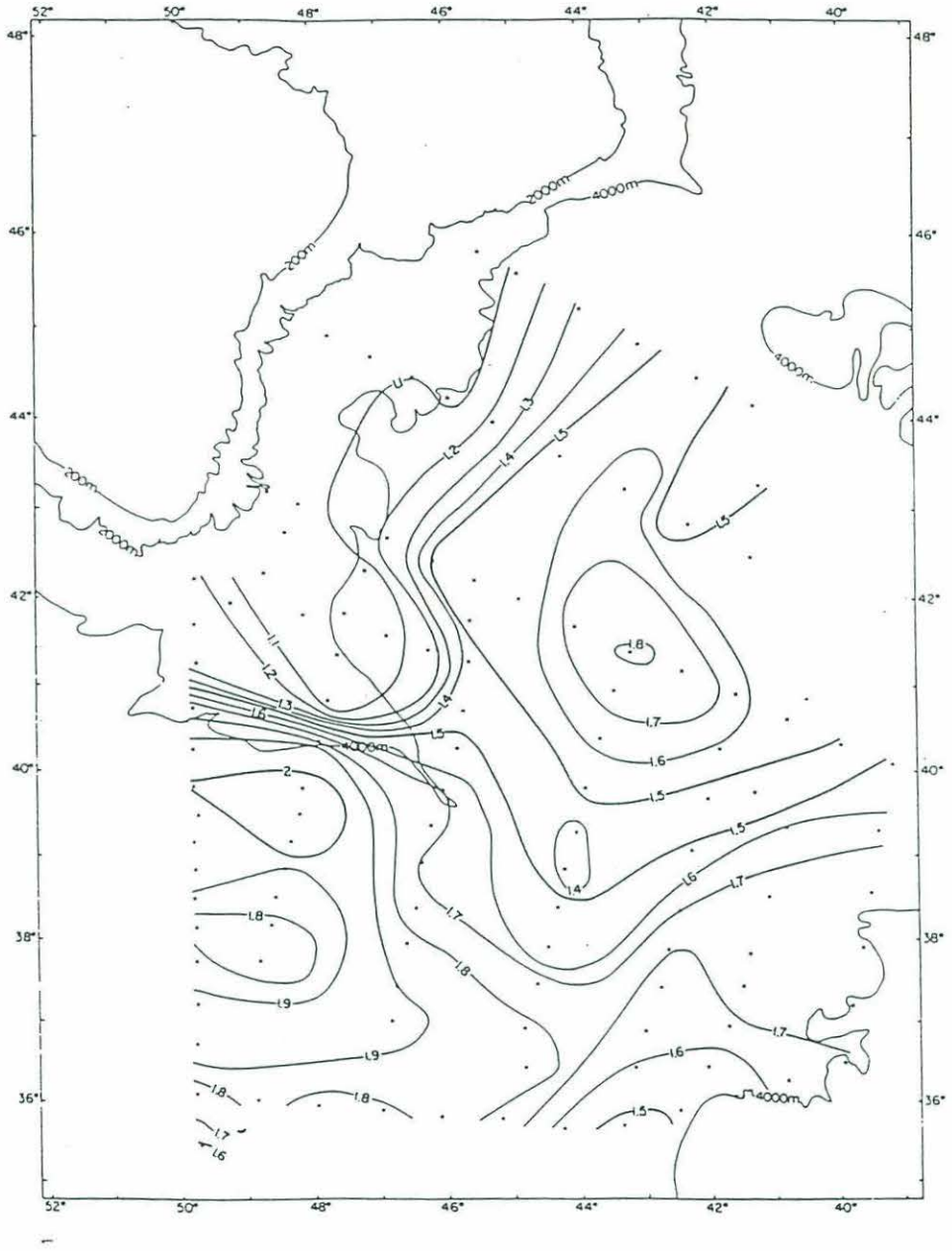

Figure 1-2: Dynamic topography relative to $2000m$, from Clarke *et al.*, 1980.

Chapter 2

Steady Alternate Flows

2.1 Introduction

Jets in the atmosphere and ocean are continually disturbed by external forcing. These forcings often generate waves that evolve into patterns that bear little resemblance to the initial forcing. Pattern formation in atmospheric and oceanic jets can be understood in terms of scale-selective shear instabilities caused by excessive horizontal shear (barotropic instabilities) or vertical shear (baroclinic instabilities). Recently, much work has been done on the non-dissipative equilibration of these instabilities; as the flow evolves to some new state it must do so with the same potential vorticity and pseudo-momentum. On the other hand, Armi (1989) and others (Pratt, 1989; Woods, 1993; Haynes et al., 1993) have suggested that an eastward jet on the β-plane may behave as a hydraulic system because they found examples of jets which have an "alternate state," i.e. another flow with the same transport and energy flux. This suggests another mechanism (transition to the alternate state) by which the flow can equilibrate after a perturbation. In this chapter, the "hydraulic theory" of planetary shear flows is examined in more detail to determine whether shear flows do indeed have all the identifying characteristics of a hydraulic system. This examination in turn will shed some interesting light on the instabilities of these flows.

It is helpful to review the simplest and most studied example of a hydraulic system to understand how transitions between alternate states may take place. Open channel

flows are gravitationally driven flows which have a laterally uniform velocity in the downstream direction. For a given mass transport and energy transport two flows are possible. One is a fast, shallow flow that is supercritical; [1] the other is deep, slow and subcritical. The subcritical flow has an excess of momentum flux compared to the supercritical flow with the same transport and energy.

Consider an obstacle in a subcritical stream which exerts a force against the flow. This force must be balanced by a reduction of the momentum flux in the fluid. For a small obstacle, the reduction occurs as lee waves form downstream of the obstacle. If the obstacle is large enough, the reduction is brought about by a transition to the supercritical alternate state in the region downstream of the obstacle. In this case the entire flow is controlled by the obstacle; waves in the subcritical upstream propagate from the obstacle up- and downstream, while waves in the supercritical flow only propagate downstream. At the control the flow is critical and through the wave propagation, the relationship between the depth of the fluid and the velocity in the entire domain is determined.

If the upstream flow is supercritical, then a transition to the subcritical alternate state would result in an excess of momentum, i.e. an external force must push downstream to stem the excess momentum associated with the rise in water level. Instead, the flow "breaks" at the transition and a hydraulic jump forms. The downstream subcritical conjugate state (which is a different subcritical flow than the alternate state) is one that has the same fluxes of mass and momentum as the supercritical upstream. However, it is important to note that the downstream flow is not *caused* by the upstream conditions but rather by some control or forcing further downstream. If this downstream establishment of the flow produces the required subcritical conjugate state, then a jump will form somewhere between the upstream and downstream flows.

There have been numerous studies of "hydraulic" behavior in geophysical flows.

[1] The terminology "super-" and "sub-critical" is confusing in a discussion that involves hydraulics and instabilities. Because the present work is an exploration of the possibility of hydraulics behavior, the hydraulics terminology will be used. Flows on either side of a stability threshold will simply deemed "stable" or "unstable."

In particular for flows through straits and over sills. A single-layer rotating channel model was introduced by Whitehead *et al.* (1974), and Gill (1974) who considered the behavior of steady flow in a rotating channel. The theory of rotating hydraulics has been further explored by Pratt (1983, 1984a, 1985), and Hogg (1983) considered a two-layer rotating hydraulics problem. This work, and more recent work on rotating channel flow has been reviewed by Pratt and Lundberg (1991). In these examples, the boundary Kelvin waves are the dominant wave which determines the structure of the flow.

A hydraulics theory has also been invoked to determine the point at which the Gulf Stream separates from the coast. Charney (1955) identifies the point of separation as the position at which the isopycnal surfaces at the base of the current outcrop. In Charney's $1\frac{1}{2}$ layer model, this is located where the single interface outcrops and this position is coincident with the point at which a southward propagating Kelvin wave is arrested by the northward velocity of the current. Blandford (1965) considered a multi-layer model and the outcropping is again coincident with the point at which the slowest-moving Kelvin wave is arrested. However, the latitude of the outcropping surface was much lower than Charney's separation latitude, and too low to be considered for the Gulf Stream separation problem. Luyten and Stommel (1985) explained this problem in terms of the hydraulics of a Kelvin wave. The inertial boundary current is the site of a control which determines the upstream relationship between the thermocline structure and the layer depth. Luyten and Stommel considered a zero potential vorticity case in which the water comes entirely from the equator. In contrast, Huang (1990a, 1990b) considered a flow with non-zero potential vorticity, which better mimics the Gulf Stream structure, whose waters come from mid-latitudes. Huang finds multiple solutions, lying along separate branches which connect at a critical set of parameters. The critical solution, where the two solutions merge, is the solution for which the Kelvin wave speed vanishes (Huang, *pers. comm.).*

In all of these cases, the waves that establish control are the " fast" modes due to boundary or coastal Kelvin waves. Hughes (1985, 1986, 1987) has also considered the criticality of Kelvin wavs in coastal boundary currents. However, by considering flows

with a potential vorticity gradient, Hughes also found that a "slow" mode, in the form of a topographic Rossby wave, can also serve as the means of control. In addition, Pratt and Armi (1987) analyzed in detail a rotating channel flow with non-uniform potential vorticity and identified a series of multiple states, associated with both gravity waves and Rossby waves. In these cases, where the effect of gravity plays a dominant role, it is difficult to isolate control due to the vorticity waves alone. Since in the open ocean inertial jest like the Gulf Stream, the Antarctic Circumpolar current, or the atmospheric jet stream are free of boundary Kevin waves, it is important to consider the control problem in terms of vorticity waves alone.

Berggren, *et al.* (1949) and Rossby (1950) first proposed a hydraulic theory of planetary flow to suggest that atmospheric blocking may be analogous to a hydraulic jump. Rossby's 1950 paper, summarized by Rex (1950) shows that there may be two uniform flows on the β-plane with different widths but the same transport and momentum flux. Armi (1989) re-introduced this work and argued that subcritical flow may pass through a control region (due to along-flow pressure changes) and become supercritical. In both of these works, the velocity up- and downstream of the transition is assumed; however, the velocity structure must be determined by the dynamics of the flow. By assuming conservation of potential vorticity, Pratt (1989) analytically constructed two alternate quasi-geostrophic jets which have the same piecewise-linear potential vorticity but different widths. Using a piecewise constant potential vorticity, Haynes *et al.* (1993) also constructed alternate quasi-geostrophic shear flows. They were able to classify them as supercritical and subcritical with respect to the long waves. Woods (1993) analytically constructed smooth alternate shallow water states by finding similarity solutions using the method of Benjamin (1981). The authors of these three papers carefully constructed alternate states which are consistent with potential vorticity conservation and explicitly showed that topography acted as a mechanism for control in their examples.

This chapter further explores the steady state theory of alternate planetary flows which have the same transport and potential vorticity - streamfunction relation but different velocity profiles. As in Pratt (1989) and Haynes *et al.* (1993), the quasi-

geostrophic approximation is made. However, rather than explore a single example of alternate flows, the goal of this chapter is to determine a general criterion for which potential vorticity - streamfunction relationships have alternate states. Section 2.2 reviews the model used in the present study, and section 2.3 reviews how alternate shear flows are characterized in terms of their momentum fluxes. The next section explains how parallel flows are characterized by the behavior of small amplitude waves. This characterization is important in a hydraulics interpretation of alternate flows and was not carried out fully by Pratt (1989) or by Woods (1993). Using mathematical theorems on the uniqueness of solutions to a differential equation, §2.5 explores which shear flows may have alternate solutions. In the remaining sections, several examples of alternate shear flows are studied numerically and characterized in terms of their momentum flux and their wave dynamics. These sections indicate that "alternate states" arise from the existence of unstable equilibria and do not fit all the criteria of a hydraulics system. Using ideas from hydraulics theories and from instability theories, §2.8 suggests two mechanisms by which flows may pass to their alternate states. These ideas are tested more fully in chapter 3.

2.2 The model

As described in Chapter 1, we consider the simplest example of shear flow in a geophysical setting. The fluid is assumed to be a single, steady, inviscid layer subject to the constraints of quasi-geostrophy on the $\beta-$plane. In the absence of forcing, the $O(\epsilon)$ equations of motion are

$$\frac{Du_0}{Dt} - v_1 - \beta y v_0 = -\frac{\partial \eta_1}{\partial x}, \tag{2.1}$$

$$\frac{Dv_0}{Dt} + u_1 + \beta y u_0 = -\frac{\partial \eta_1}{\partial y}, \tag{2.2}$$

$$-u_0\frac{\partial \eta_B}{\partial x} - v_0\frac{\partial \eta_B}{\partial y} + \left(\frac{\partial u_1}{\partial x} + \frac{\partial v_1}{\partial y}\right) = 0. \tag{2.3}$$

The notation is standard

$$\begin{aligned} & & u, v & \quad \text{(zonal, meridional velocities)} \\ \frac{D}{Dt} &= \frac{\partial}{\partial t} + u_0 \frac{\partial}{\partial x} + v_0 \frac{\partial}{\partial y} & & \quad \text{(the material derivative)} \\ & & \eta & \quad \text{(the pressure at the top surface)} \\ & & \eta_B & \quad \text{(the bottom elevation).} \end{aligned}$$

The variables have been non-dimensionalized using typical scales U, L, D for the horizontal velocity, horizontal length, and fluid depth. The relevant dimensionless parameters are

$$\begin{aligned} \epsilon &= \frac{U}{fL} << 1 && \text{the Rossby number} \\ \beta &= \frac{\beta^* L^2}{U} = O(1) && \text{the dimensionless planetary vorticity gradient.} \end{aligned}$$

The numeric subscripts refer to the order in the asymptotic expansion in ϵ.

Conservation of potential vorticity is established by taking the curl of the momentum equations and using continuity

$$\frac{D}{Dt} Q = 0. \tag{2.4}$$

The quasi-geostrophic potential vorticity is defined as

$$Q = \nabla^2 \psi + f(x, y)$$

where f is the ambient vorticity due to the Coriolis effect and bottom topography and the streamfunction ψ is the geostrophic streamfunction

$$\begin{aligned} \psi_x &= v_0 \\ -\psi_y &= u_0. \end{aligned}$$

Because the flow is steady, the conservation equation may also be expressed as

$$J(\psi, Q) = 0, \tag{2.5}$$

where $J(A, B)$ represents the Jacobian of $A(x, y)$ and $B(x, y)$ with respect to the coordinates x and y. By definition, when the Jacobian of two fields vanishes, we may regard one as a function solely of the other. In the absence of forcing the $Q(\psi)$ relation must have been determined upstream where forcing such as wind stress and dissipation due to eddies are more important than inertial effects. The $Q(\psi)$ relation is carried from there along the streamlines into the free inertial region of interest.

In hydraulic theories, we assume that the structure of the basic flows are slowly-varying in x, the direction of flow. The flow structure $\psi(y)$ is then determined by the long-wave potential vorticity equation:

$$\frac{\partial^2 \psi}{\partial y^2} + f(y) = Q(\psi). \tag{2.6}$$

The boundary conditions for this second order differential equation depend on the physical domain of the problem. If the flow is bounded at $y = \pm L$, the geometry is a channel. Since the flow can not pass through the channel walls the normal velocity must vanish there, implying that the streamfunction is constant along the walls. Without any loss of generality, these constants are defined as

$$\psi = \pm \psi_w \ \ at \ \ y = \mp L. \tag{2.7}$$

The streamfunction at the wall is determined by the dynamics of the flow and may vary in time. However, in the present problem, we will be considering disturbances that are isolated in x. In this case

$$\frac{\partial \psi_w}{\partial t} = 0,$$

since ψ_w cannot change far away from the disturbance. Often in geophysical fluid

problems the channel is assumed to be periodic, representing a complete latitude circle. If this is the case, the integrated x-momentum equation (2.1) leads to

$$\frac{\partial}{\partial t}\int_{-\infty}^{\infty} u dx \;=\; 0 \quad at \quad y \;=\; \mp L. \tag{2.8}$$

In a hydraulic system, the up- and downstream flows are not necessarily the same and we are not considering a periodic channel. In this case, the boundaries at $\pm L$ are not closed, and (2.8) need not apply. Instead, the ageostrophic pressure gradient compensates for the change in momentum. This ageostrophic pressure will be discussed further in section 2.3.

The possibility of alternate flows depends on whether a particular $Q(\psi)$ allows non-unique solutions to (2.6) for the same ambient potential vorticity. This question of non-uniqueness will be taken up in section 2.5; first we consider how to classify the flows by considering fluxes of energy and momentum and also the speed of long-waves.

2.3 Fluxes of Energy and Momentum

In this inviscid, unforced system several quantities are conserved. One, the potential vorticity, was discussed in the previous section. A second conserved quantity is the energy. An energy equation can be constructed by adding $u_0 \times$ (2.1) + $v_0 \times$ (2.2)

$$\frac{D}{Dt}\left(\frac{u_0^2 \;+\; v_0^2}{2} \;+\; \eta_1\right) \;+\; v_0 u_1 \;-\; u_0 v_1 \;=\; 0. \tag{2.9}$$

This equation may be expressed as a quantity conserved along geostrophic streamlines by mathematically constructing an $O(\epsilon)$ "streamfunction" from the $O(\epsilon)$ continuity equation

$$\begin{aligned} \frac{\partial \psi_1}{\partial x} \;&=\; -v_0 \eta_B \;+\; v_1, \\ \\ \frac{\partial \psi_1}{\partial y} \;&=\; u_0 \eta_B \;-\; u_1. \end{aligned} \tag{2.10}$$

Using this "streamfunction" in the steady form of (2.9) we find the equation,

$$u_0 \frac{\partial B}{\partial x} + v_0 \frac{\partial B}{\partial y} = 0 \tag{2.11}$$

i.e B is conserved along geostrophic streamlines where

$$B(\psi) = \frac{u_0^2 + v_0^2}{2} + \eta_1 - \psi_1. \tag{2.12}$$

In fact, by using this $O(\epsilon)$ "streamfunction" in the momentum equations

$$\left(\beta y + \eta_B + \frac{\partial v_0}{\partial x} - \frac{\partial u_0}{\partial y}\right) v_0 = \left(u_0 \frac{\partial u_0}{\partial x} + v_0 \frac{\partial v_0}{\partial x} + \frac{\partial(\eta_1 - \psi_1)}{\partial x}\right) = \frac{\partial B}{\partial x} \tag{2.13}$$

$$-\left(\beta y + \eta_B + \frac{\partial v_0}{\partial x} - \frac{\partial u_0}{\partial y}\right) u_0 = \left(u_0 \frac{\partial u_0}{\partial y} + v_0 \frac{\partial v_0}{\partial y} + \frac{\partial(\eta_1 - \psi_1)}{\partial y}\right) = \frac{\partial B}{\partial y}. \tag{2.14}$$

we find that

$$\frac{dB}{d\psi} = Q(\psi_0). \tag{2.15}$$

The function $B(\psi)$ is a quasi-geostrophic version of the β-plane Bernoulli function discussed by Ball (1954) and Woods (1993).

The Bernoulli function may be used to show that energy is conserved in an inviscid transition between two zonal flows with the same $Q(\psi)$ in a channel of width $2L$, since if potential vorticity is conserved, then the Bernoulli function (and therefore energy) are also. The energy equation (2.11) is integrated over the domain of the fluid

$$0 = \int_{-L}^{+L} \int_{x=A}^{x=B} \left(u_0 \frac{\partial B}{\partial x} + v_0 \frac{\partial B}{\partial y}\right) dx dy$$

$$= \int_{-L}^{+L} u_0 B dy|_{x=A}^{x=B} + \int_{x=A}^{x=B} v_0 B dx|_{-L}^{+L}.$$

The second term must vanish because there can be normal flow through the channel walls. Thus, the energy flux, $G = \int_{-L}^{+L} u_0 B dy$, must be the same upstream (at $x = A$) and downstream (at $x = B$) of a transition. This can be seen more easily by direct integration of 2.15 across the streamlines in the channel (which is what the

previous integration is).

The drawback of the quasi-geostrophic Bernoulli function is the presence of the ageostrophic pressure $\eta_1 - \psi_1$. However, for strictly zonal flows, these ageostrophic terms may be re-expressed as an $O(1)$ quantity using (2.14)

$$\int_{-L}^{y} (\beta y + \eta_B)\, u_0\, dy = \eta_1 - \psi_1. \tag{2.16}$$

The ageostrophic pressure gradient is due to meridional variations in the Coriolis force and the bottom topography.

The amount of momentum flux is used to classify alternate flows in open channel hydraulics; subcritical flows have an excess of momentum flux. If a control is established, then momentum flux is lost in the transition to supercritical flow due to topographic drag on the flow. For the quasi-geostrophic flow a similar loss is found by integrating the zonal momentum equation (2.1) across the channel in y and along x from a point ($x = A$) upstream of the transition to downstream ($x = B$). Using ψ_1 again, this leads to

$$M|_A^B = -\int_{-L}^{+L} \int_A^B \frac{\partial \eta_B}{\partial x} \psi dx dy, \tag{2.17}$$

where

$$M = \int_{-L}^{+L} \left(u_0^2 + \eta_1 - \psi_1 \right) dy.$$

Equation (2.17) shows explicitly that any difference in the momentum flux (the left hand side) is due to the momentum loss from form drag (the right hand side). Using (2.16) for the ageostrophic pressure, the momentum flux for zonal flows may also be expressed in terms of $O(1)$ quantities.

An alternative approach is to follow the method of Benjamin (1984) and consider the impulse. The fluid impulse is the amount of force needed to generate the entire flow from rest (Batchelor, 1985). For a two-dimensional, non-rotating system with

vorticity $\vec{\omega}$, the total impulse vector is therefore

$$\vec{I} = \frac{1}{2}\int \vec{x} \times \vec{\omega} dA,$$

where the integral is taken over the entire fluid domain. On the β-plane, the total vorticity includes the ambient vorticity, and the total zonal impulse is therefore

$$I = \frac{1}{2}\int yQ dA.$$

Conservation of I is determined from (2.4) by multiplying the equation by y

$$\frac{\partial}{\partial t}(yQ) + u_0(yQ)_x + v_0(yQ)_y - v_0 Q = 0,$$

or, with the continuity equation $\frac{\partial u_0}{\partial x} + \frac{\partial v_0}{\partial y} = 0$,

$$\frac{\partial}{\partial t}(yQ) + (u_0 yQ)_x + (v_0 yQ)_y - v_0 Q = 0.$$

The final term may be written as the divergence of a flux (Bretherton, 1966a) and, if topography is present, a drag term

$$v_0 Q = \frac{\partial}{\partial x}\left[\beta y\psi + \eta_B \psi + \frac{1}{2}v_0^2 - u_0^2\right] - \frac{\partial}{\partial y}[u_0 v_0] - \frac{\partial \eta_B}{\partial x}\psi.$$

The conservation law becomes

$$\frac{\partial}{\partial t}(yQ) + \frac{\partial}{\partial x}\left(-\frac{1}{2}v_0^2 + \frac{1}{2}u_0^2 - \beta y\psi - \eta_B\psi + y u_0 Q\right) + \frac{\partial}{\partial y}(u_0 v_0 + y v_0 Q) = -\frac{\partial \eta_B}{\partial x}\psi. \tag{2.18}$$

This equation is integrated over the domain in y, and from $-\infty$ to ∞ in x. The application of the boundary conditions (2.7) on $v(\pm L)$ causes the third term on the left hand side to vanish. In many other geophysical applications, the second term on the left hand side cancels due to periodicity, and in the absence of topography the

right hand side cancels also, leaving

$$\frac{\partial}{\partial t}\int_{-L}^{+L}\int_{-\infty}^{+\infty} yQ\,dx\,dy \;=\; \frac{\partial}{\partial t}I \;=0$$

i.e. pseudo-momentum is conserved. Conservation of I is used to calculate bounds in nonlinear global stability problems (i.e. Arnol'd (1966), Shepherd (1988), Dritschel (1988), Bell and Pratt (1994)).

In the present search for hydraulic behavior, periodicity in x is not assumed. If the transition is an example of a hydraulic control then the controlled flow has different flow structures upstream and downstream of the control. In addition, the flow is assumed to have reached steady state after some adjustment that has established the control. Because the alternate flows have no x-variations away from any transitions between them, the integrated conservation equation (2.18) reduces to

$$S|_{x=-\infty}^{x=+\infty} \;=\; -\int_{-L}^{+L}\int_{-\infty}^{+\infty}\frac{\partial \eta_B}{\partial x}\psi\,dx\,dy, \tag{2.19}$$

where

$$S \;=\; \int_{-L}^{+L}\left(\frac{1}{2}u_0^2 - \beta y\psi + yu_0Q\right)dy \tag{2.20}$$

Equation (2.19) also shows explicitly that any difference in the flux as the flow passes from subcritical to supercritical at the control is due to the momentum loss from form drag. Integration by parts (using $Q = \psi_{yy} + \beta y$) shows that this form of the momentum equation is equivalent to (2.17), which is hardly surprising since conservation of momentum and conservation of pseudo-momentum differ only by the divergence of a flux.

The flux of impulse, S, is equivalent to the "flow-force" used by Benjamin (1984) in many examples of hydraulics problems. Benjamin demonstrated that the dynamical problem (2.6) is equivalent to the variational equation $\delta S = 0$. If the integrand of S is abbreviated as $s(\frac{\partial\psi}{\partial y}, \psi, y)$, then $\delta S = 0$ is true if ψ satisfies the Euler equation

(Courant and Hilbert, 1953)

$$\frac{\partial}{\partial y}\left(\frac{\partial s}{\partial \psi_y}\right) - \frac{\partial s}{\partial \psi} = 0,$$

$$+\frac{\partial u}{\partial y} - \beta y + Q(\psi) = 0$$

which is precisely equation (2.6). Each alternate state which satisfies (2.6) must be an extremum of S.

2.4 Wave Properties

Alternate flows may also be classified by the behavior of long-wave small amplitude disturbances. As in open channel hydraulics, flows are supercritical [2] if long-wavelength disturbances can only propagate downstream, which means that small amplitude stationary waves can not form. Because stationary waves are not possible, Rossby wave radiation is prevented and a supercritical flow may support stationary coherent, finite amplitude structures.

In a hydraulics interpretation, flows are classified as subcritical if long-wavelength disturbances can propagate both upstream and downstream. Because upstream propagation is possible, subcritical flows are capable of supporting stationary waves. These waves have a group velocity directed downstream, and so stationary waves can form in the lee of an obstacle.

A flow is critical if the long-wave disturbances are stationary. By considering a general class of "hydraulics" problems, Gill (1977) showed that the critical flow is also the flow for which two alternate states are equal because a flow that is close to critical will differ from its alternate by only a small disturbance; as the flow approaches criticality the speed of this disturbance must approach zero.

In order to determine the propagation speed and classify a quasi-geostrophic flow,

[2] see note on pg. 24

the background state is disturbed so that the streamfunction Ψ of the perturbed state is given by

$$\Psi(x,y,t) \;=\; \psi(y) \;+\; \tilde{\phi}(x,y,t).$$

These disturbances, denoted by $\tilde{\phi}$, are long enough for the flow to be considered uniform and parallel to the axis everywhere, yet short enough so that along-stream changes in the flow can be ignored over a wavelength. The latter assumption allows any disturbance to be expressed as a superposition of plane waves of the form

$$\tilde{\phi}(x,y,t) \;=\; \phi(y)e^{ik(x-ct)},$$

where the symbol ϕ is now taken to denote only the meridional variation of the disturbance. The dispersion relation is found by substituting the perturbed streamfunction into the potential vorticity equation (2.4)

$$\left(\frac{\partial}{\partial t}+U_0\frac{\partial}{\partial x}\right)\nabla^2\tilde{\phi} \;+\; \frac{\partial\tilde{\phi}}{\partial x}\frac{\partial Q}{\partial y} \;+\; \left(\frac{\partial\tilde{\phi}}{\partial x}\frac{\partial\nabla^2\tilde{\phi}}{\partial y}-\frac{\partial\tilde{\phi}}{\partial y}\frac{\partial\nabla^2\tilde{\phi}}{\partial x}\right) \;=\; 0, \qquad (2.21)$$

and linearizing. For the geophysical shear flows considered here, the phase speed of a disturbance is determined by the well-known eigenvalue problem (Rossby, 1939; Kuo, 1949):

$$\begin{aligned}(U(y)-c)\left(\phi_{yy}-k^2\phi\right) \;+\; (\beta \;-\; U_{yy})\,\phi \;&=\; 0 \qquad (2.22)\\ \phi \;=\; 0 \qquad\quad at \qquad\quad y \;&=\; \pm L\end{aligned}$$

By considering this eigenvalue equation, we will attempt to classify examples of alternate flows as supercritical and subcritical with respect to the speed of the appropriate long-wavelength wave mode. Because of the application to jet splitting, the wave of interest is the second cross-channel mode, the varicose wave.

Much of the previous work on this eigenvalue equation has focused on finding the unstable modes with complex eigenvalues c. Howard (1964) showed that on the f-plane the number of unstable modes is equal to the number of inflection points in the

flow. A neutral wave is found by setting $U - c = 0$ at the inflection point in (2.22). The eigenfunction ϕ is non-singular and the mode is marginally stable. These neutral waves are contiguous to a set of unstable modes with complex eigenvalue c. Howard's (1961) semicircle theorem, extended to the β-plane by Pedlosky (1964), states that for an arbitrary unstable velocity profile, $U(y)$, the complex eigenvalues lie within a semicircle

$$\left(c_r - \frac{1}{2}(U_{min} + U_{max})\right)^2 + c_i^2 \leq \left(\frac{1}{2}(U_{max} - U_{min})\right)^2 + \frac{\beta(U_{max} - U_{min})}{2k^2}$$

in the complex c-plane, where $c_r < U_{max}$ (Pedlosky, 1964).

In addition to these unstable modes and the neutral mode, there may be a countable number of non-singular stable modes. These propagating modes will be most important in a hydraulics interpretation of shear flows. Pedlosky (1964) showed that there is no mode with c_r greater than U_{max}, and modes with c_r in the range $U_{min} \leq c_r \leq U_{max}$ must either be unstable, stable and moving with a phase speed equal to the velocity at the critical latitude, or singular at the critical latitude. Thus, any stable, non-singular mode has $c < U_{min}$ (other than the finite number of neutral modes). These modes, which are essentially Rossby waves modified by shear (or Rayleigh shear waves modified by β), have been studied by Drazin *et al.* (1982) in the asymptotic limit of large β. In the limit as $\beta \to \infty$, the waves become the classic Rossby waves of which there can be an infinite number of cross-channel modes. In the present study we are interested in $\beta = O(1)$ which makes an analytic investigation of the waves more difficult.

For a given flow, the propagation of disturbances with wavenumber k is found by solving (2.22) numerically. The eigenvalues are found by discretizing (2.22) using center differencing, and then solving the the linear algebra problem numerically (Yanai and Nitta, 1968). The domain is divided into $M + 1$ grid-points (labeled i) with spacing $dy = 2L/M$. The second derivatives in (2.22) are expressed in center differences at the interior points, and the boundary conditions, $\phi = 0$ are used at

the end points. This turns (2.22) into a linear homogeneous system

$$(B - cD)\, P \;=\; 0,$$

or

$$\left(D^{-1}B \;-\; c\delta_{i,j}\right) P \;=\; 0, \tag{2.23}$$

where

$$\begin{aligned} B(i,j) &= (\beta \;-\; U(y(i))_{yy})\,\delta_{i,j} \;+\; U(y(i))D(i,j); \\ D(i,j) &= \frac{1}{dy^2}\left(\delta_{i,j+1} - 2\delta_{i,j} + \delta_{i,j-1}\right) \;-\; k^2\delta_{i,j}; \\ P(i) &= \phi(y(i)). \end{aligned}$$

The eigenvalues of this matrix (2.23) are easily found using standard routines and this method is used later in the chapter when specific velocity profiles are considered.

This section and the preceding one have discussed how to classify flows as subcritical or supercritical based on their wave properties and the amount of momentum flux associated with them. A supercritical flow has less momentum flux than its subcritical alternate state and a supercritical flow does not support infinitesimal stationary waves. Following an argument by Benjamin (1962) these two properties are now shown to be equivalent. Using variational calculus in §2.3 we established that a solution to the dynamical equation (2.6) subject to the boundary conditions (2.7) was an extremal of the integral S. A solution is an actual minimum of S if the second variation $\delta^2 S$ is positive (Courant and Hilbert, 1953). To prove this the expression

$$S[\psi] \;=\; \int s(\psi_y, \psi, y)dy'$$

is expanded by Taylor's theorem

$$S[\psi + \epsilon\phi] \;=\; S[\psi] \;+\; \delta^2 S$$

where

$$\delta^2 S = \frac{\epsilon^2}{2} S_2[\psi,\phi] = \frac{\epsilon^2}{2}\int\left(\frac{\partial^2 s}{\partial\psi^2}\phi^2 + 2\frac{\partial^2 s}{\partial\psi\partial\psi_y}\phi\frac{\partial\phi}{\partial y} + \frac{\partial^2 s}{\partial\psi_y^2}(\frac{\partial\phi}{\partial y})^2\right)dy'.$$

The first order term in the Taylor expansion has vanished because S is stationary for the solution ψ. Using the definition of S (2.20) with $Q = \frac{dB}{d\psi}$ and integrating by parts yields

$$\delta^2 S = \frac{\epsilon^2}{2}\int\left(\frac{d^2 B}{d\psi^2}\phi - \frac{\partial^2\phi}{\partial y^2}\right)\phi dy.$$

Clearly $\delta^2 S$ is zero for critical flow because the integrand is just the wave equation for a $k = 0$ wave with zero phase speed. If the flow is subcritical, then stationary waves of finite wavenumber k are possible and the integrand is equal to $-k^2\phi^2$ which is clearly negative. A minimum of S can only occurs when the flow is supercritical and $\delta^2 S$ is positive.

2.5 Multiple solutions for general $Q(\psi)$

According to Armi (1989), a uniform eastward flow on the β plane may be either subcritical or supercritical as waves can be advected downstream or propagate upstream depending on the strength of β. On the other hand, westward flow can not be subcritical because both the β effect and advection cause waves to propagate to the west. If the flow has some shear associated with it this argument is not rigorous because the propagation speeds of the waves depends on the shear and, in fact, the strength of the shear determines whether a particular mode exists at all. Also, the mere existence of some flows that allow stationary waves and some that do not is not enough to show that alternate states are possible. True alternate flows must have the same energy (or, equivalently, potential vorticity) so that they may pass from one to the other in a conservative manner. The purpose of this section is to explore which shear flows have alternate states by determining which $Q(\psi)$ relations allow non-unique solutions to (2.6) with a given ambient potential vorticity $f(y)$.

In a bounded domain such as the channel with the boundary conditions (2.7),

equation (2.6) is a two point boundary value problem and there have been several theorems, dating back to Picard (1893), which determine when such systems have unique solutions (Bailey *et al.* (1968) and Bernfeld and Lakshmikanthan (1974)). If $\frac{dQ}{d\psi}$ is a constant (Λ), (2.6) is linear and the problem is easily solved and, as §2.6 will demonstrate, a linear $Q(\psi)$ does not allow alternate states. Depending on the sign of Λ, the solution is either exponentially decaying, or a sinusoidal free mode, the wavenumber of which is determined by Λ.

If $Q(\psi)$ is nonlinear, the structure of $\psi(y)$ is no longer simply sinusoidal, but instead has a local wavenumber which depends on $\frac{dQ}{d\psi}$, which is a function of ψ. Unlike the linear problem, the nonlinear problem may have several different solutions with different meridional structures. According to Bailey *et al.* (1968), if $Q(\psi)$ is continuous and smooth ($\frac{dQ}{d\psi}$ is continuous) and $\frac{dQ}{d\psi}$ is positive for all ψ, then the solution to (2.6, 2.7) is unique. If $\frac{dQ}{d\psi}$ is bounded from below by $-\mathcal{K}$ then the system has a unique solution if

$$\sqrt{\mathcal{K}} \; < \; \frac{\pi}{2L}. \tag{2.24}$$

This places a bound on the size of the domain that may have unique solutions and if L exceeds this bound, it is possible, although not guaranteed, that non-unique solutions exist. The actual number of solutions will depend on the other parameters of the problem, i.e. β and ψ_w (which determines the net transport of the flow).

Formal proofs of this theorem may be found in Bailey and Waltman (1966) and Lettenmeyer (1944). The idea behind the proofs is that solutions to a nonlinear equation, bound in the manner described, will have a wavy structure with a minimum wavelength set by the bound of $\frac{dQ}{d\psi}$. Assume a function $\tilde{\psi}$ satisfies one boundary condition and the equation (2.6). If the domain is large enough, the fluctuations may allow $\tilde{\psi}$ several ways to meet the boundary condition at the opposite edge. However, if the domain is smaller than the minimum wavelength then it is too small for there to be several paths to the opposite side.

The bounds which guarantee uniqueness are the same as the bounds found by Arnol'd in his two theorems on stability of a fluid in a bounded domain (Arnol'd

(1966) as reported in McIntyre and Shepherd,(1987) and Ripa (1992)). Arnol'd's first theorem guarantees stability if $\frac{d\psi}{dQ}$ is positive everywhere and his second theorem guarantees stability if $\frac{d\psi}{dQ} < -\left(\frac{\pi}{2L}\right)^{-2}$; thus when the domain is small enough so that the flow is stable in the sense of Arnol'd, solutions are unique.

If $\mathcal{K}$ exceeds the limit set in (2.24) the equation may have non-unique solutions. Perov (1962), explored the special case where $f(y) = \psi_w = Q(0) = 0$. When $\frac{dQ}{d\psi}$ is negative, then (2.6) has solutions $\psi(y)$ that oscillate in y with a local wavenumber $\sqrt{-\frac{dQ}{d\psi}}$. If the domain is smaller than half of the minimum wavelength only the trivial solution is possible. As the domain size increases, more solutions are added with more "nodal" points in the domain. There are $2n$ non-trivial solutions where n is the greatest integer that satisfies

$$n < \frac{2L\sqrt{\mathcal{K}}}{\pi}. \tag{2.25}$$

A consideration of specific $Q(\psi)$ relations that violate (2.24) allows an explicit demonstration of when alternate flows are possible. Multiple solutions to the two point boundary value problem (2.6) are found with a shooting method. For simplicity the ambient potential vorticity gradient will be taken to be linear, $\frac{df}{dy} = \beta$, in all of the examples. The domain is divided into $M+1$ grid-points (labeled i) with spacing $dy = 2L/M$. Starting at the southern boundary, we use the appropriate boundary condition for ψ and an estimate for $u = -\frac{\partial\psi}{\partial y}$ to begin the integration northward. The integration is carried out using a three-point difference for the second derivative. At the northern boundary the discrepancy between ψ_{M+1} and $-\psi_0$ is used to re-estimate the velocity at the southern boundary. The process is iterated until the discrepancy at the northern boundary is reduced to within a predetermined tolerance. This method leaves us with a set of zonal velocities at the southern boundary $u_{y=-L} = u_S$ which correspond to different solutions $\psi(y)$ that satisfy (2.6).

2.6 Linear $Q(\psi)$

$Q(\psi)$ is commonly chosen to be linear everywhere which makes the problem of finding the flow structure analytically tractable. For instance, Fofonoff (1954) solved for the free inertial modes of a closed rectangular basin using a linear $Q(\psi)$. In addition, scatter plots of Q vs. ψ in the atmosphere show that a nearly linear relationship between Q and ψ often holds (Butchart *et al.,* 1989). In a blocking episode, the relationship is piecewise linear and the interior of the block has a steeper slope than the exterior. However, we will demonstrate that a linear $Q(\psi)$ is not an appropriate model for multiple equilibria. Consider the equation

$$\frac{\partial^2 \psi}{\partial y^2} + \beta y = \Lambda \psi$$

with the antisymmetric channel boundary conditions (eq. 2.7). If Λ is positive, the unique solution is

$$\psi = (u_0 L - \psi_w) \frac{\sinh \Lambda^{-\frac{1}{2}} y}{\sinh \Lambda^{-\frac{1}{2}} L} - u_0 y$$

where

$$u_0 = -\beta/\Lambda. \tag{2.26}$$

If Λ is negative, the number of antisymmetric solutions depends on its value. The streamfunction is given by

$$\psi = (u_0 L - \psi_w) \frac{\sin\left((-\Lambda)^{-\frac{1}{2}} y\right)}{\sin\left((-\Lambda)^{-\frac{1}{2}} L\right)} - u_0 y. \tag{2.27}$$

If $(-\Lambda)^{\frac{1}{2}} \neq \frac{n\pi}{L}$, where n is an integer, then there is a unique solution that satisfies the boundary conditions. However, if $(-\Lambda)^{\frac{1}{2}} = \frac{n\pi}{L}$, there are no solutions if $\psi_w \neq +u_0 L$. For the special case when $\psi_w = +u_0 L$ the amplitude of the free, sinusoidal mode is unspecified by the boundary conditions and an infinite number of solutions satisfy

the equation. These solutions are of the form

$$\psi = A \sin \frac{n\pi}{L} y - u_0 y.$$

Tollmein (1935) investigated the stability properties of this sinusoidal flow, and showed that the flow is stable when the domain half width L is less than $\frac{\pi}{(-\lambda)^{\frac{1}{2}}}$. Note that this is the same cut-off width for the flow to be unique.

The infinite number of modes correspond to Rossby waves of arbitrary amplitude which satisfy the full perturbation equation (2.21) because the nonlinear terms vanish. These waves are not alternates to each other or the uniform flow ($A = 0$) because the energy associated with them depends on the amplitude A. Also, the momentum flux

$$S = \int \left(\frac{u^2}{2} - \beta y \psi + y u \Lambda \psi \right) dy = \frac{\beta^2 L^5 (3 + 4\pi^2)}{3\pi^4}$$

is independent of the amplitude of these waves. According to the classification given in §2.3, these waves can not be alternates since they all have the same momentum flux. Of course, this restriction on linear $Q(\psi)$ does not apply to flows with piecewise linear $Q(\psi)$ which do have alternates states (Pratt, 1989 ; Haynes *et al.*, 1993) since a nonlinearity arises at the discontinuities of potential vorticity.

2.7 $Q = -\sin \psi$

Consider the nonlinear potential vorticity distribution in a flat-bottomed channel

$$\frac{\partial^2 \psi}{\partial y^2} + \beta y = -\sin \psi \tag{2.28}$$

with Dirichlet boundary conditions (eq. 2.7). The derivative $\frac{dQ}{d\psi}$ is bounded from above and below by ± 1. If $L < \frac{\pi}{2}$ a solution is unique and, according to Arnol'd's theorem, also stable. Because $-\sin \psi$ is an odd function, if $\psi(y)$ is a solution then $-\psi(-y)$ is also. Therefore the unique solution ψ must also be antisymmetric. As the domain width increases beyond the critical width of $L = \frac{\pi}{2}$, multiple solutions are

possible.

2.7.1 Zero Transport

First consider the special case of flow with no net transport ($\psi_w = 0$) on the f-plane. According to Perov's theorem (2.25), when the domain has a half-width of $L = 4$ there are four non-trivial solutions. These are determined by the shooting method with $M = 48$ and are shown in Figure 2-1. Two of the flows are antisymmetric and two are symmetric about the midpoint of the channel. In addition, there is a trivial solution.

If the ambient potential vorticity gradient changes (as it would if a fluid parcel passes over an isolated ridge) while the $Q(\psi)$ relation is maintained, then the velocity structure is forced to change. For each value of β, the shooting method determines all the flows that satisfy (2.28) and characterizes them in terms of u_S, the velocity at the southern channel wall. Solutions are summarized by figure 2-2. Each point that lies along the curves corresponds to a solution of the potential vorticity equation (2.28) and the velocity profiles of several solutions are indicated in the figure. Negative values of β correspond to negative values of the scaling velocity U and the curves show the symmetry $(\beta, u_s) \rightarrow (-\beta, -u_s)$, i.e. solutions corresponding to points in the lower left quadrant are the same as the ones represented by points in the upper right quadrant.

Every solution $\psi(y)$ that lies along the S-shaped curve is antisymmetric, so the velocity profiles $u(y)$ are symmetric. The curve includes the trivial solution at the origin and extends to infinity as $\beta \rightarrow \infty$, implying that at least one antisymmetric solution ψ exists for all values of β. The curve has two turning points at $\beta = \pm 0.103$ and when β is between these critical values three antisymmetric solutions exist. At the point P a symmetry-breaking bifurcation occurs as another solution curve bifurcates off of the S-shaped curve. Points on this curve represent asymmetric solutions ψ. This curve has two turning points at $\beta = \pm 0.39$. Beyond this value of β the only solution is an antisymmetric ψ.

The critical latitudes of the marginally unstable modes are the latitudes at which

$\frac{dQ}{dy}$ vanishes. In this example these are determined by

$$\begin{aligned} \frac{dQ}{dy} &= \frac{dQ}{d\psi}\frac{d\psi}{dy} \\ &= (\cos\psi)\, u. \end{aligned}$$

With a net eastward transport of zero, u must vanish somewhere in the flow or be identically zero everywhere in the flow. Other critical latitudes may occur whenever $\psi = \frac{\pi}{2}$. The presence of these latitudes suggest that unstable modes may be found for this flow and indeed, because the half-width of the channel is $L = 4$, we are well beyond the necessary condition for instability which, for the present problem, is $L > \frac{\pi}{2}$. The dispersion relations for four symmetric velocity profiles (on the S-shaped curve) are described in figure 2-3. The eigenvalue equation (2.22) has been solved for these velocity profiles using the matrix method described in §2.4 using $M = 48$ points. The method finds all of the normal modes and a set of other eigenvalues which represent the discretized version of the continuous spectrum. No information on this continuous spectrum (whose eigenfunctions have discontinuous derivatives at the critical latitude) will be presented.

In figure 2-3 we see that all of the solutions are unstable to the sinuous mode. For profile a the unstable modes lie within two bands. The longer waves have a positive real part, so $U - c_r$ vanishes along the wall. For the shorter waves $U - c_r$ vanishes in the center region of the flow. Both of these bands correspond to symmetric eigenfunctions ϕ which are the sinuous mode. Profile d also has two bands of unstable sinuous waves. The critical latitude for the longer waves is again at the edges of the flow but because the velocity profile is reversed, c_r is negative for the longer waves and the longest waves have stabilized with $c < U_{min}$. The band of shorter waves has positive phase speeds and vanishingly small growth rates. This band is quite narrow, and for smaller values of β on the outer branch it disappears. Solutions b and c have a single band of unstable sinuous waves which are contiguous to long stable sinuous waves with westward phase speeds.

The dispersion diagrams for the second gravest mode, the varicose wave, are also

shown in figure 2-3. No varicose wave exists for any of the solutions along the outer branches (i.e. profiles a and d). At the point of the curve where two symmetric solutions merge, profile c, a long ($k = 0$) stationary ($c = 0$) wave emerges, as expected by Gill, 1977. This wave is stable, but only marginally so; on the other side of the turning point the mode becomes unstable. All solutions on the center branch are unstable to both the sinuous and varicose waves with the exception, of course, of the null solution at $\beta = 0$. The dispersion diagram for profile b is typical. The longest sinuous waves are stable and the longest varicose waves are unstable. The two bands overlap at moderate wavelengths and as k increases further only the sinuous mode is unstable. The largest growth rate for the varicose mode is smaller than the largest growth rate of the sinuous wave.

In this example it appears that the multiplicity of symmetric solutions is linked to the instability of the symmetric (varicose) mode. This can be seen more clearly by considering the other parameter in this problem: L, the half-width of the channel. Since Q and $\frac{dQ}{d\psi}$ were non-dimensionalized, L is a measure of the instability according to Arnol'd's theorem. The solution curves at a fixed β, i.e. $\beta = 0.05$, with variable L show that the instability is tied to the existence of multiple equilibria (fig. 2-4). For small L, the flow is unique and stable (a) . As the half-width increases beyond $L = \frac{\pi}{2}$ a pitchfork bifurcation occurs as two other solution branches emerge (b and d). The center branch represents symmetric velocity profiles which are unstable to the long sinuous wave (c), the symmetry-breaking mode. The two outer branches represent stable, asymmetric velocity profile, which do not support a sinuous mode. Note that the bifurcation occurs right at Arnol'd's necessary condition for instability, $L = \frac{\pi}{2}$. As the half-width increases beyond $L = 3.5$, two more solution branches emerge (f and g) with symmetric velocity profiles. All of these symmetric solutions (e,f and g) are unstable to the sinuous mode. Only the center solution (f) is also unstable to the long varicose mode, and the outer solutions do not support a varicose mode.

For the special case of $\beta = 0$ (fig. 2-5) the first set of multiple equilibria emerge via a pitchfork bifurcation at $L = \frac{\pi}{2}$ again. Because $\beta = 0$ the center branch only

represents the null solution, which of course is stable. The increase in channel width beyond $L = \frac{\pi}{2}$ does allow the gravest wave to satisfy the boundary conditions and so a stable normal mode does exist for $L > \frac{\pi}{2}$. The second set emerges at $L = \pi$, where Perov's theorem predicts the formation of more solutions. These new solutions are symmetric and unstable to the sinuous mode alone (just as e and g were in the previous plot). The pitchfork bifurcation is structurally unstable which means that any non-zero value of β leads to a structural change of the bifurcation to that of figure 2-4. It is clear that the onset of each instability corresponds to a bifurcation of solution branches and that Arnol'd's necessary condition for instability is the minimum value of L at which these bifurcations may take place. As β increases, multiple equilibria occur for larger values of L, the exact value of which depends on β.

As in many other nonlinear systems (Arnol'd, 1992) the existence of an unstable equilibrium depends on the multiplicity of solutions to the governing equation. In fact, if we consider the solution surface $u_s(\beta, L)$ for the symmetric velocity profiles (fig. 2-6) we see that the surface is folded; the projection of the fold onto the (β, L) plane is a cusped region within which three solutions are possible. The entire center branch is unstable with the exception, of course, of the null solution. This structure of the solution surface is ubiquitous in systems described by catastrophe theory, and a further discussion of what such a solution surface might indicate about the barotropic instability problem will be postponed until the discussion section of this chapter.

2.7.2 Eastward Transport

Because we are primarily interested in eastward jets, we continue this analysis for streamfunctions with the boundary condition $\psi_w = 1$. This addition of a net eastward flow with $\overline{u} = \frac{\psi_o}{L}$ does not simply shift the solutions of the previous example by $\overline{u}$. That kind of Galilean shift would cause $Q(\psi)$ to have a different functional form. Instead we keep $Q = -\sin\psi$ and search for the new streamfunctions that satisfy (2.6). To focus on symmetric jets and their alternates, only the antisymmetric streamfunctions are examined which allows us to use u_c, the center velocity to characterize the flow as a function of the external parameters β and L. Because the

folded catastrophe surface is structurally stable, a similar solution surface exists for this example (figure 2-7). When L exceeds π, the surface corresponding to symmetric velocity profiles will fold and three solutions are possible for a range of β. The exact range differs from the previous example because of the change in transport.

As an example, only the solutions for a channel half-width of $L = 4$ is examined in detail. The solution curve (figure 2-8) is again S-shaped (the choice of the center velocity, u_c, instead of u_s has reversed the S) with turning points at $\beta = 0.07$ and $\beta = 0.26$. For $0 < \beta < 0.26$, an eastward jet (a) exists with westward return flow along the channel walls. These jets are unstable with respect to the sinuous mode and the unstable portion of the spectrum is a single band of moderate wavelengths. The long sinuous waves are stable and propagate westward. No normal varicose mode exists for any of the jets along this outer branch. The other outer branch, extending from $\beta = 0.07$ to infinity corresponds to a "split jet" with a westward center and eastward jets along each channel wall. This flow is also unstable to a sinuous mode and, again, no varicose mode is present. In the range of $0.07 < \beta < 0.20$, the center branch represents flows with weak westward centers and eastward jets along the walls. They are unstable to both the sinuous and varicose waves. The sinuous waves are stable at long wavelengths, but in general have a larger growth rate than the varicose wave. All of these properties are analogous to the preceding example with $\psi_w = 0$, and do not fit into hydraulics interpretation.

On the other hand, when $0.2 < \beta < 0.26$, the flows on the center branch are entirely eastward and have small shear. These flows have no critical latitudes and so are stable even though they lie on the center branch. However, since they do not have the full range of $Q = [-1, 1]$ they are not true alternates to the solutions on the outer branches. A pair of stable sinuous waves and a pair of stable varicose waves with $c < U_{min}$ exist for these flows. These waves are contiguous to the unstable waves for $\beta < 0.2$. Each pair has a mode that can propagate upstream ($c < 0$) and one that propagates with the flow ($c > 0$), which fits the definition of sub-critical hydraulic flow given in §2.4.

The other hallmark of subcritical flow is that the group velocity of the stationary

waves is directed downstream, i.e. it is positive. By considering the dispersion relation for $\beta = 0.21$ this is clearly true since

$$c_g = c + \frac{dc}{dk}$$

and, where $c = 0$ for the varicose mode, $\frac{dc}{dk}$ is positive.

As discussed in §2.4, the flux of momentum may also be used to classify alternate flows because sub-critical flows have more momentum flux than their alternates. Figure (2-9) shows that at any given β the flow on the center branch carries more momentum flux than either flow on the outer branches. Solutions on the center branch are classified as subcritical, and a transition to a solution on either outer branch would result in a loss of momentum flux. Thus the stable flows on the center branch may be classified as subcritical.

2.8 Transitions

Can one of the zonal flows described in the preceding subsection undergo a transition to one of its alternates? This question is considered more carefully in Chapter 3, where time-dependent adjustments are carried out in a quasi-geostrophic numerical model. In this section we suggest two differing scenarios based on the steady, long-wave theory for how an isolated topographic feature may cause a zonal flow to pass to an alternate state. One scenario is based on a hydraulics interpretation of the solution curve. The other is based on an interpretation of how the flow will evolve due to instabilities if $Q(\psi)$ is maintained from its upstream structure.

We assume that the functional form of the topography is separable, i.e.

$$\eta_b = g(x)h(y),$$

where $g(x) \to 0$ as $x \to \pm\infty$, and that $g(x = 0)$ is unity. Other than this, the

topography may take any shape; however, for simplicity, $h(y)$ is assumed to be linear

$$h(y) \;=\; \beta_T(-L \;+\; y).$$

Other choices for this meridional function will alter quantitative features of the suggested transition, such as the exact value of the critical slope or the latitude of the flow as it passes over the topography, but the qualitative nature of the transition will be the same. The actual shape of this topography is shown in figure (2-10). While it may appear unusual, it should be remembered that other choices for η_B will still allow alternate states, since their existence depends only on L and not on the specific functional form of the ambient potential vorticity gradient. Although this η_B is, frankly, chosen for simplicity, it could be argued that the nose-shaped topography qualitatively resembles the South East Newfoundland Ridge near where the Gulf Stream bifurcates (fig. 1-1).

It is also assumed that the topography and the flow vary more slowly in the x-direction than in the y-direction, so that $\nabla^2\psi$ is approximated by $\frac{\partial^2\psi}{\partial y^2}$. With this choice of topography, the potential vorticity equation is simply

$$\frac{\partial^2\psi}{\partial y^2} \;+\; (\beta + \beta_T g)\, y \;-\; \beta_T g L \;=\; Q(\psi),$$

$$\psi \;=\; \pm 1 \quad \text{at} \quad y \;=\; \mp 4.$$

The long-wave character of the topography makes the x-dependence parametric and is simply denoted by the slowly varying function g. The flow field over the topography is determined by solving this ordinary differential equation in y for each value of g between zero and unity. As a fluid parcel passes over the ridge, it experiences a change in the ambient potential vorticity which causes $\psi(y)$ to vary. Of course, this equation is just the potential vorticity equation considered in the preceding subsection with the addition of a constant vorticity term which arises from the stretching over the topography. The solution curve in figure 2-8 may then be used to predict how a

non-unique zonal flow passes over topography.

Suppose that the background potential vorticity gradient is $\beta = 0.21$. The three possible alternate states corresponding to flow far away from the topography lie at the intersection of the solution curve and the line $\beta = 0.21$ (fig. 2-8). Suppose that the upstream flow is represented by the center alternate flow which is stable and subcritical (velocity profile b). As the ridge is approached the $Q(\psi)$ relationship must stay the same as its upstream form, so the flow at any ambient vorticity gradient is determined by the solution curve. As the effective β increases, the velocity structure adjusts itself causing the center velocity of the jet to increase. If the maximum ambient potential vorticity gradient is less than 0.26, then, when the crest of the ridge is met, u_c has reached its maximum; passing down the other side of the ridge causes the flow field to return along the curve to its upstream value.

The difference in interpretation enters if the effective β exceeds the critical value of $\beta = 0.26$. First consider a hydraulics interpretation. Although some of the flows are unstable, the hydraulics interpretation will assume that the long - wave hydraulics character will be present despite smaller wavelength instabilities. If $\beta_T = 0.05$, i.e. so that the total ambient potential vorticity is equal to the value at the turning point of the solution curve (fig. 2-8), then the flow can pass from one branch of the curve to the other. For instance, if the upstream flow is profile (a) then u_c decreases continuously as the topography is passed and reaches the value on the center branch far downstream. In open channel hydraulics this transition is unstable as waves are directed to the ridge from the upstream and downstream which causes energy to be concentrated at the critical point. This results in a hydraulics jump which dissipates the energy and allows the flow to pass to a new state with a different $Q(\psi)$ (since the jump is non-conservative).

In the present case, the upstream flow does not support varicose waves so a convergence of energy does not take place and the flow could possibly pass smoothly from the narrow flow (a) to the broader flow (b). If β is small enough, the flow downstream of the topography may be split. An example of this type of flow is shown in figure (2-11) for $g(x) = e^{-\left(\frac{x}{5\pi}^2\right)}$. Upstream of the topography is a single eastward

jet. The background potential vorticity gradient is taken to be $\beta = 0.08$, so that the jet is a narrow jet with westward return flow along the channel walls. As the topographic slope increases, some of the streamlines are blocked forming a recirculation. Downstream of the topographic center the eastward jet continues to widen forming a stagnation point on the eastern slope. Further east, as the potential vorticity gradient decreases below 0.2, the flow is split into two eastward jets. Far downstream, where β returns to its upstream value of 0.08, the flow is decidedly split, with a recirculation in the interior. This transition bears a qualitative resemblance to the splitting observed in the Gulf Stream (Clarke *et al.,* 1980) and to blocking in the atmosphere (Shutts, 1986). A defect in this interpretation is that east of the stagnation point some of the streamlines originate from the east where $Q(\psi)$ is determined by different dynamics than in the west; the assumption that $Q(\psi)$ has the same functional form there may not be good. However, since the range of Q is the same up- and downstream, perhaps a transition such as fig. 2-11 qualitatively takes place as the contours "fold" into their steady-state position after some time-dependent adjustment.

The analogue to a control is difficult to imagine for the stable subcritical flow (b) since it does not contain all of the Q values as the other states that exist for $\beta_T = 0$. Perhaps some other alternate state can be constructed using the original range of Q to fill in the regions not covered by the streamlines extending from upstream but there is no a priori way of determining how to do this within the steady-state long wave theory. A more serious defect is the lack of a varicose mode on the outer branches of the solution curve. The absence of this wave allows no passage of information downstream from the topography and thus no mechanism to establish a supercritical state downstream. Nevertheless, we presume for the sake of argument that some kind of transition from the subcritical flow (b) to a supercritical flow can take place which conserves $Q(\psi)$ on all streamlines that originate from upstream and that momentum is lost at the transition. The flow should exhibit upstream influence and adjust to a new flow that has the value of β_T at the turning point of whatever new solution curve that it lies upon.

The examination of the wave properties in the previous subsections indicate that

the existence of multiple states has more to do with the instability of the flow rather than hydraulics. This interpretation leads to a different prediction of transitions from one state to the other. The flow should maintain its original $Q(\psi)$ relationship on all streamlines that originate from upstream. For instance, if $\beta = 0.21$ and the upstream flow is stable (b), then a localized change in the effective β will cause stable waves to be excited in the lee. However, a transition to another parallel flow is not expected and no upstream influence should be present. If the flow is unstable, then the perturbations excited by the topography will grow. If the instability is localized so that the upstream conditions are unaffected by it, then the original $Q(\psi)$ must still be maintained on all streamlines that originate from upstream despite the instability. The localized instability will cause the zonal flow to equilibrate into a new form with the same $Q(\psi)$. This new shape is not necessarily one of the zonal flows depicted in figure 2-8, since the long-wave behavior is not assumed to dominate the instability process (as it is assumed to dominate a hydraulic transition). Of course, if the perturbation excites modes that are globally unstable then the upstream structure will change and the entire flow field will evolve into a new equilibrated state, or a turbulent flow.

2.9 Discussion

The previous work of Pratt (1989), Woods (1993), and Haynes *et al.* (1993) on hydraulic shear flows examined specific examples of alternate states with a given potential vorticity - streamfunction relation, but left unanswered the question of which $Q(\psi)$ relations may undergo hydraulic transitions. Here, by considering when the potential vorticity equation may have non-unique solutions, a necessary condition for alternate states was established namely that $\frac{dQ}{d\psi}$ is negative, and bounded from above by

$$\frac{dQ}{d\psi} < -\left(\frac{\pi}{2L}\right)^2. \tag{2.29}$$

This type of analysis may easily carry over to other fluid systems that undergo hydraulic transitions, the dynamics of which are governed by equations similar to (2.6). A list of such problems including gas flow from a nozzle, open channel hydraulics, stratified hydraulics and vortex breakdown in tubes has been compiled by Binnie (1949) and more recently by Benjamin (1984). The present idea of finding a condition for multiple solutions like condition (2.29) has not been exploited before, although recently Beran and Culick (1992) considered an example of non-uniqueness for the vortex breakdown problem and found a solution curve of symmetric solutions that is S-shaped and similar to (2-8). However, they did not find a condition for non-uniqueness, nor was the connection to hydraulics or instabilities made.

It is interesting to note that the violation of (2.29) is the same condition that Arnol'd (1966) found for nonlinear stability. In fact, the non-unique solutions for linear $Q(\psi)$ in a channel (§2.6) are a common example of Arnol'd's theorem (e.g. McIntyre and Shepherd (1987) §6 ex. 1). The onset of instability and the existence of multiple equilibria were shown to coincide for the barotropic instability problem considered here. This places the instability problem into a large set of nonlinear systems described by bifurcation theory. In fact, this has been suggested by Ukhovskii and Iudovich (1963) and Benjamin (1976,1978a) for the stability problem of a viscous fluid. Benjamin was not able to explicitly show the bifurcation for a specific example of the instability problem. However, he was able to find laboratory evidence for a bifurcation of equilibrium states similar to the branching diagrams shown here (e.g. figures 3 and 4 of Benjamin, 1978b). Based on a weakly nonlinear solution and numerical calculations, Helfrich and Pedlosky (1994) have recently found evidence for a bifurcation at the onset of baroclinic instability (their figure 14).

Because the instability problem considered is explainable by bifurcation theory, several interesting questions and conjectures are suggested. For instance, the solution surfaces found in catastrophe theory are universal, meaning that they can always be mapped to a few elementary forms whose shape depends on the number of free parameters (Thom, 1975). Although a specific example is considered here, $Q = -\sin\psi$, other flows with different $Q(\psi)$ should behave the same way as β and L are varied.

This also suggests that a sufficient condition for instability could perhaps be found, based on fixing the location of the flow on the universal solution surface.

As more parameters are added to the problem the complexity of the solution surface increases, yet Thom was able to show that when the number of parameters was increased to four there were only seven elementary catastrophes and all other solution surfaces can be mapped into these. Therefore, more complicated flows such as stratified flows should still fall within bifurcation theory, but bifurcations also take place along other axes in the parameter space, corresponding to the additional mechanisms for instability (i.e. baroclinic instabilities).

An accurate estimate of $\frac{dQ}{d\psi}$ is important for the present theory on multiple alternate states, and many other theories of nonlinear planetary flow. For example, Marshall and Marshall (1992) noted that poor model resolution could lead to inaccurate estimates of $\frac{dQ}{d\psi}$, and thus poor zonal penetration scales of jets. Weakly nonlinear theories such as Malguzzi and Malanotte-Rizzoli (1984) and Helfrich and Pedlosky (1993) rely on the even more delicate second derivative $\frac{d^2Q}{d\psi^2}$. These derivatives may be estimated from scatter plots of ψ vs. Q, although the relative paucity of oceanic compared to atmospheric data makes such estimates difficult. Despite these difficulties the present work is expected to apply to realistic atmospheric and oceanic flows because they are known to be unstable.

The examples in this chapter, constructed from artificial $Q(\psi)$ relations, bear a qualitative resemblance to blocking and jet splitting. However, the analogy with hydraulic systems is not complete because of dispersion, instability, and the absence of a varicose mode for the narrow eastward jet. These complications suggest considering the time-dependent evolution of the jets in §2.7.2 to consider whether transitions among alternate states take place and whether these are due to hydraulic behavior or the equilibration of localized instabilities.

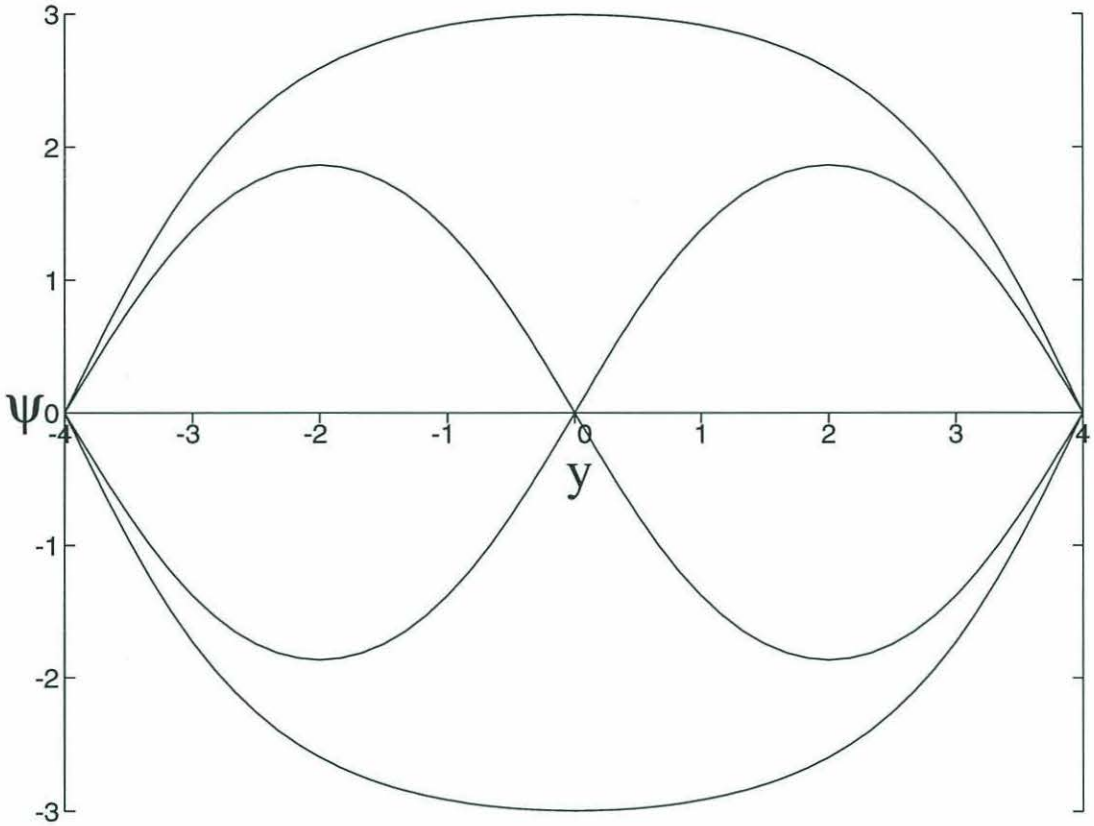

Figure 2-1: The four non-trivial solutions to (2.13) on the f-plane with zero transport. The half-width of the channel is $L = 4$.

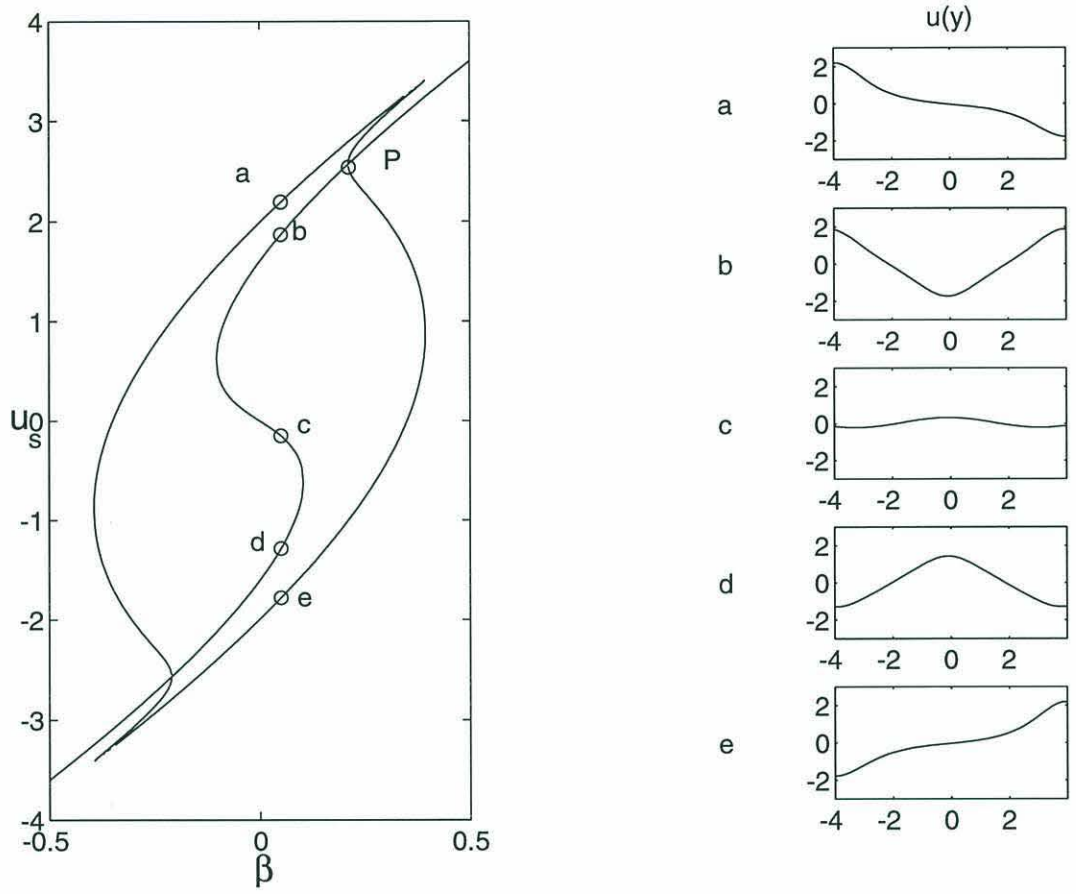

Figure 2-2: Solution curves showing u_S as a function of β for the zero transport flow. The S-shaped curve corresponds to symmetric velocity profiles (and antisymmetric streamfunctions). The solutions that correspond to points on the closed path are asymmetric. The velocity profiles $u(y)$ on the right correspond the points labeled on the curve.

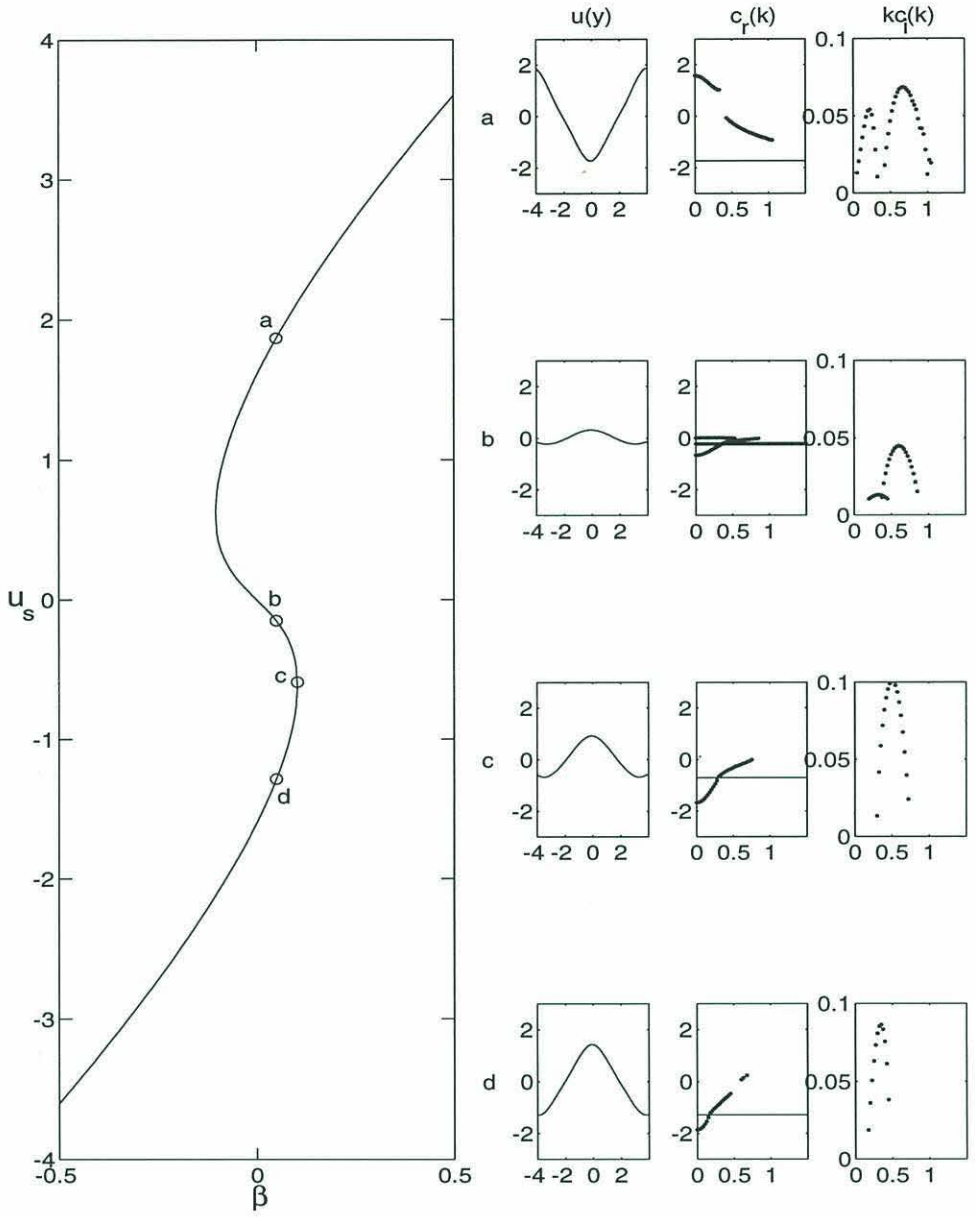

Figure 2-3: Dispersion diagrams for four symmetric velocity profiles labeled on the solution curve. The first column is the velocity profiles. The second column is the real part of the phase speed c_r as a function of the wavenumber k. The solid line denotes the velocity U_{min}. The third column is the growth rate as a function of k. $\beta = 0.05(a), 0.05(b), 0.103(c), 0.05(d)$. Solution b is the only profile indicated which supports bands of both sinuous and varicose modes. Solution c supports a long $(k \approx 0)$ stationary $(c \approx 0)$ which is varicose.

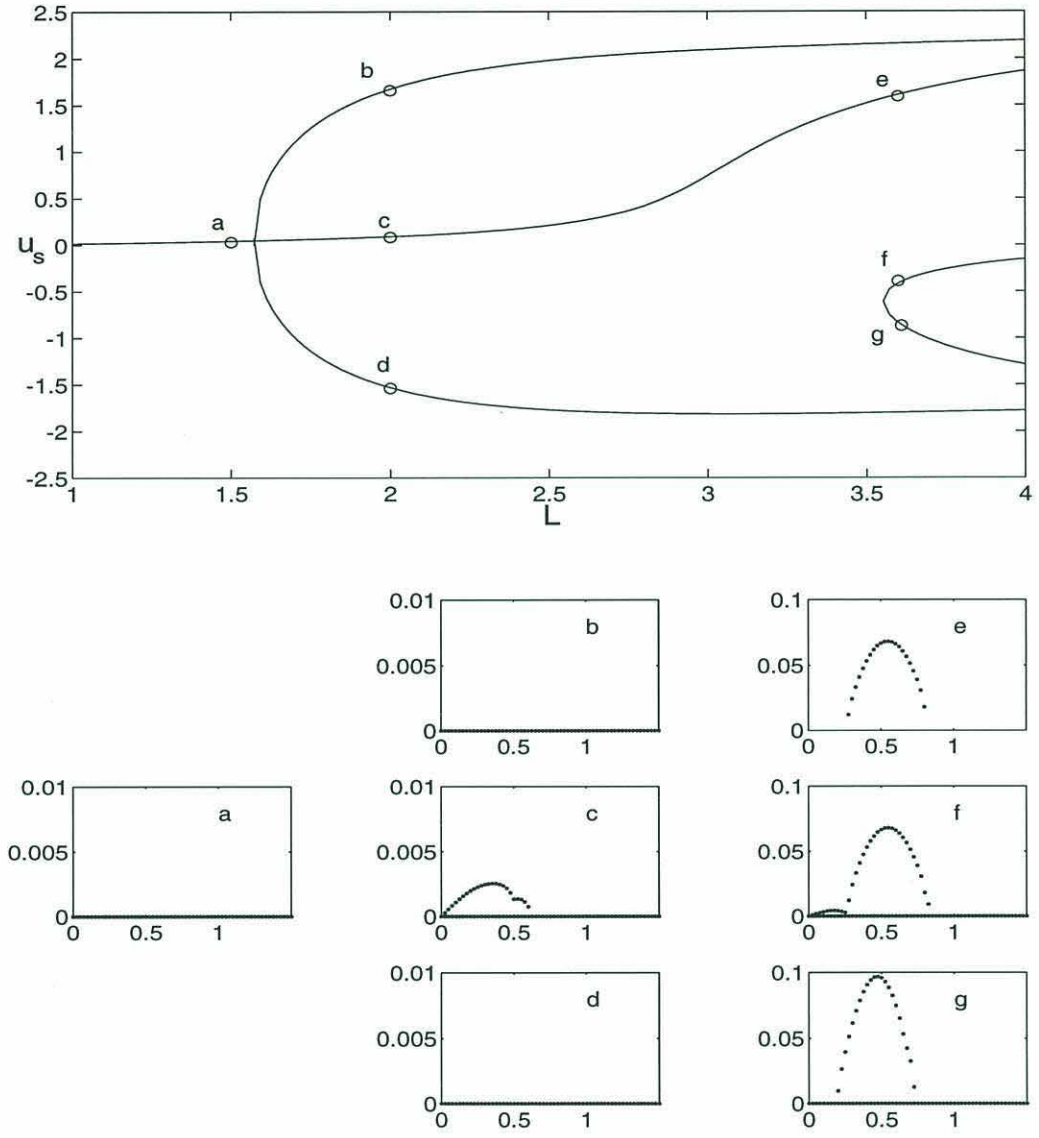

Figure 2-4: Solution curves u_s as a function of L for $\beta = 0.05$. The lower panels show the growth rate as a function of wavenumber k, for the velocity profiles on the solution curve above.

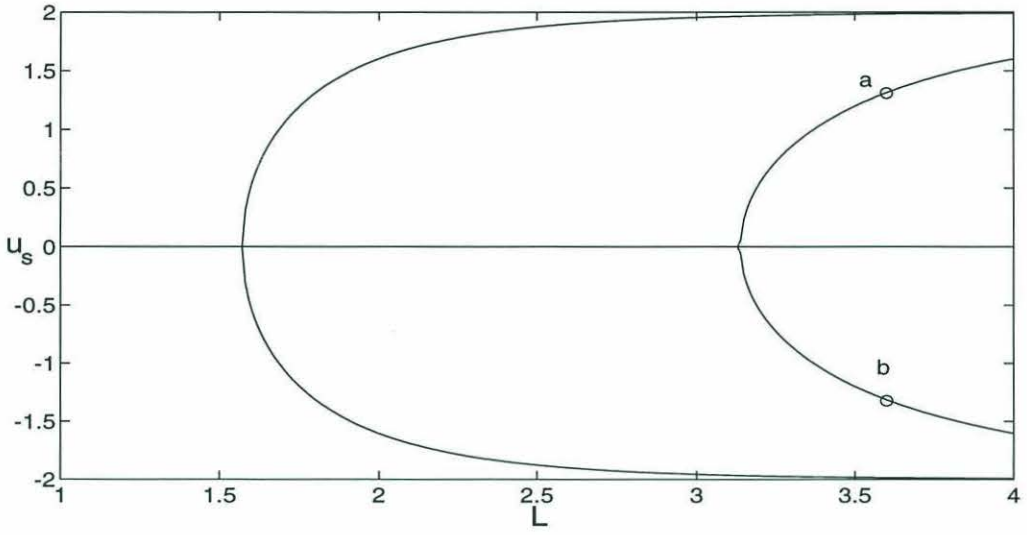

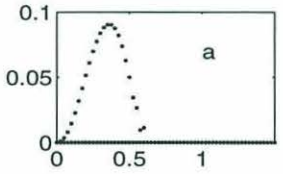

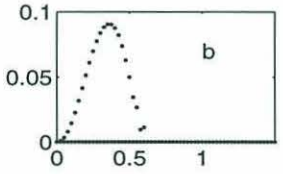

Figure 2-5: Solution curves u_s as a function of L for $\beta = 0.0$. The lower panels show the growth rate as a function of wavenumber k for the two velocity profiles indicated above.

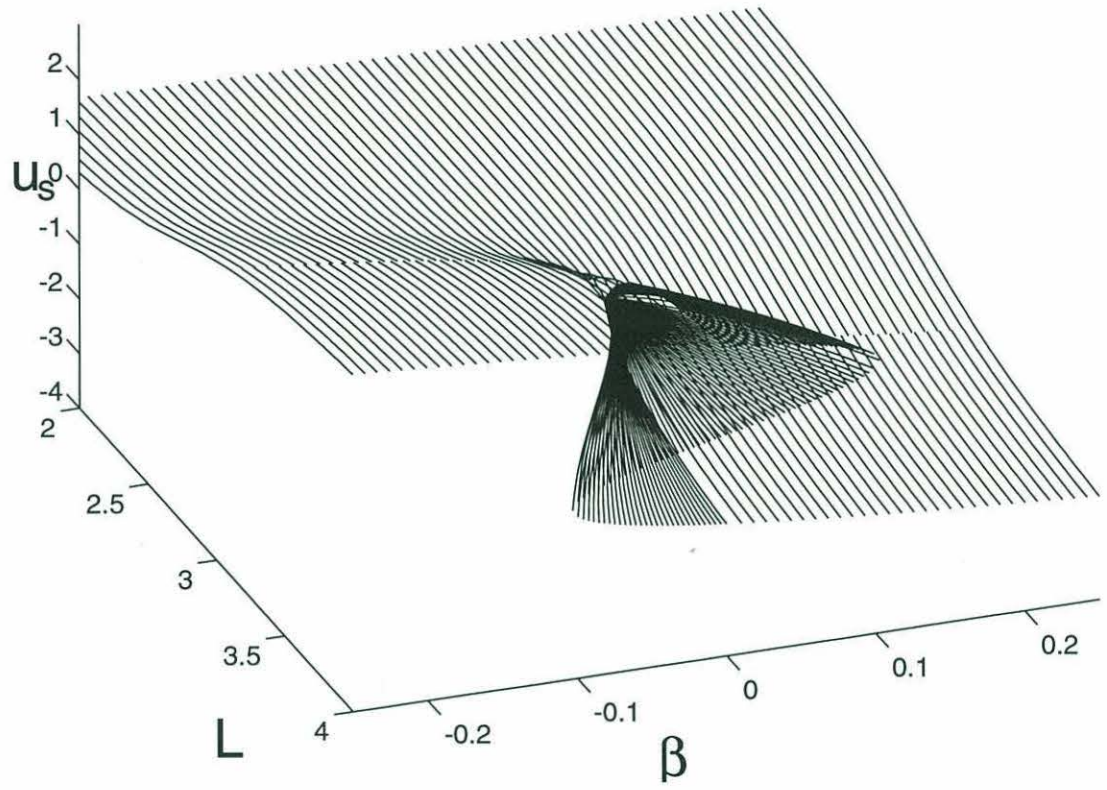

Figure 2-6: Solution surface $u_s(\beta, L)$ for the symmetric velocity profiles. The projection of the surface onto the parameter plane (β, L) forms a cusp, within which there are three solutions.

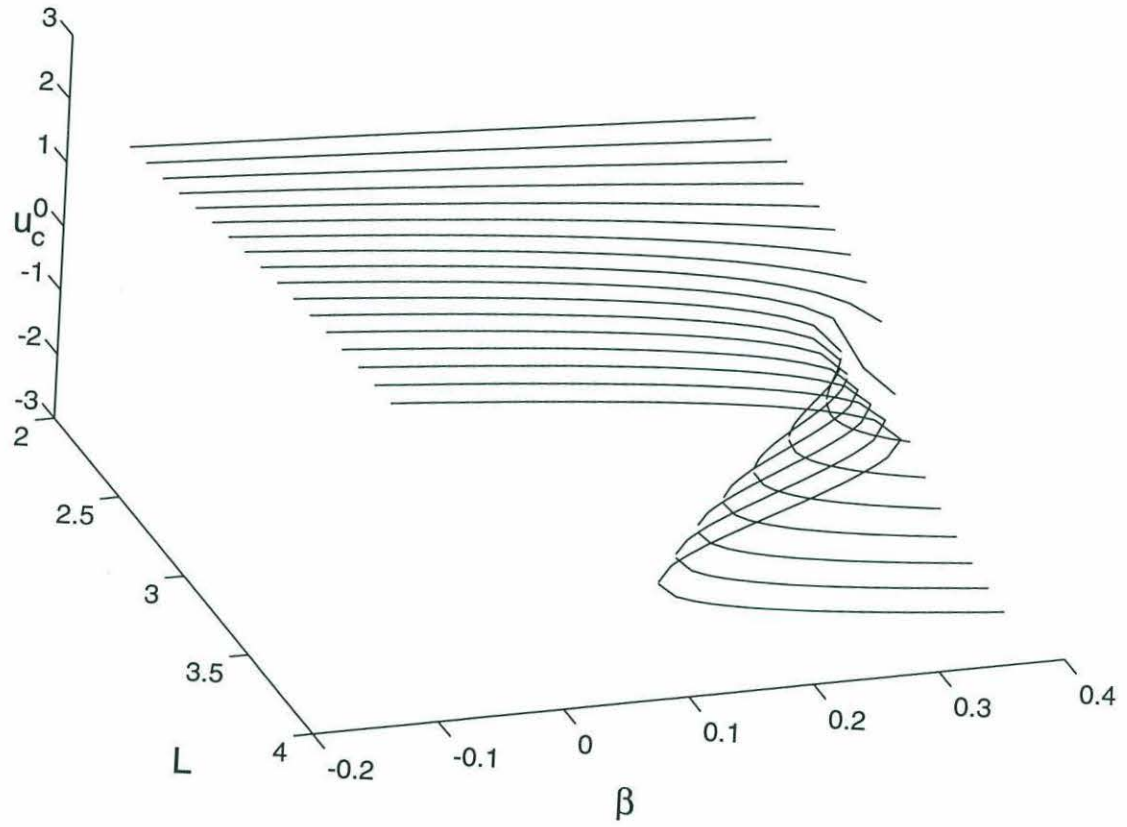

Figure 2-7: Solution surface $u_c(\beta, L)$ for the symmetric velocity profiles with eastward transport.

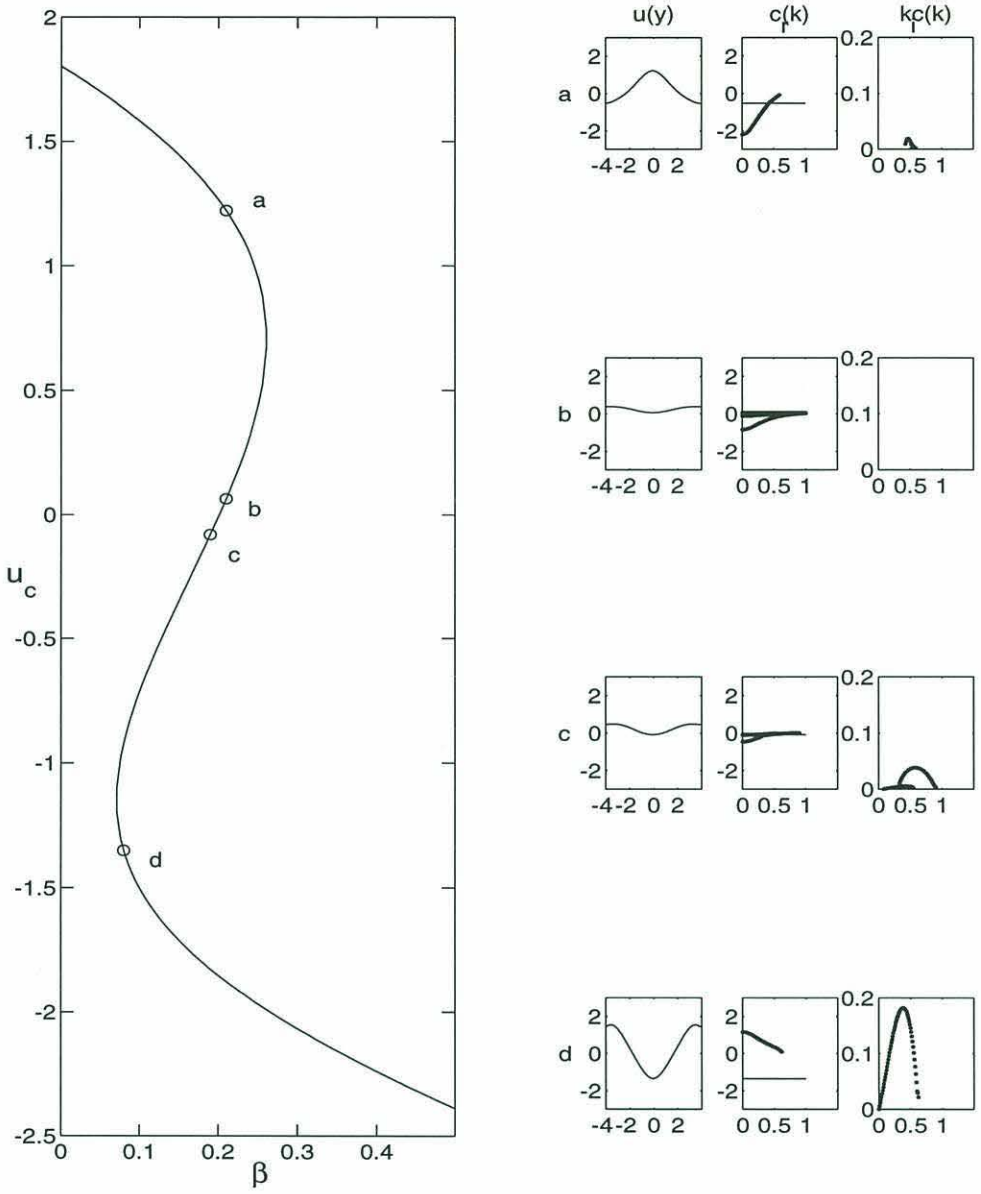

Figure 2-8: Solution curves showing $u(y=0)$ as a function of β for the symmetric velocity profile with $\psi_w = 1$. Also included are the dispersion diagrams for the four velocity profiles. $\beta = 0.21(a), 0.21(b), 0.19(c), 0.08(d)$.

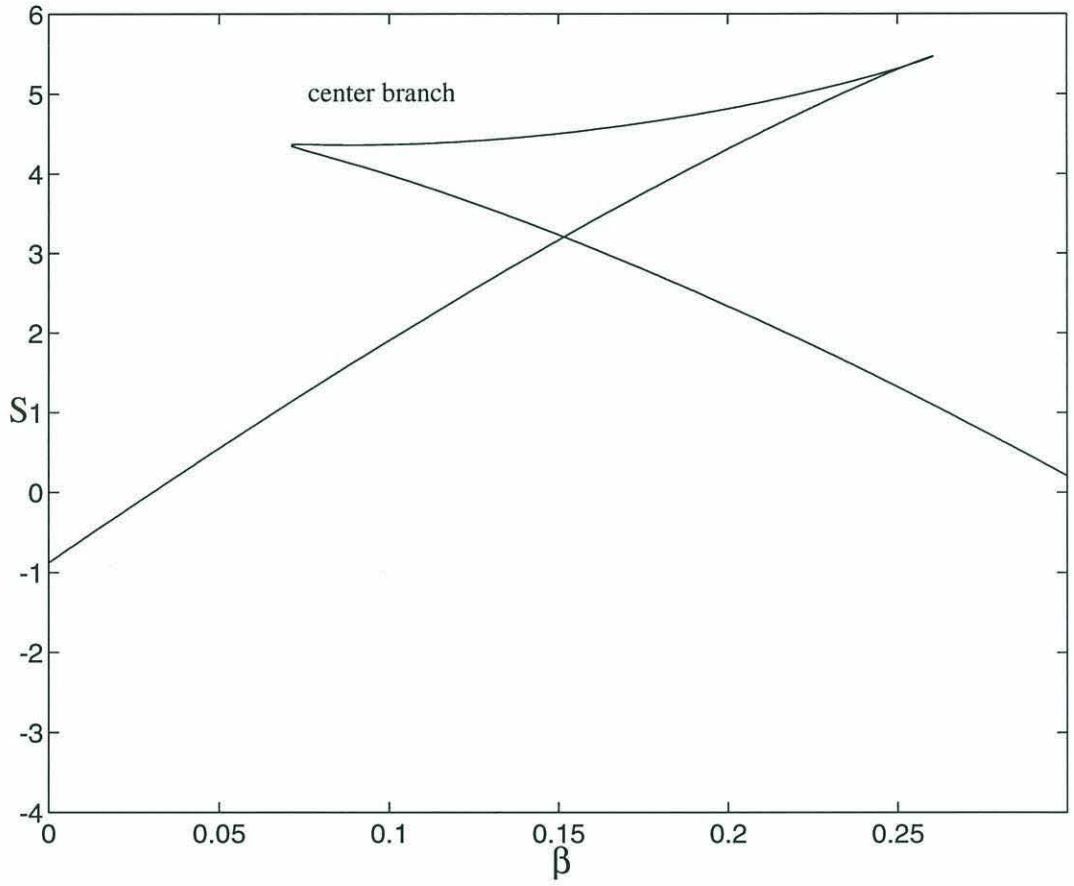

Figure 2-9: The momentum flux S (defined in §2.3) as a function of β for the three branches of the solution curve.

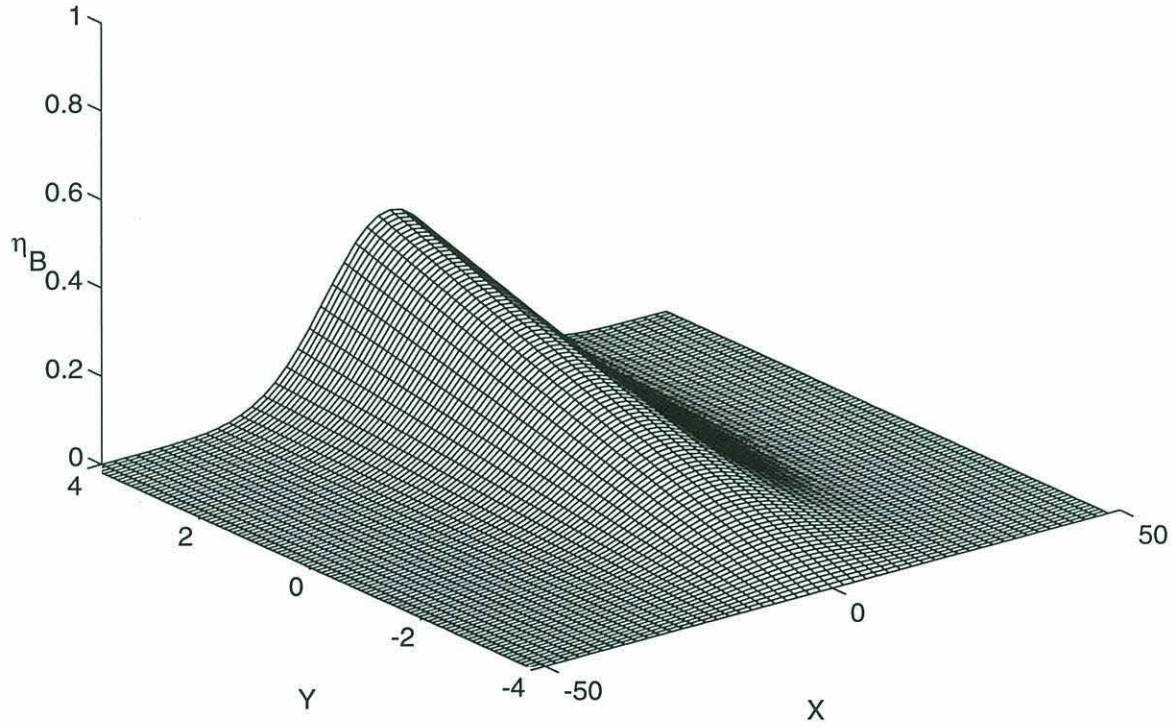

Figure 2-10: A schematic of topography with a slowly varying linear meridional slope.

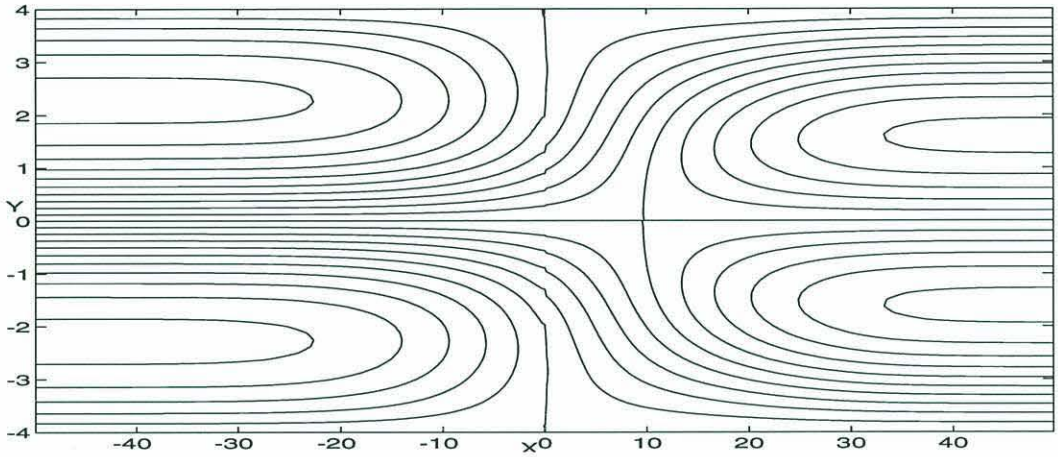

Figure 2-11: A contour plot of the streamfunction ψ for the hydraulic transition over a meridionally antisymmetric topography. The contour interval is 0.2.

Chapter 3

Time-dependent Alternate Flows

3.1 Introduction

Atmospheric blocking and the splitting of oceanic jets, such as the Gulf Stream are characterized by their unusual persistence in time and by the longitudinal extent of the double-jet system. Rex (1950) states that a block is characterized by a transition from a single jet to a double-jet system which must remain split over 45^o in longitude and must persist for at least ten days. The branching of the Gulf Stream is clearly persistent in time, and the split is permanent in space; the waters never re-merge to form a single current. While these features are persistent, observations also stress the importance of time-dependent forcing in the maintenance of the block. Green (1977) and Illari and Marshall (1983) established that a particular block was maintained by the convergence of vorticity fluxes that arise from transient eddies. Krauss *et al.* (1990) remarked that the branching of the Gulf Stream was marked by intense eddy activity, even though the current always bifurcates near $40^oN, 44^oW$. These observations suggest considering the effect of time-dependent forcing and whether, as a result of such forcing, transitions between zonally-uniform equilibrium states can take place.

The theories on equilibrium states also provide compelling reasons to consider the effects of time-dependence. Previous authors (Pratt, 1989 and Woods, 1993) have interpreted the existence of multiple flows with the same $Q(\psi)$ relationship as an

indication that the flow behaves as a hydraulic system if the multiple states can be connected by smoothly varying the ambient potential vorticity gradient. This suggests that hydraulic behavior may be possible in planetary scale flows. In particular, critical control could be established if Rossby waves can propagate upstream and if these waves are of sufficient amplitude to cause a permanent change in the upstream flow. Experiments in other hydraulic systems, such as those considered by Long (1954) or Pratt (1983), have demonstrated that a transition between two alternate states is established when a disturbance of sufficient amplitude is introduced. However, a careful consideration of the wave properties in chapter 2 indicates that the multiple solutions of the quasi-geostrophic potential vorticity equation are not clear examples of hydraulic systems, but rather they correspond to stable and unstable equilibria. If the equilibrium is unstable, then the disturbance may cause the flow to equilibrate to some new, stable equilibrium as the instability mechanism saturates, or the flow may break apart into a turbulent system if saturation does not occur. These two scenarios, hydraulics and instabilities, must be examined with a time-dependent numerical calculation to determine whether transitions between zonally uniform flows can take place, and whether they do so as the result of a stable, hydraulic adjustment or due to the equilibration of an unstable state.

Haynes et al. (1993) considered the establishment of hydraulically controlled flows in a single layer subject to the constraints of quasi-geostrophy. A zonally uniform flow in a channel was perturbed by the sudden introduction of a topographic shelf which varies in width along the channel. They chose the shelf to be a single height so that after the disturbance the potential vorticity is piecewise constant, with a value of η_B over the shelf, and zero where there is no topography. The two regions are separated by a front of potential vorticity upon which vorticity waves can travel. Of course, after this disturbance, the flow is no longer in steady state and the resulting adjustment exhibited hydraulic behavior including upstream influence and bores when the width of the shelf extended beyond a critical value determined by steady state theory. The purpose of this chapter is to test whether such hydraulic behavior is possible when the potential vorticity gradient of the zonal flow is not concentrated in a single front

but rather is smoothly distributed. In particular, by allowing the potential vorticity gradient to vary it may pass through zero, a condition which allows the flow to be unstable.

As in Haynes et al. (1993), the numerical experiments in this chapter have been designed to search for hydraulic behavior. We consider an adjustment problem similar in spirit to their work and the work of Long (1954) and Pratt (1983). Initially the flow is one of the symmetric, zonally-uniform flows with $Q = -\sin\psi$ on the β plane. The flow has a net eastward transport, and is described by the solution curve in §2.7.2, which is reproduced here (figure 3-1). At $t = 0$ an obstacle, localized in x, is introduced and the flow is forced to adjust. As in Haynes et al. (1993), the sudden introduction of the topography introduces potential vorticity into the flow causing Q to be disturbed from its equilibrium position along contours of $-\sin\psi$. In addition, the obstacle has a linear meridional slope, β_T, which locally alters the propagation characteristics of the vorticity waves by changing the ambient potential vorticity gradient from β to $\beta + \beta_T$. The variable topographic slope may cause hydraulic effects by bringing the speed of long waves to zero or it may alter the stability characteristics of the waves.

The adjustment calculations are carried out in a numerical model described in section 3.2. In the sections following this description, the four zonal flows labeled in figure 3-1 are considered. The initial conditions are perturbed by several topographies which alter the total ambient potential vorticity gradient as indicated by the figure. To examine the possible upstream influence, the momentum flux is measured up- and downstream of the topography. In addition, scatter plots of $Q(\psi)$ are monitored throughout the adjustment to steady state.

Transitions between alternate states are observed in the adjustment problems. If the flow is subcritical and stable, then hydraulic control is established when $\beta + \beta_T$ exceeds the critical value, β_c determined by the steady state theory. Downstream of the control an unstable narrow front of potential vorticity forms, which is analogous to supercritical hydraulic flow. Hydraulic behavior is not present when the initial flow is unstable to the varicose mode or when the varicose mode is not present. However,

transitions to other zonal flows still take place when the flow is locally unstable, or when disturbed by a large topographic feature.

3.2 Numerical Model

The initial value problems are solved numerically using a pseudo-spectral model of the quasi-geostrophic vorticity equation for a single layer on the β plane:

$$\frac{\partial}{\partial t}\nabla^2\psi \; + \; \beta\frac{\partial}{\partial x}\psi \; + \; J(\psi, \nabla^2\psi) \; + \; J(\psi, \eta_B) \; = \; \nu\nabla^6\psi. \tag{3.1}$$

The code typically uses 256×48 grid points with $\Delta x = 0.59$ and $\Delta y = 0.166$, so that the total zonal extent of the domain is 150 non-dimensional units, and the channel is 8 units wide. The time step was $\Delta t = 0.02$ and $\nu = 4.0e^{-7}$. The pseudo-spectral model can adequately resolve features with fewer gridpoints than a finite difference model. This feature makes the method a natural choice for this problem because the transitions between zonal flows may be abrupt. For instance, in Pratt (1983), the hydraulic jumps took place over only a few gridpoints and he used a Lax-Wendroff method to ensure that conservation laws held over shock regions. Transitions in the present numerical experiments will also take place over several gridpoints, and as the resolution was increased the transitions occur over smaller zonal distances.

If the disturbance is localized, the boundary conditions are independent of time so that

$$\psi = \pm\psi_w \quad \text{at} \quad y = \mp L.$$

By taking a constant velocity field ($u_b = -\frac{\psi_w}{L}$) out of the flow, the total streamfunction may be expressed as a sum of the background field and of sin ly terms

$$\psi \; = \; -u_b y \; + \; \sum_{l=\pi/2L}^{M\pi/2L} \left[\sum_{k=0}^{2\pi(N-1)/L_x} \left(A_{k,l} e^{ikx} \; + \; * \right) \right] \sin(ly).$$

where L_x is the zonal extent of the domain, M is the number of gridpoints in y and N

is the number of gridpoints in x. With this expansion the spectral form of equation (3.1) is

$$-(k^2+l^2)\frac{\partial A_{k,l}}{\partial t} \; + \; \left(ik\beta \; - \; iku_b(k^2+l^2) \; + \; \nu(k^2+l^2)^3\right) A_{k,l} \; + \; N_{k,l} \; = \; 0$$

where $N_{k,l}$ is simply the (k,l) Fourier component of the nonlinear terms that arise from the Jacobian terms in the original equation. The linear constant coefficient terms are integrated exactly to yield

$$\frac{\partial}{\partial t}\left(A_{k,l}e^{\sigma t}\right) \; + \; N_{k,l}e^{\sigma t} \; = \; 0 \tag{3.2}$$

where

$$\sigma = -i\left(\beta k/(k^2+l^2) - u_b k\right) - \nu\left(k^2+l^2\right)^2.$$

The Rossby wave dispersion relation and the exponential decay due to the friction are readily apparent. Exact integration is preferred because it allows the numerical stability limit to be increased (Canuto et al. 1987). Equation 3.2 is then integrated forward in time with a leapfrog scheme

$$A_{k,l}(t+\Delta t) \; = \; A_{k,l}(t-\Delta t)e^{-2\sigma\Delta t} \; + \; 2\Delta t N_{k,l}(t)e^{-\sigma\Delta t}.$$

The nonlinear term, $N_{k,l}$ is calculated by passing to real space, performing the multiplications and then passing back to Fourier space. The aliasing inherent in the pseudo-spectral transform is removed by a truncation technique which is described in Canuto et al. (1987). For both the x and y spectra of Fourier coefficients, $\tilde{M}$ (or $\tilde{N}$) components rather than M components are used, where $\tilde{M} \geq 3M/2$. The first M coefficients are identical to the original Fourier coefficients, and the rest of the coefficients, corresponding to high wavenumbers, are padded with zeros. This Fourier series is transformed into real space where it is multiplied by another, similarly treated, real function. The product is then transformed back to Fourier space, using all of the $\tilde{M}$ components. This spectrum is then truncated to the first M components. With this method, the aliasing has been removed, but any enstrophy

that has cascaded to wavenumbers beyond the highest wavenumber, (corresponding to M), is lost.

Because of dispersion, different length scales propagate up- and downstream and the physical problem is not periodic in x. To prevent "wrap-around" from one edge of the channel to the other, absorbing regions are used which gradually damp the amplitude of the solution over forty grid points. The amplitude of the damping is chosen by trial and error to minimize reflections off of the sponge into the domain of interest. Typically, the streamfunction in the absorbing region is multiplied by the factor $G = exp(-(0.005(40-i))^2)$, where i denotes the number of the gridpoint. This gives a value of unity for $i = 40$ at the interior boundary and a value of 0.96 for $i = 1$ at the edge of the computational domain.

The right hand side of 3.1 is a "friction" which is included to dissipate the enstrophy that has cascaded down to the spectral resolution of the model. Because it is a higher order friction, it should have little effect on the low-wavenumber dynamics of interest. However, a drawback of the biharmonic friction, as opposed to a Laplacian friction, is that it may actually intensify vorticity maxima that arise during the evolution. This problem is helped by increasing the spatial resolution of the model and it is monitored by keeping track of histograms of Q during the evolution. In the few places where this error has not been completely eliminated it appears that the enhanced maxima do not determine the overall dynamics of the flow.

The obstacle itself has a meridional slope that slowly varies from zero at the far ends of the channel to a maximum at the midpoint. This causes the ambient potential vorticity gradient to vary from its background value of β to $\beta + \beta_T$. The functional form of the topography is

$$\eta_B = \beta_T (y + L) exp\left(-(x/5\pi)^2\right).$$

The zonal extent of the topography is chosen to be quite long so that the change in ambient potential vorticity gradient is gradual.

3.3 Broad eastward flow

When $\beta = 0.21$ and the channel half-width is $L = 4$, there are three symmetric solutions to the potential vorticity equation with $Q = -sin\psi$. We first consider an initial condition, depicted in figure 3-2, which lies on the center branch of the solution curve. The flow is nearly uniform and stable and because the flow is completely eastward, upstream is well-defined as the west (left) of the channel. According to the dispersion relation (figure 3-2), this flow is subcritical with respect to both the sinuous and varicose modes because long waves can propagate upstream. The sinuous mode has a stationary wavelength of $2\pi/k \approx 7$, and the varicose mode's stationary wavelength is $2\pi/k \approx 11$. Both of these waves have a group velocity directed downstream and so they can both form lee waves. Since the stationary wavelengths are smaller than the scale of the topography, these lee waves are only very weakly excited.

Figure 3-3 depicts the evolution of the potential vorticity when $\beta_T = 0.03$, a value forty percent less than the critical gradient. In this example, the domain has been elongated to $L_x = 300$ to follow the disturbances further before they pass out of the computational domain. At $t = 100$, the initially zonal flow has deflected southward over the upstream face of the ridge, and northward over the downstream face. Subsequently, this pattern breaks into two isolated dipoles, one that propagates upstream and another traveling downstream. Because the dipoles are weakly nonlinear, they are difficult to see in the contours of potential vorticity. Therefore, at $t = 800$, contours of the streamfunction are superimposed on top of the potential vorticity field to highlight the dipoles. The upstream dipole is centered at approximately $X = -79$ and the downstream dipole is centered at $X = +68$. As these dipoles pass out of the computational domain, at $t = 1700$, the flow is left in a steady state that appears symmetric in X about the topography.

Measurements of the $Q(\psi)$ relationship and the momentum flux show that the flow is indeed symmetric, and no hydraulic control has been established. Scatter diagram of Q vs. ψ are shown in figure 3-4. At $t = 0$, Q is scattered about the functional form

established upstream. As the flow equilibrates, the potential vorticity collapses back onto a single curve which is the original upstream function $Q = -sin\psi$. At $t = 1700$ and $t = 2000$, there is a small range of points clustered near $Q = 0.5$, for which Q is nearly constant with ψ. These points lie right over the peak of the topography where the fluid has come from close to the wall. Despite these minor differences, the flow has generally maintained its original $Q(\psi)$ form as it passes over the topography even though the zonal velocity field has changed structure there.

Measurements of M, the flux of momentum defined in chapter 2, are made with time at points up- and downstream of the topography (figure 3-5). As the dipoles pass by the measurement points at $t = 300$, M increases and then returns to near its original value both up- and downstream. Both positions show a slight loss of the momentum flux and surprisingly the loss is slightly greater in the upstream flow. Still, the difference between the two values is less than one-half of one percent of the original momentum flux. Thus, there has been no upstream influence due to the topography and there is no topographic drag on the flow. The final steady state is subcritical everywhere in the flow because the topographic slope never exceeds the critical value.

The presence of the weakly nonlinear dipoles makes this an appropriate place to mention a few results from previous work on weakly nonlinear waves. This theory was originally developed by Malguzzi and Malanotte-Rizzoli (1984) and extended to include time-dependence by Helfrich and Pedlosky (1993). In the latter work, the authors consider the evolution of a solitary wave in a flow that is near the stability threshold. They find that the solitary wave itself is often unstable, even when the flow lies just on the stable side of this threshold. The time-dependence of solitary waves in flows that are well-within the stable regime are also discussed briefly in their Appendix and since the flow considered here is firmly stable, these results are of immediate interest. Their calculations are carried out for a two-layer fluid, but nothing in the asymptotic calculations depends on the baroclinicity of the flow, so their results may be simplified to the one layer case. They find that a weakly nonlinear wave in a stable flow obeys the classic KdV equation and the solitary wave moves, in a non-translating

frame, with a constant speed $c_0 + u$. The speed c_0 is the speed of the second cross-stream mode with infinite wavelength. Because the flow is stable, two of these modes are possible with different values of c_0. For the present flow, the dispersion diagram (3-2) shows that the infinitely long varicose modes have $c = +0.044$ and $c = -0.120$. Since the dipoles travel with speeds of

$$c_d \approx +0.075 \quad \text{and} \quad c_d \approx -0.09,$$

the speeds of each of the dipoles in the appropriately translating frames is $u \approx +0.03$. The theoretical value of u is difficult to calculate because it depends on the shear of the basic flow and the amplitude and meridional structure of the solitary wave and is given by equation A4 of HP. However, their discussion, based partly on work by Haines and Malanotte-Rizzoli (1991), shows that a small amplitude solitary wave in a stable, widening flow will have a positive value of u.

The adjustment over the topography is quite different when β_T exceeds the critical value of 0.05. Figure 3-6 shows the evolution of Q when $\beta_T = 0.06$, a value which is twenty percent above the critical slope. Because the initial perturbation due to the topography is so large, a large amplitude response is quickly seen in the flow. By $t = 100$, the $Q = 0.8$ contour is beginning to pinch together, near $X = 10$. Since a small amount of friction is present, this contour can form a closed loop, as can be seen at $t = 150$. As this potential vorticity contour and other, nearby contours "fold-up," they are forced northward to the channel wall, widening the flow on the upstream face of the topography (i.e. negative X). The arrow above the $t = 150$ panel denotes this "fold-up." This pushes the potential vorticity that was originally along the wall ($Q = -sin(-\psi_w) \approx 0.84$) downstream of the topography so that it must pull down from the wall. A small pocket of this fluid can be seen on the downstream face of the topography, near $X = 10$ in the $t = 150$ frame. A similar effect also begins to happen along the southern wall ($t = 425$). At later times, more fluid is forced along the walls because of changes upstream, causing the downstream region of constant Q to lengthen. The center contours of potential vorticity are squeezed together, forming a

front of potential vorticity, and consequently a strong eastward flow. Because of this effect, upstream and downstream influence occur simultaneously. The integration is halted as the front reaches the sponge region.

Clearly the adjustment bears a qualitative resemblance to a hydraulic control because of the broad sub-critical flow upstream and a swift, narrow flow downstream. To examine this resemblance more carefully, the flux of momentum was measured just upstream of the topography at $X = -8$, and downstream at $X = +20$ (figure 3-7). At $t \approx 300$, when the potential vorticity contours are squeezed together downstream, the downstream momentum flux drops, and then remains below the upstream value for the rest of the integration. Approximately ten percent of the momentum flux is lost due to topographic drag.

In classical free-surface hydraulics, the establishment of a hydraulic control causes a decrease in the transport. In the present application, the streamfunction along the walls must be fixed because the disturbance is localized in X, so a similar reduction in transport can not take place. Instead, when β_T exceeds the critical value for a given $Q(\psi)$ relation, the function $Q(\psi)$ itself must change as the system equilibrates to allow the flow to be on another curve representing steady solutions. Because of the meandering downstream flow and other changes in the upstream flow, a steady state has not been reached and $Q(\psi)$ at every longitude shows some scatter. Unfortunately then, it is not possible to say anything definitive about how the $Q(\psi)$ relationship has changed, or even if it has the same form up- and downstream of the transition. Instead of looking at the entire $Q(\psi)$ field as before, figure 3-8 shows a comparison of the original $Q(\psi)$ function and scatter plots of $Q(\psi)$ for two longitudes, one in the wide, upstream flow and the other in the narrow front. The potential vorticity distributions are similar at these two longitudes except for the constant Q regions that lie north and south of the front in the downstream flow. These regions arise from the fluid that was squeezed from along the walls to downstream of the transition where it spreads to fill the nearly homogeneous pools. This homogenization does not necessarily occur as a result of friction in the model, since the region is filled with fluid that originates near the boundary and always has nearly constant Q. The

scatter plots show that there is a plateau of constant Q located upstream as well, at $Q \approx 0.4$. Figure (3-6) shows that this pool of potential vorticity is homogenized; the small scale features in the Q field are lost by $t = 975$.

Because the propagation characteristics of long waves are so important in hydraulics, a dispersion relationship for the downstream flow is considered. A velocity profile taken from the jet is shown in figure 3-9 along with the phase speed and growth rates of the normal modes for this jet. The phase speed for the varicose wave is positive and so the zonal flow downstream of the topography is supercritical, albeit unstable in the range $k = 0$ to $k = 0.9$. The sinuous mode is stable and westward for wavenumbers less than 0.65. The fastest growing sinuous wave has a wavelength of 9 in the non-dimensional model units and the eastward jet in the model does have a strong meander pattern at this wavelength.

Because of the momentum loss across the transition and the change in the wave properties downstream of the transition, the final state is consistent with a hydraulic control. In the theory of hydraulics, this sub- to supercritical transition is primarily an inertial phenomenon where frictional effects are unimportant. To verify that the control seen in this numerical run is independent of the level of friction, a series of experiments were conducted in which the frictional coefficient takes on a range of values. In figure (3-10), the positions of the sub- to supercritical front and the super- to subcritical front are plotted as a function of the magnitude of ν. The position of the transitions are, to a first approximation, independent of friction until ν is an order of magnitude larger than that the value used in the reported numerical runs. At this large value of ν, the front does not even form, presumably because the large friction at high wavenumbers prevents the abrupt transitions from taking place. Reducing ν by an order of magnitude leads to no significant change in the positions of the fronts, although the potential vorticity field is much noiser at the resolution of the grid.

This transition did not arise from any kind of instability of the original stable, zonal flow because the local increase in the topographic gradient only made dQ/dy more positive. However, a decrease in the topographic gradient could cause the flow to be locally unstable and it is this case that will be considered next. If β_T is less than

-0.01, then the flow enters the unstable portion of this solution branch which causes a localized region of unstable flow. As an example, the evolution for $\beta_T = -0.03$ is shown in figure 3-11. Initially, the flow widens over the topography, and in particular the $Q = 0$ contour sharply deflects to the north. By $t = 200$, this contour has begun to "roll-up," forming an elongated eddy. A close-up of this region is shown in figure 3-12 at $t = 240$. Note that the pool of nearly homogeneous potential vorticity arises from the breaking of the highly convoluted $Q = -0.05$ contour that extends from upstream. To the south and east of this pool are sharp fronts of potential vorticity which have been swept around from the north. The western edge of the eddy is determined by a stagnation point at the maximum topographic gradient (located at $X = 0$) in the center of the channel where the $Q = -0.01$ contour extends to the northeast and southeast. In the interior of the eddy the flow is zonal with reversed flow. In an ideal model, with infinite resolution, all of the interior Q contours would smoothly connect to the upstream flow (although they would be highly convoluted). By this time, the instability has reached its maximum meridional amplitude. At later times (figure 3-11), the eddy elongates as more fluid is swept into the interior and the eastern front of potential vorticity advances with speed $c = 7.7$ in the non-dimensional units. The western edge of the eddy continues to be the stagnation point fixed at $X = 0$. Upstream of the topography the interior potential vorticity contours have narrowed, presumably as fluid is entrained into the recirculation zone. The integration is halted as the front of potential vorticity nears the downstream sponge region. The final state ($t = 480$) shows two distinct zonal flows on the up- and downstream faces of the topography. Upstream, the flow is similar to the original broad zonal flow. Downstream, the eastward flow is intensified along the northern wall, and the flow is westward in the interior. This zonal flow bears a qualitative resemblance to the "split" jet belonging to the lower branch of the solution curve (3-1).

A consideration of the $Q(\psi)$ scatter plots 3-13 at longitudes up- and downstream of the maximum topographic gradient as well as at $X = 0$, shows that the functional relationship between Q and ψ is maintained along all streamlines that pass over the topography, despite the $O(1)$ difference in the structure. Curiously, for positive values

of potential vorticity, the function $Q(\psi)$ has shifted slightly from its original, upstream form. This occurs as the interior fluid is swept northward and is then entrained into the recirculating region which displaces the fluid originally along the wall to the west. In fact, a "trough," marked by the arrows, is visibly moving upstream along the northern wall. This wave produces "upstream influence" which slightly changes the $Q(\psi)$ function. A wave is also present along the southern wall, which produces a similar effect, albeit much smaller since the topographic disturbance is much smaller along this wall. This scenario is consistent with critical control. Exceptional points, with differing $Q(\psi)$ functions, also lie in the the "roll-up" region of reversed flow and these points form a "loop" in the $Q(\psi)$ plane. The loop in the $Q(\psi)$ plane indicates that the flow in this region has not yet reached a steady state. Presumably a new $Q(\psi)$ relationship is being established in the recirculation as a result of the stirring of potential vorticity, and as the dissipation slowly acts on the flow. The close-up of the eddy (figure 3-12) shows that the tongue of potential vorticity has spread out near $X = 15$, $Y = 0$, presumably because of the viscosity.

Because the artificial viscosity appears to be playing some role in the equilibration of the flow, a discussion of the quantitative effects of the viscosity is warranted. The steady-state theory of chapter 2 considered alternate states in an inviscid, unforced system and ideally a numerical model that considered the transition between such flows would also be inviscid. In such an inviscid model, enstrophy would be conserved, even as it cascades to smaller scales. Unfortunately, this is impossible, because the finite resolution of a numerical model causes problems as enstrophy cascades to scales smaller than the scale of the grid. However, with a de-aliasing procedure, and adequate spatial resolution, enstrophy is very nearly conserved (Orszag, 1971).

In the present model, a small biharmonic friction was included in the model in order to keep the potential vorticity field smooth at the scale of the grid. How does the inclusion of viscosity alter the conservation of total enstrophy? In many of the model runs of this chapter, this question can not be addressed, because the sponge regions, which are necessary to prevent wrap-around, will destroy enstrophy. In the present example, the signal does not reach the wrap-around position, and so the sponges can

be removed, allowing conservation of enstrophy to be considered. Even with the small viscosity included, the fractional change in the total enstrophy is $O(10^{-3})$ during the course of the model run. This indicates that the dynamics are conservative, and the artificial viscosity only serves to smooth out the field.

Since the conservation of total enstrophy is a global measure, a more useful measure of the viscosity might be to consider how well potential vorticity is conserved following a parcel as it moves through the evolving Eulerian field. Unfortunately, this Lagrangian calculation is fraught with difficulties, due to the loss of information caused by the inevitable truncation of the Eulerian field at the resolution of the numerical model (Haidvogel, 1982). Despite these difficulties, Lozier and Riser (1989) have considered Lagrangian trajectories in an Eulerian model. However, the potential vorticity along such a trajectory varied by as much as 20%. Such variations do not necessarily invalidate their Lagrangian information. Since the potential vorticity field can contain small scales, a small error in the location of a parcel may lead to large errors in the measurement of its potential vorticity. However, these errors do present a problem when conservation of potential vorticity is the issue, as it is here. For instance, Hua (1994) advocates the use of Lagrangian potential vorticity conservation as an independent method for checking the consistency of a numerical model. By comparing model runs with different horizontal and vertical resolution, he concludes that adequate resolution is achieved when the error in the potential vorticity is approximately 25%. These variations in potential vorticity reported by Lozier and Riser (1989) and Hua (1994) show the difficulty in using Lagrangian information to measure conservation of potential vorticity.

However, since I am interested in determining the effect of the artificial viscosity term on the dynamics, I will compare potential vorticity conservation for the model run presented earlier (fig. 3-11 with a new run with no artificial viscosity present. This run also conserves total enstrophy; the fractional change is $O(10^{-3})$, similar to the run with viscosity. The potential vorticity field for this run is shown in figure 3-14. The filaments of potential vorticity are more connected in the "roll-up" region, and the tongue of potential vorticity is less diffuse. However, the most obvious difference

between the two fields, is the ragged structure at the scale of the grid when the viscosity is not present to smooth out the field.

The parcel trajectories are determined by the kinematic equations

$$\frac{d\vec{x}_i}{dt} = \vec{u}_i(\vec{x}_i, t), \tag{3.3}$$

where $\vec{u}_i(\vec{x}_i, t)$ is the velocity field at the position of the i^{th} parcel. Equation (3.3) is solved with a 4^{th} order Runge-Kutta scheme, where the values of $\vec{u}_i$ are calculated by summing up their Fourier series. This method is much slower than interpolating the velocity field from its grid point values, but it is a more accurate method. Using this procedure, individual parcels are followed as the Eulerian velocity field evolves. Figure 3-15 shows the "spaghetti diagram" from 24 parcels which began at two lines across the channel, at $X = -50$ and $X = 0$. These parcels are for the case with artificial viscosity, and show little qualitative difference from the case with no viscosity. The parcels clearly separate as the "roll-up" develops, and some parcels are caught in this interior recirculation.

Figure 3-16 compares potential vorticity conservation for the two runs for the parcels which began at $X = 0$, and it is clear that potential vorticity is better conserved when the small viscosity is present to keep the potential vorticity filaments smooth and connected. The maximum loss of potential vorticity for this case is 29%, while in the absence of viscosity the parcels completely lose track of their original values of potential vorticity.

Given that total enstrophy is conserved and that potential vorticity is better conserved in the presence of the small viscosity, I conclude that the artificial viscosity is serving its purpose in keeping the potential vorticity field smooth at the scale of the grid. The equilibration of the flow appears to be due to the adjustment from the time-dependent terms, and not the dissipation.

3.4 Split flow

The development of a hydraulic control in the stable, subcritical flow is interesting. but how robust is the control if the initial flow is unstable? After all, much of the center branch of the solution curve is unstable. Do these flows produce hydraulic control? To examine this question, a slightly split flow with $\beta = 0.19$ and shown in figure 3-17 was chosen for the initial condition. The long, varicose waves are marginally unstable and the sinuous waves are unstable at moderate wavelengths. Because the flow has a westward center, some of the streamlines originate from $X = +\infty$ and upstream is no longer well defined. However, the initial value problem is still well-posed, and figure 3-18 shows the evolution when $\beta_T = 0.03$, less than half of the value needed to reach the critical point on figure 3-1. Note that the zonal length of the domain is twice that of the previous runs, but Δx, and therefore Δt and ν remain the same. This unstable flow adjusts quite differently than the similar stable adjustment depicted in 3-3, although the localized topographic perturbation is identical. Instead, the northern potential vorticity contours are pushed northward to the wall, and then roll up into a reversed zonal flow near the center ($X = 0$) of the topography ($t = 225$). Until this point, the adjustment looks very similar to the locally unstable example in figure 3-11. However in the present example, the background initial flow is more unstable than the localized region over the topography. Thus, the disturbance excites unstable, periodic waves. The final state, halted as the signal reached the eastern sponge layer, shows that the initial disturbance has excited a sinuous wave, with a wavenumber of $k \approx 0.45$, which is near the fastest growing sinuous wave of the initial flow. Experiments with larger values of β_T show similar evolution patterns, and hydraulic control is not established. Because the entire region off of the topography is more unstable then the region of the initial disturbance, the plane wave instability is excited and then dominates the evolution. The instantaneous field at $t = 350$ shows a difference between east and west of the maximum topographic slope. This difference is due to the different dispersion characteristics of the waves. During the initial adjustment, long waves propagate westward and short waves propagate to the

east. However, since a periodic instability is being excited, off of the topography the final state will be a global instability with a wavelength determined by the global dynamics. The periodic instability is suppressed in the present model by the absorbing boundary conditions.

By reversing the topographic slope, the most unstable region is then localized at the topographic perturbation. The adjustment (figure 3-19) then follows the now-familiar pattern of "roll-up" at the topography, which strengthens the westward center. An intense meridional jet forms at the eastern edge of the "roll-up" connecting the new zonal flow to the original system. The western edge of this interior recirculation is determined by a stagnation point, fixed at $X = 0$. The southern potential vorticity contours pass between the southern wall and the recirculation. This flow is subject to a short-wavelength instability that causes the southern jet to meander with a zonal wavelength of 6 non-dimensional units.

3.5 Swift eastward flow

We next consider the $\beta = 0.21$ flow with a strong eastward center and westward return flow along the channel wall (figure 3-20). This zonal jet lies along the outer branch of the solution curve described in chapter 2 and accordingly does not have any kind of varicose mode, stable or unstable. However, the flow does have two critical latitudes where dQ/dy vanishes; they are located at $Y = \pm 2.25$, the latitudes at which the zonal velocity vanishes. There is a band of unstable, sinuous waves for which the dispersion diagrams are shown in figure 3-20. The shortest marginally unstable wave, with $k \approx 0.65$, has the quantity $U - c$ vanishing at the critical latitude and so $c = 0$ at the short wave cutoff. The latitudes at which $U - c_r$ vanishes for the other unstable waves lies between the critical latitude and the wall; thus, their phase speeds are always westward. The longest marginally unstable wave, with $k \approx 0.45$ has c equal to the velocity at the wall; all longer waves are stable, westward-propagating waves. The fastest growing wave has a non-dimensional wavelength of $2\pi/0.47 \approx 13.3$ and an exponential growth rate of 0.019.

The adjustment that occurs when $\beta_T = 0.03$ is depicted in figure 3-21 which shows the potential vorticity contours at various times of the evolution. At $t = 0$, the introduction of the topography causes the formerly steady Q contours to shift from their initial zonal configuration. An anomalous, closed patch of potential vorticity is introduced by the topography in the interior of the domain. This patch of high potential vorticity is advected towards the west along the channel wall and towards the east by the core of the jet. By $t = 210$, the northern patch of potential vorticity is stretched so thin that it breaks and an equilibrium state is eventually reached. The anomalous potential vorticity is advected out of the domain, and the steady state Q contours have widened slightly over the topography to compensate for the increased ambient potential vorticity gradient.

Scatter plots of potential vorticity versus streamfunction (figure 3-22) show that the adjustment causes the points to collapse along a single line. The final plot also includes a line of the $Q(\psi)$ function for the original upstream flow. Clearly the points for the equilibrium state are indistinguishable from the $Q = -\sin\psi$ line. When the topographic slope lies below the critical value, the flow equilibrates to have the same functional relationship between the two fields as the upstream flow has.

Although $Q(\psi)$ is the same everywhere in the flow, the flow field is not quite symmetric in x, due to the presence of a large amplitude sinuous wave which arises from the instability of the flow. Initially, this mode is not excited by the topography, and so no instability is present. As the signal reaches the sponge region a small reflection takes place and an unstable sinuous wave with a wavelength of $L \approx 13$, i.e. near the fastest growing wave, is excited. Although this wave is artificial, since it is due to the sponge, the model run is continued because sinuous modes are a dominant feature of geophysical jets. This wave grows and potential vorticity is cast out to the north and south of the eastward jet. It appears that this instability does not destroy the overall structure of the eastward jet, so that potential vorticity contours are unbroken from upstream; however, the equilibration of this unstable wave is not really adequately resolved in this model. The initial zonal jet was also perturbed by a periodic, unstable, sinuous wave with a finer resolution model and the instability

still did not disrupt the eastward jet because the critical latitudes for the unstable flow lie outside of the core of that jet.

The adjustment of the potential vorticity contours when $\beta_T = 0.06$ is shown in figure 3-23. When β_T exceeds the critical value of $\beta_T = 0.05$ by only this small amount, the adjustment that takes place is very similar to the previous run. As before, the initial maximum of potential vorticity is stretched out by advection, and the contours widen over the topography to compensate for the topographic stretching. In addition, the $Q(\psi)$ relationship is maintained on all streamlines that originate from upstream (figure 3-24). However, because β_T exceeds the critical value for this potential vorticity function, the functional relationship can not be maintained at the crest of the ridge. Instead, a small, closed region of the anomalous potential vorticity is trapped over the topography at the northern channel wall. This patch of potential vorticity accounts for the points of potential vorticity that abruptly rise from the $Q = -sin\psi$ curve in the final scatter plots.

Because ψ varies slowly in this region, the zonal flow is nearly zero there. Figure 3-25 shows the velocity field right at the crest of the ridge ($X = 0$), and at points east and west of the ridge. The velocity fields are nearly identical away from the ridge, with a strong eastward core and westward flow along the walls. At the ridge crest, the flow has clearly slowed down due to blocking of some streamlines by the topography. The dispersion relationship for the velocity field at $X = 0$ and $\beta = 0.21 + 0.06$ shows that only a sinuous mode is present for this flow (figure 3-25) and thus no transition to a state that is subcritical with a varicose mode has been made. Unlike open channel flow, no hydraulic jump forms in the narrow, swift current as the topographic gradient is raised beyond the critical value. However, a hydraulic jump is the result of the convergence of energy that arises when the upstream flow has waves propagating downstream and the downstream flow allows upstream propagation. In this case, the upstream flow does not allow a varicose wave of any kind and so the hydraulic jump is not necessary. Instead, a local response is felt both upstream and downstream of the topography. This is consistent with a feature of this dispersive flow mentioned in Chapter 2. While subcritical flows may have stationary waves of finite wavelength,

their alternates only have $c = 0$ when k is imaginary; thus, the response of the flow to a perturbation is exponentially decaying and nothing resembling a hydraulic jump takes place.

The cusp-shaped solution curve, discussed in chapter 2, suggested that if the original solution lay on the outer branch and β_T was varied so that this branch no longer existed, then the solution would jump to the other outer branch. However, in catastrophe theory, for which this jumping behavior occurs, the center branch is always unstable, and it is the instability at the cusp which causes the flow to equilibrate to the new, stable state. In this case, the center branch is stable just on the other side of the cusp, and so no such jump takes place (as seen in the previous run). The topographic gradient must be raised all the way to $\beta_T = 0.09$, nearly twice the value of the critical gradient, before this kind of response is seen (3-26). With the large topography, the flow widens over the topography enough so that by $t = 360$ the inner $Q = \pm 0.84$ contours reach the wall and block all but the inner fluid (with $-0.84 < Q < 0.84$) from passing over the topography. This reduced range of Q abruptly widens and fills the width of the domain for a small region in X that is connected to the original flow by intense meridional jets. The fluid is squeezed into a narrow, northern jet that passes between the northern channel wall and the recirculation, and a broader, southern flow between the southern wall and the recirculation. As in the previous two runs, some waves reach the eastern sponge region and an unstable sinuous mode is excited; by $t = 640$, the potential vorticity to the north of the eastern zonal jet has been cast off. However, this process plays little role in the evolution of the split flow since the instability does not break up any of the contours that pass through the localized region to the west of this zonal flow. At later times, the localized region widens as the downstream meridional front expands eastward, as more of the fluid from the upstream jet is entrained in the recirculation. The western front slowly propagates westward until it reaches the longitude at which β_T is equal to the critical value $\beta_c - \beta = 0.05$. At this point, the growth of the region halts and the flow has achieved a new steady state. The integration has been carried out to $t = 4000$, with no significant change in the final structure. The split flow does

not expand to fill the eastern portion of the channel, but halts when the western front reaches its equilibrium position which prevents more fluid from being entrained. Throughout the slow growth of the localized flow, the $Q(\psi)$ relationship maintains its original functional form (3-27), with the exception of some of the interior points which belong to filaments of the initial potential vorticity disturbance. This trapped anomaly is initially consistent with a modon-like solution, which has $dQ/d\psi$ more negative in the interior of the closed contours. However, with time, friction tends to destroy the potential vorticity gradient, and the slope in the $Q - \psi$ plane of the interior points is nearly constant.

When β_T exceeds the critical value, the behavior of this narrow, eastward jet is quite different than the two predictions in chapter 2. If this jet behaved as a supercritical, hydraulic flow, then presumably a westward-propagating dissipative jump would form at the topography. As the jump passes out of the domain of interest, the final state would resemble figure 3-6: a subcritical flow passing to supercritical flow in the lee of the topography. However, this jet does not ever form a dissipative, propagating front with subcritical flow in the lee. On the other hand, if the system behaved as a typical catastrophic system, then the flow would undergo an abrupt transition when β_T reached its critical value, passing to the only solution possible, the westward flow lying on the other outer branch of the solution curve. However, in a typical catastrophic system, the critical value of β_T occurs when a stable equilibrium and unstable equilibrium merge. It is the passage to an unstable state that causes the system to amplify the disturbance until a new, stable equilibrium is reached. In the present example, the merger at $\beta_T = 0.05$ occurs between two stable states and so there is no mechanism to cause an $O(1)$ change in the flow. Only when $\beta_T = 0.09$, nearly twice as large as the critical value, is the disturbance introduced by the topography large enough to cause the flow to pass to the new zonal flow.

3.6 Swift westward flow

It is natural to consider an initial flow lying on the other outer solution branch, since it merges with an unstable equilibrium at the critical value of $\beta + \beta_T = 0.07$. The velocity profile with $\beta = 0.08$, shown in figure 3-28, was considered to test this idea. The flow still has a net non-dimensional transport of $T = +2$, but the eastward flow is split into two jets along the walls, with a westward flow in the center. The entire zonal flow-field is unstable to the sinuous mode in the range $k = 0$ to $k = 0.5$. The fastest growing wave has an e-folding time scale of 5.5 and a wavelength of $L = 16.5$, which is very close to the topographic length scale of 5π. The evolution for $\beta_T = -0.001$, which is *ninety* percent below the critical value, shows that the initial jets rapidly break down (figure 3-29). By $t = 50$, a meandering motion is set up over the topography and the trough-to-trough distance for this meander is precisely the wavelength of the most unstable mode. Very quickly, this motion amplifies and expands east and west of the topography. By $t = 80$, the potential vorticity in the two eastward jets has rolled up into closed eddies trapped between the westward flow and the channel walls. Unfortunately, because the sinuous mode is unstable to very long wavelengths, it is not practical to use a longer topography to avoid this unstable sinuous mode. No further tests with larger topographic gradients are warranted since the meandering motion will always dominate the evolution.

3.7 Discussion

The purpose of this chapter was to examine the establishment of, and the transitions between alternate zonal flows. In this case, potential vorticity was added into the flow by the introduction of a topographic feature. This disturbs the potential vorticity from its equilibrium position along the $Q = -\sin\psi$ contours. In addition, the meridional slope of the topography varies slowly in the zonal direction, allowing a slow change in the dispersion characteristics of vorticity waves which depend on dQ/dy.

For stable, subcritical flow it has been shown that the adjustment proceeds in

a similar way to the hydraulic adjustment experiments of Long (1954) and Pratt (1983). A transition to a supercritical eastward jet takes place over the topography when $\beta + \beta_T$ exceeds the critical value determined by the steady state theory. In this case the vorticity waves, and specifically the second cross-channel mode, play the role of gravity waves in the open channel hydraulic adjustment. However, in the quasi-geostrophic example presented here, the waves do not carry any mass, so the transition is effected by shifting potential vorticity into a new equilibrium state. This type of transition could possibly have applications in the question of frontogenesis. If, through some local change in the ambient potential vorticity, the initially subcritical flow was rendered critical, the potential vorticity contours could collapse, forming a strong front.

If the initial flow was unstable, or made unstable in a localized region by the topography, then the instability dominates the evolution. When the flow field outside of the topography is more unstable than the localized region, plane waves are excited and destroy any local signal of the initial perturbation. On the other hand, if the instability is localized by the topography, because the initial flow is stable or just less unstable then the local region, then the instability grows only over the topography, and spreads eastward. These results are consistent with the work on local instability by Pierrehumbert (1984) and Samelson and Pedlosky (1990) who find that the instability reaches a maximum amplitude downstream of where the maximum growth rate is located. In the present example, using the fully nonlinear quasi-geostrophic equations, the flow evolves into a split jet on the downstream face of the topography. Because of the westward interior, this final state bears a qualitative resemblance to the solutions along the lower branch of figure 3-1, and it is tempting to think of this transition between two alternate zonal flows (with the same $Q(\psi)$) as a catastrophic jump from the unstable equilibrium branch to a stable branch.

When the initial flow was a strong eastward jet with no varicose mode, then hydraulic transitions are not possible. Anomalous potential vorticity is trapped over the topography when β_T exceeds the critical value, yet the flow up- and downstream is virtually symmetric. Nothing resembling a hydraulic jump forms, precisely because

there is no varicose mode to cause energy to converge in the fluid. Only when β_T is nearly double the critical value does an abrupt transition take place. As a result of the large disturbance, the flow reaches a new zonal equilibrium with the same $Q(\psi)$ relationship everywhere in the flow. Although the transition did not take place when β_T was at its critical value, these runs are still consistent with the notion of a catastrophic jump. In the present case, as β is increased, the flow does pass along the solution branch until it merges with another equilibrium state. However, because this equilibrium is also stable, there is no mechanism to amplify small disturbances and cause the flow to move to a new equilibrium. It is only when the disturbance itself is quite large that a new state is achieved. The final state in these calculations bears a strong resemblance to the recent, localized instability calculations of Helfrich and Pedlosky (1994), which were also fully nonlinear. In their case, the flow was close to the instability threshold, and the disturbance caused the flow to be locally unstable, so the "jump" to a new zonal flow was brought about by an instability of the flow.

It appears that the "hydraulic" behavior and the localized instabilities are both manifestations of the existence of multiple equilibria in quasi-geostrophic systems on the β-plane. Both types of behavior are present for initial flows that lie on the center branch of the solution curve (figure 3-1). In all of the transitions from the center branch, the $Q(\psi)$ relationship is maintained across the transition, but has shifted from its original upstream form as vorticity waves propagate away from the initial disturbance. An outstanding problem is a satisfactory determination of how these waves alter $Q(\psi)$ and what that new functional relationship is. Pierrehumbert and Malguzzi (1984) show that within closed streamlines $Q(\psi)$ is established by a balance between weak dissipation and forcing, perhaps from eddy vorticity fluxes. In the present case, no forcing is present, and ultimately the dissipation must destroy the potential vorticity gradients. Long before this occurs, the dissipation serves to mix the fluid *along* streamlines, establishing a nearly steady state which then homogenizes (Rhines and Young, 1983). Is shear-enhanced dispersion the mechanism that ultimately equilibrates the adjustment calculations presented here or can the time-dependence alone establish the equilibrated state? Related work by several previous authors indicate

that the time-dependence alone caused the potential vorticity field to adjust to a new equilibrium in their experiments. The above-mentioned experiments conducted by Helfrich and Pedlosky (1994) were carried out with a psuedo-spectral model containing no explicit dissipation. In addition, the hydraulics problem of Haynes *et al.* (1993) were done with a contour dynamics model, for which potential vorticity is conserved. In the present study, the effect of the dissipation was estimated to be small based on measurements of the enstrophy and conservation of potential vorticity following parcels.

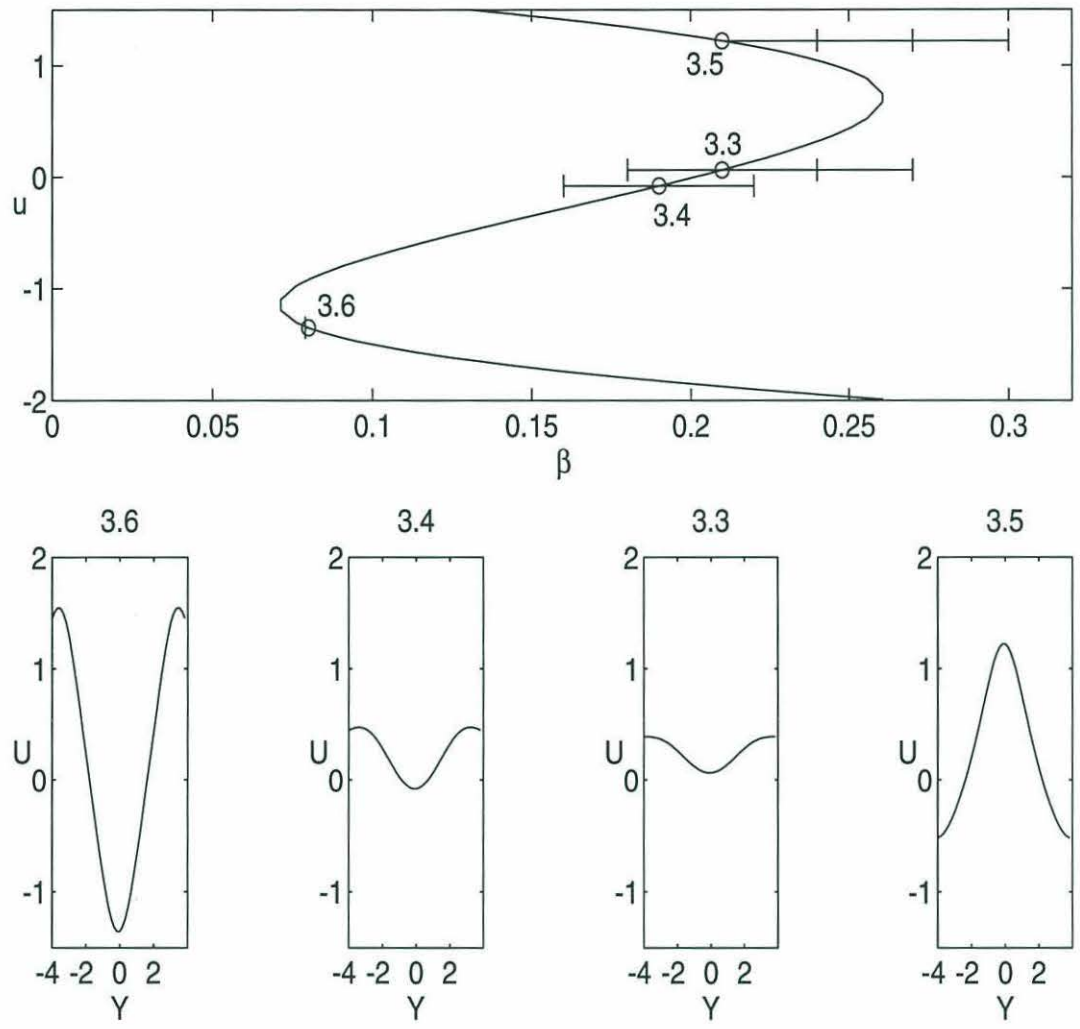

Figure 3-1: The solution curve of $u(y = 0)$ as a function of β from §2.7.2. Also included are the velocity profiles for the four initial conditions. The numbers refer to the sections of this chapter. The horizontal lines on the solution curve indicate the maximum ambient potential vorticity gradient imposed by the topography in the various runs.

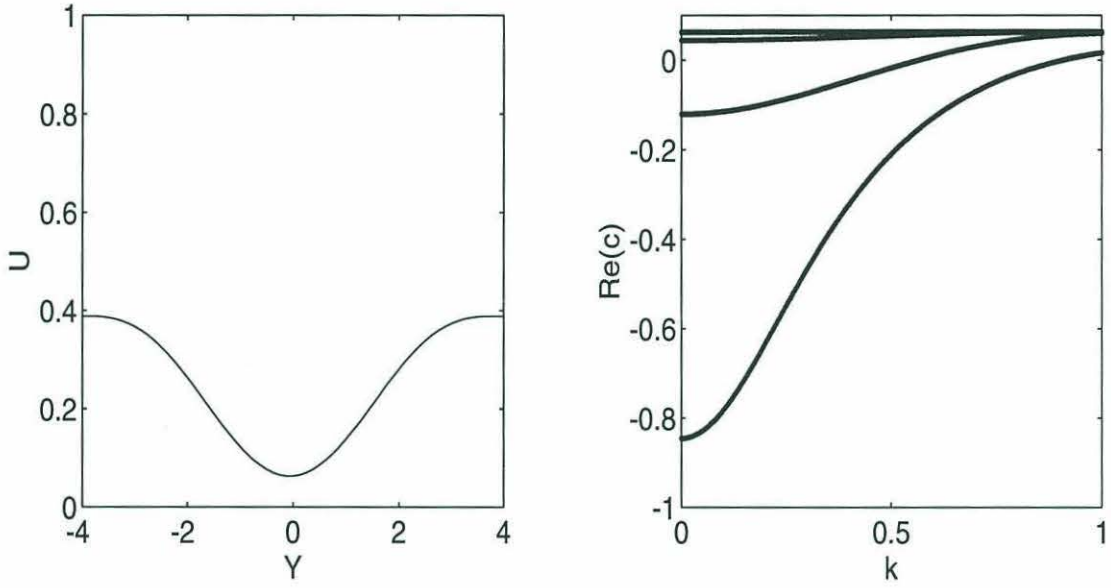

Figure 3-2: The velocity profile for section 3.3, the broad eastward flow with $\beta = 0.21$. Also included are the phase speeds for the normal modes. The inner two curves correspond to the varicose wave; the outer curves are for the sinuous wave.

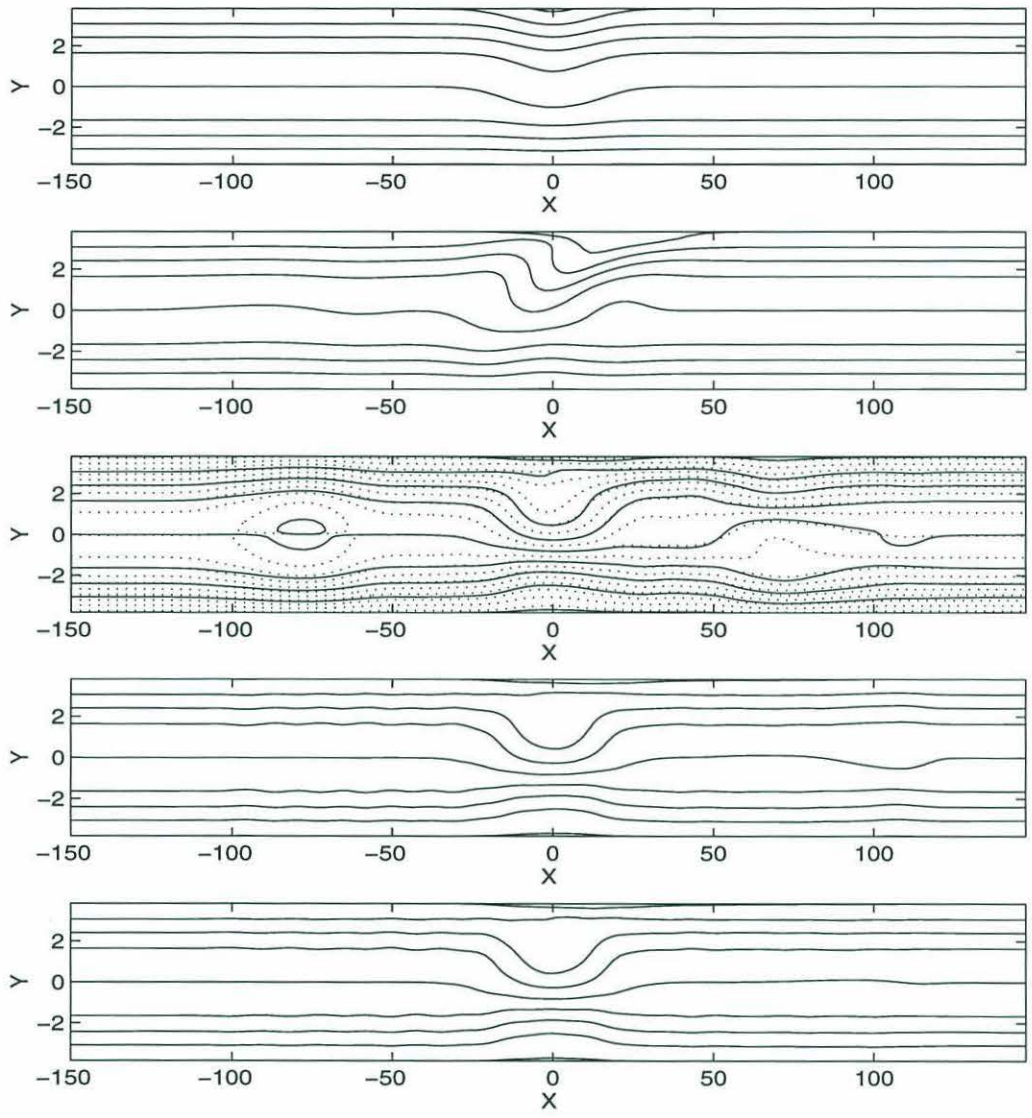

Figure 3-3: Potential vorticity contours at times 0, 100, 800, 1700, 2000 for the broad eastward flow with $\beta = 0.21$, $\beta_T = 0.03$. Contour interval is 0.2. The center plot shows the streamlines with a dotted line; the contour interval is 0.1.

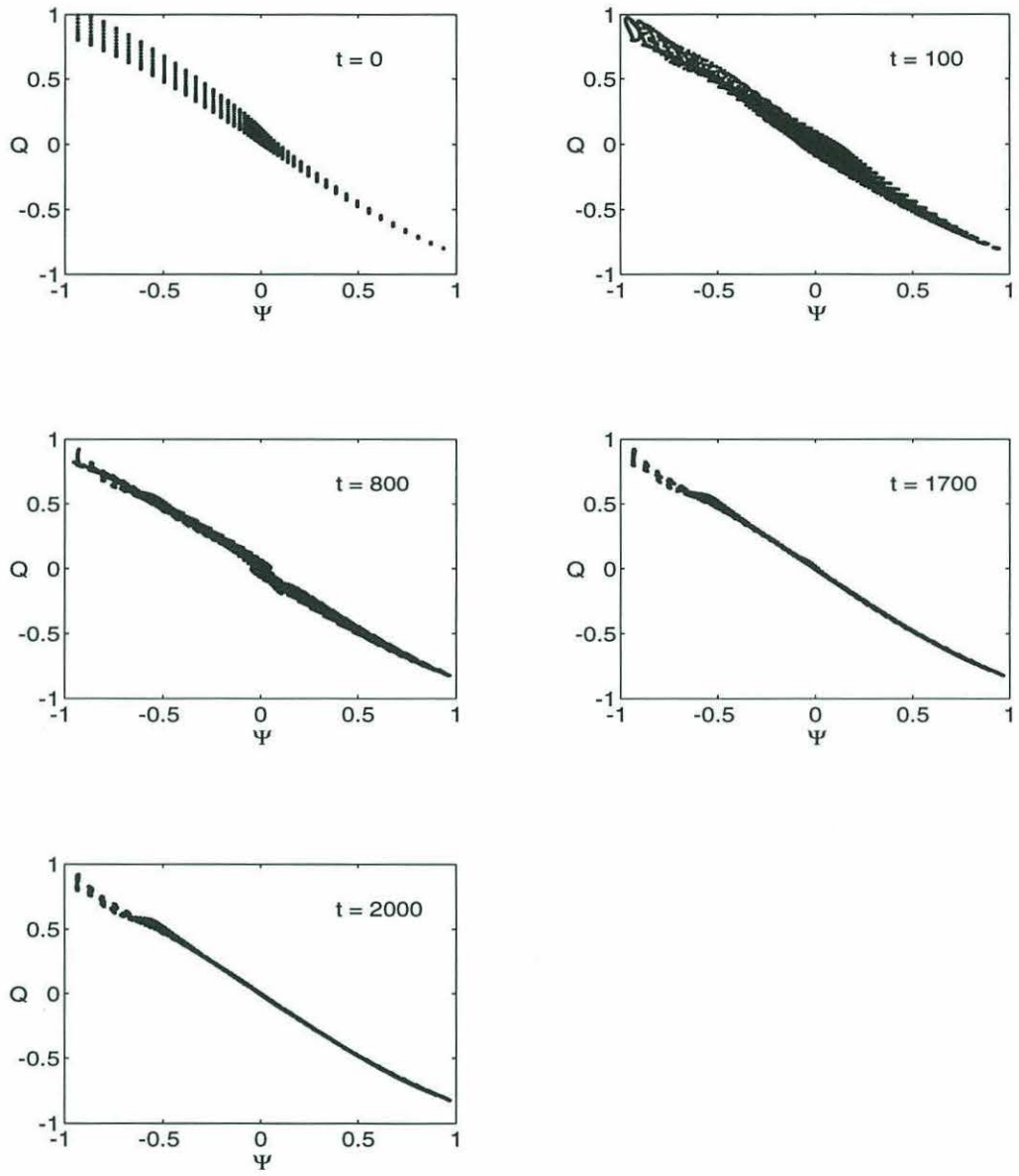

Figure 3-4: Q vs. ψ for the broad, eastward flow with $\beta = 0.21$, $\beta_T = 0.03$.

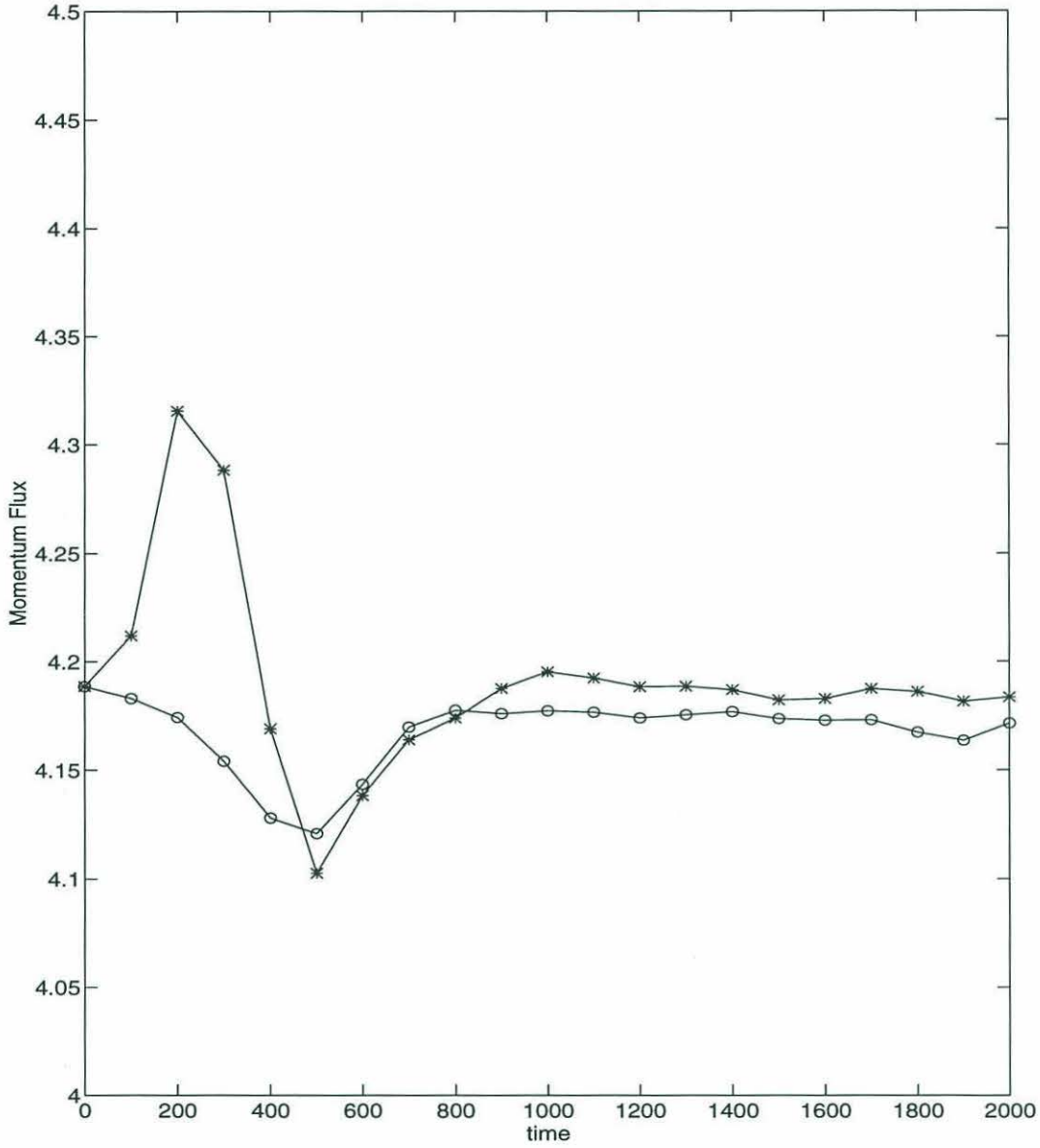

Figure 3-5: The momentum flux with time at $X = -50$ (o) and at $X = +50$ (*).

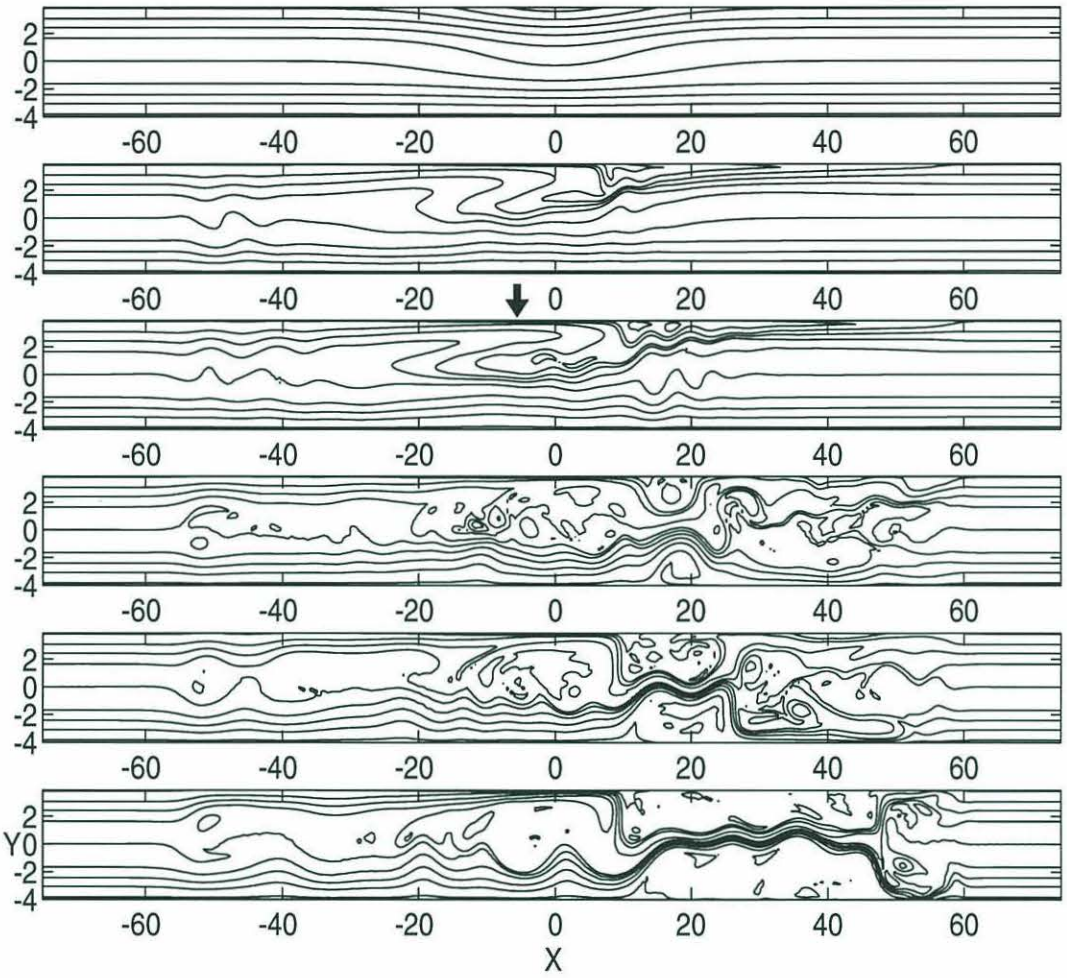

Figure 3-6: Potential vorticity contours at times 0, 100, 150, 425, 575, 975 for the broad eastward flow with $\beta = 0.21$, $\beta_T = 0.06$. Contour interval is 0.2.

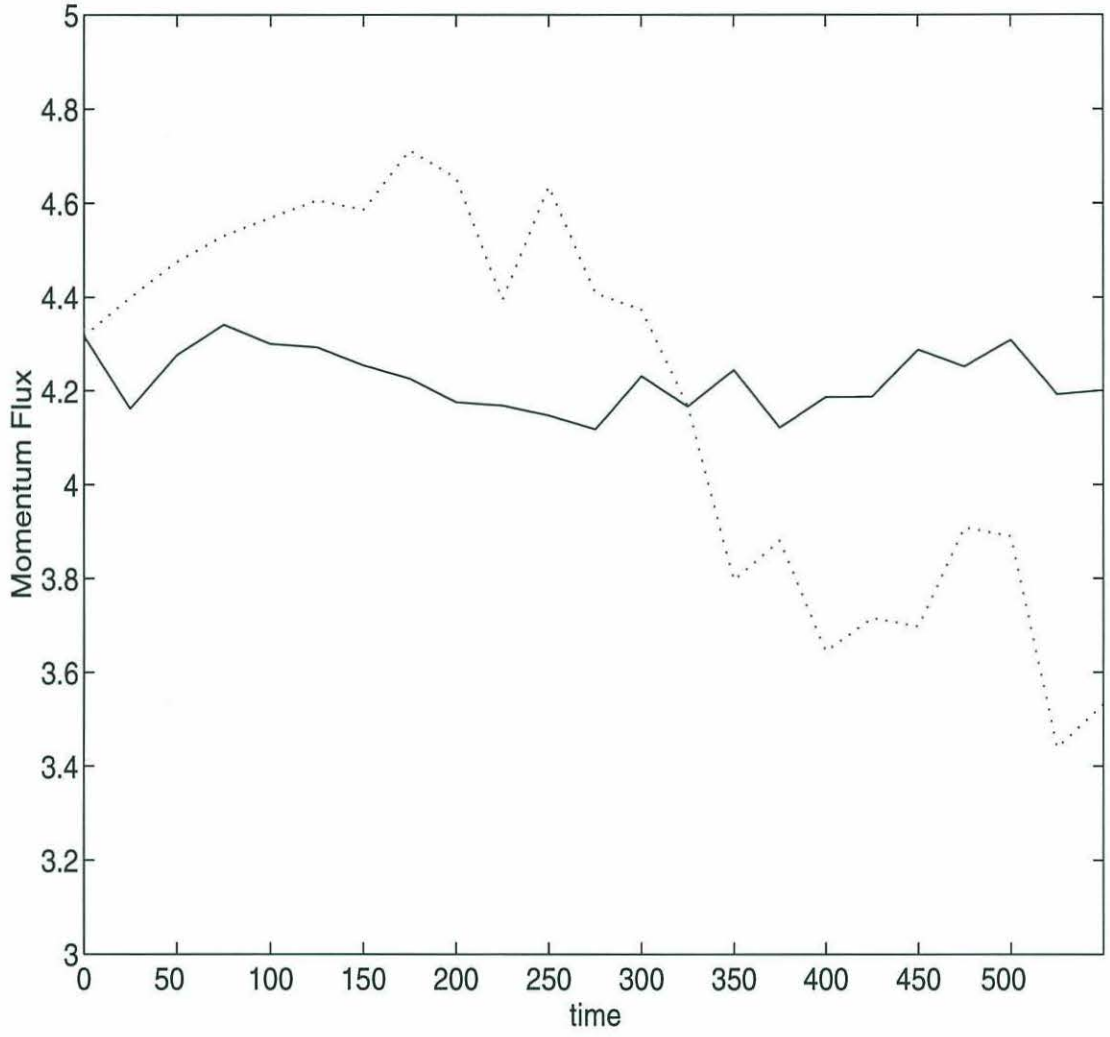

Figure 3-7: The momentum flux with time at $X = -8$ (– solid line) and at $X = +20$ (... dotted line).

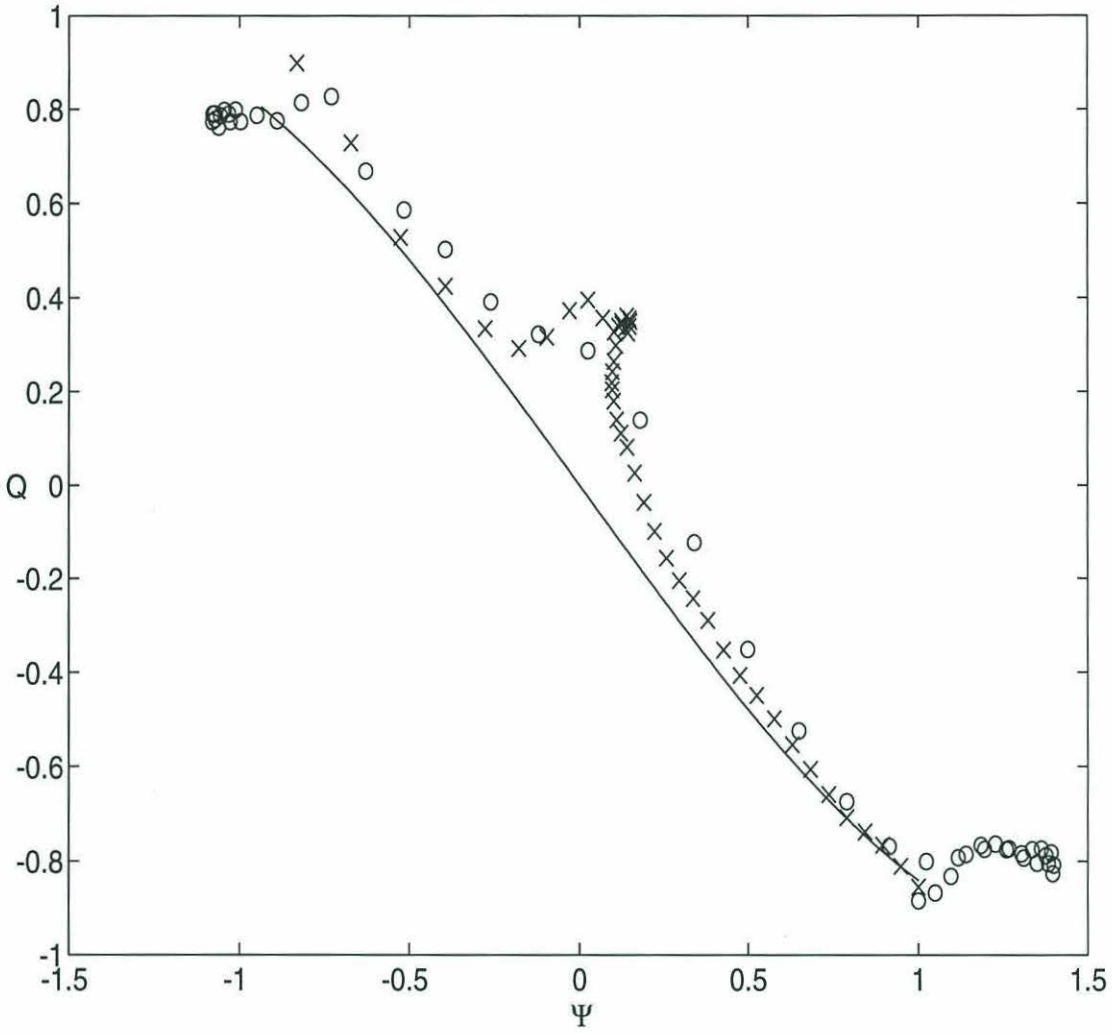

Figure 3-8: Scatter plot for Q versus ψ for $X = +20$ (o) and $X = -8$ (x). at $t = 1000$ The solid line is the original, upstream $Q(\psi)$ function.

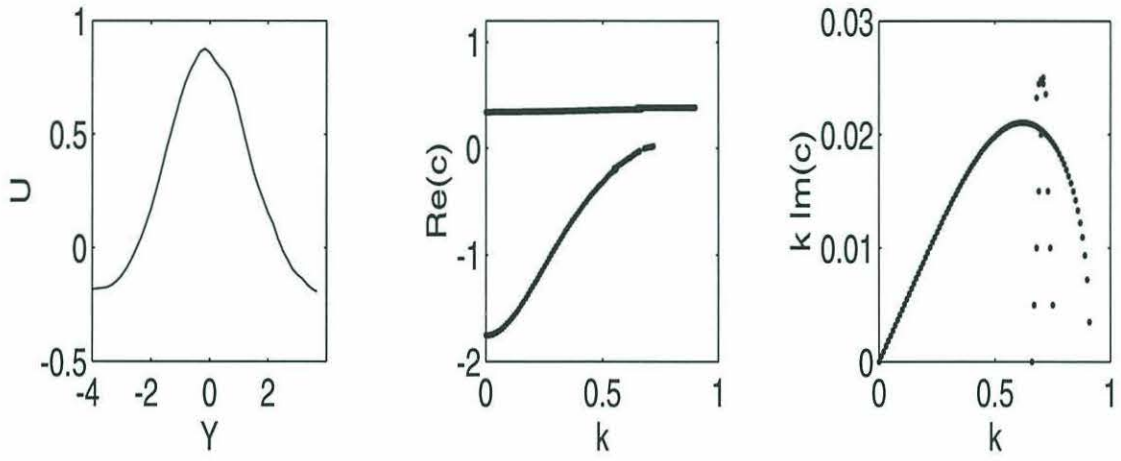

Figure 3-9: The velocity profile and dispersion characteristics for $U(y, X = +30)$ at $t = 1000$ for the originally broad flow with $\beta = 0.21$ and $\beta_T = 0.06$.

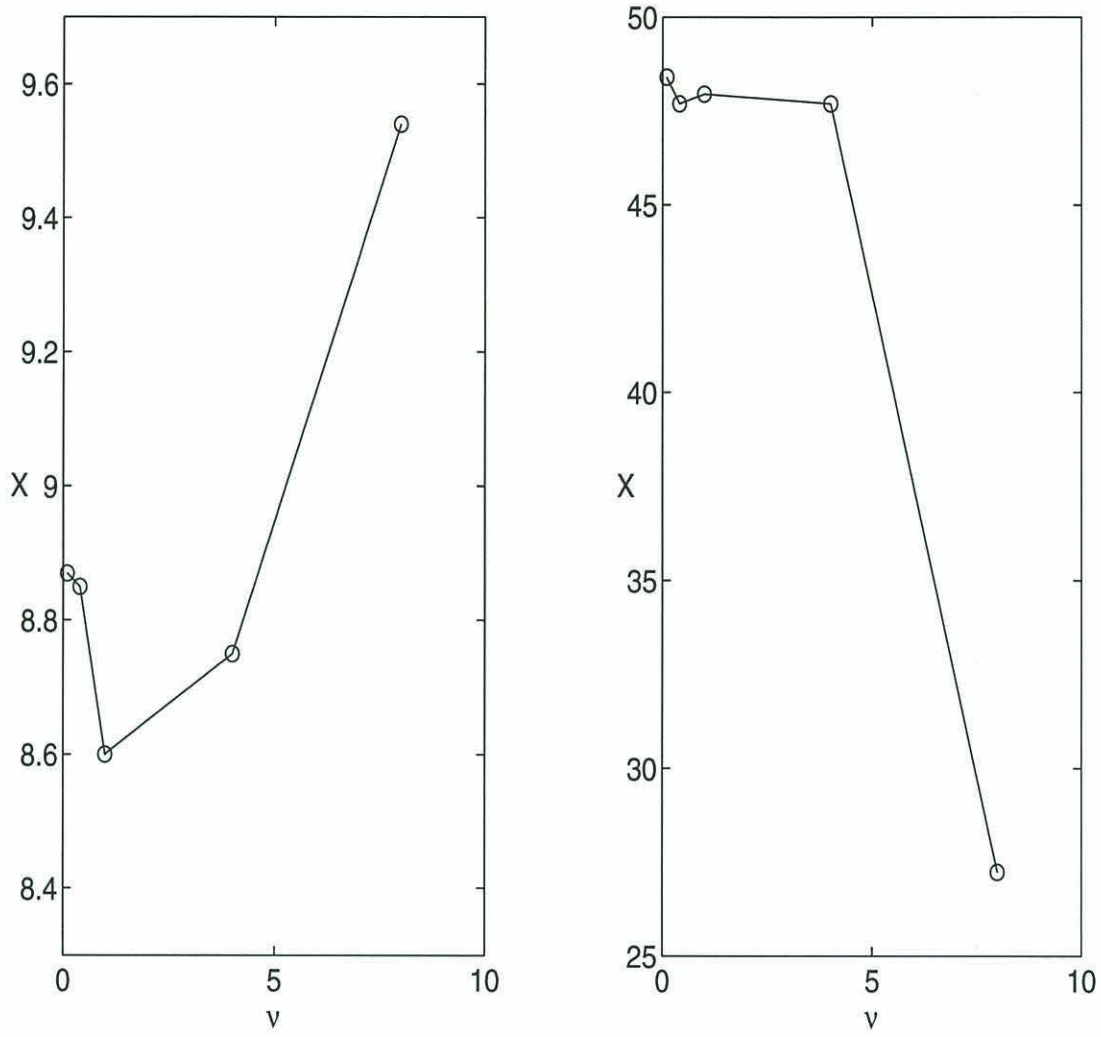

Figure 3-10: Latitudinal positions of the two meridional fronts at $t = 1000$ as a function of the biharmonic friction coefficient ν (The abscissa is scaled by $4e^{-7}$).

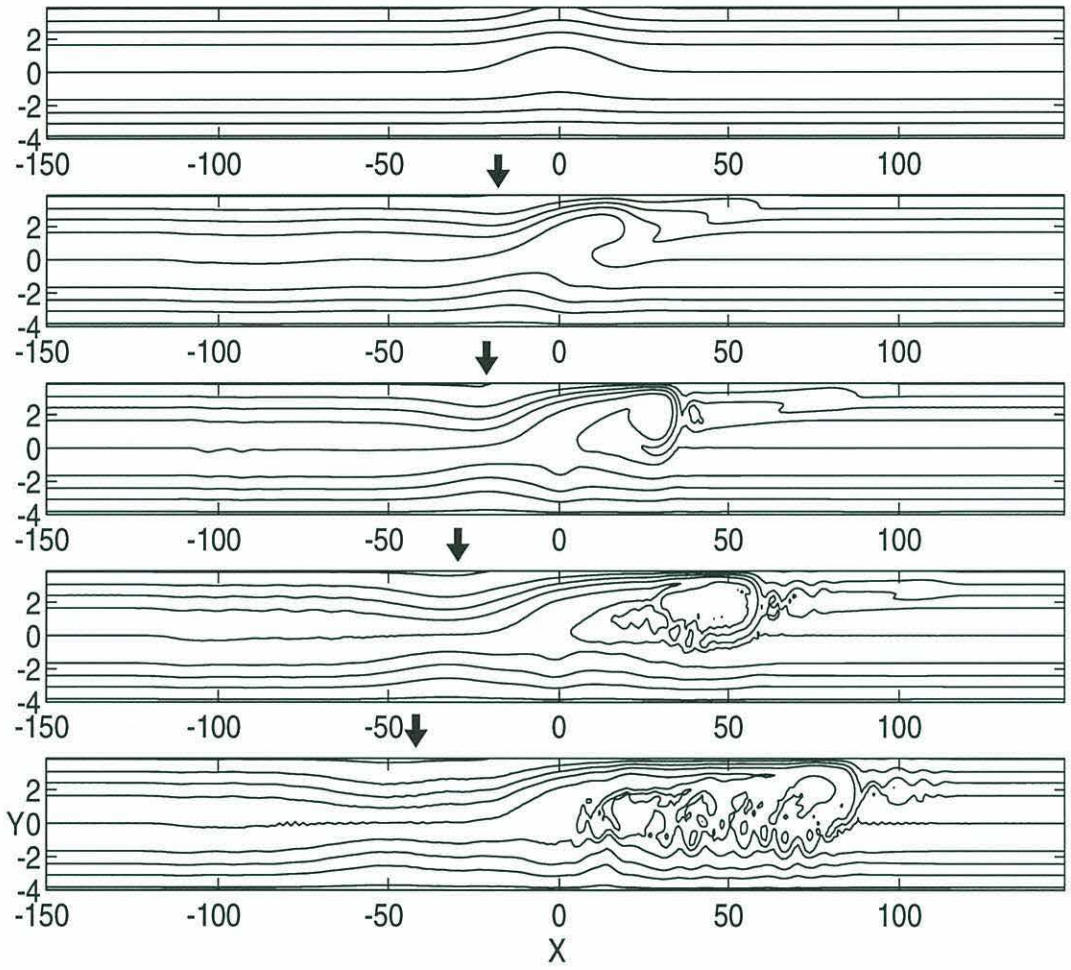

Figure 3-11: Potential vorticity contours at times 0, 120 200, 320, 480 for the broad eastward flow with $\beta = 0.21$, $\beta_T = -0.03$. The contour interval is 0.2.

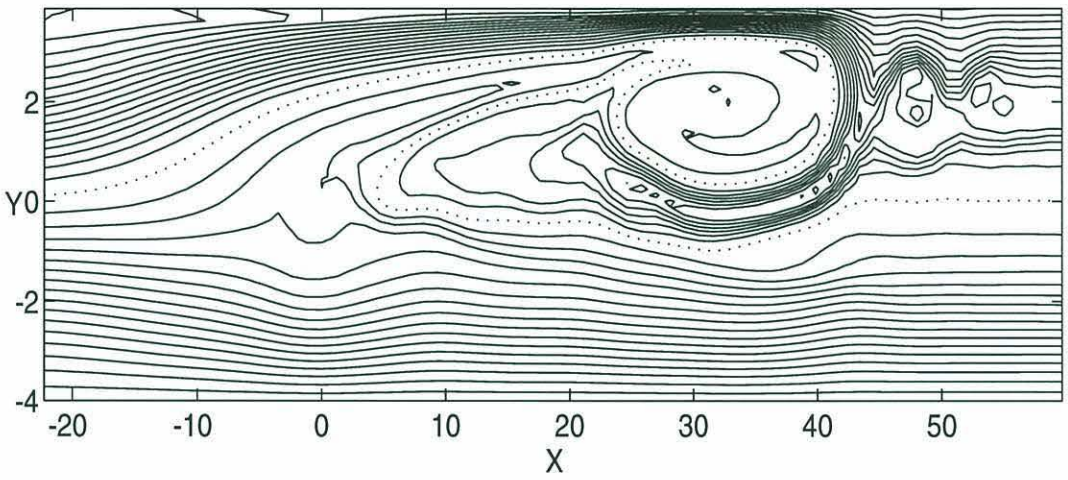

Figure 3-12: Potential vorticity contours at $t = 240$ for the broad eastward flow with $\beta = 0.21$, $\beta_T = -0.03$. The contour interval is 0.05 and the zero contour is dotted.

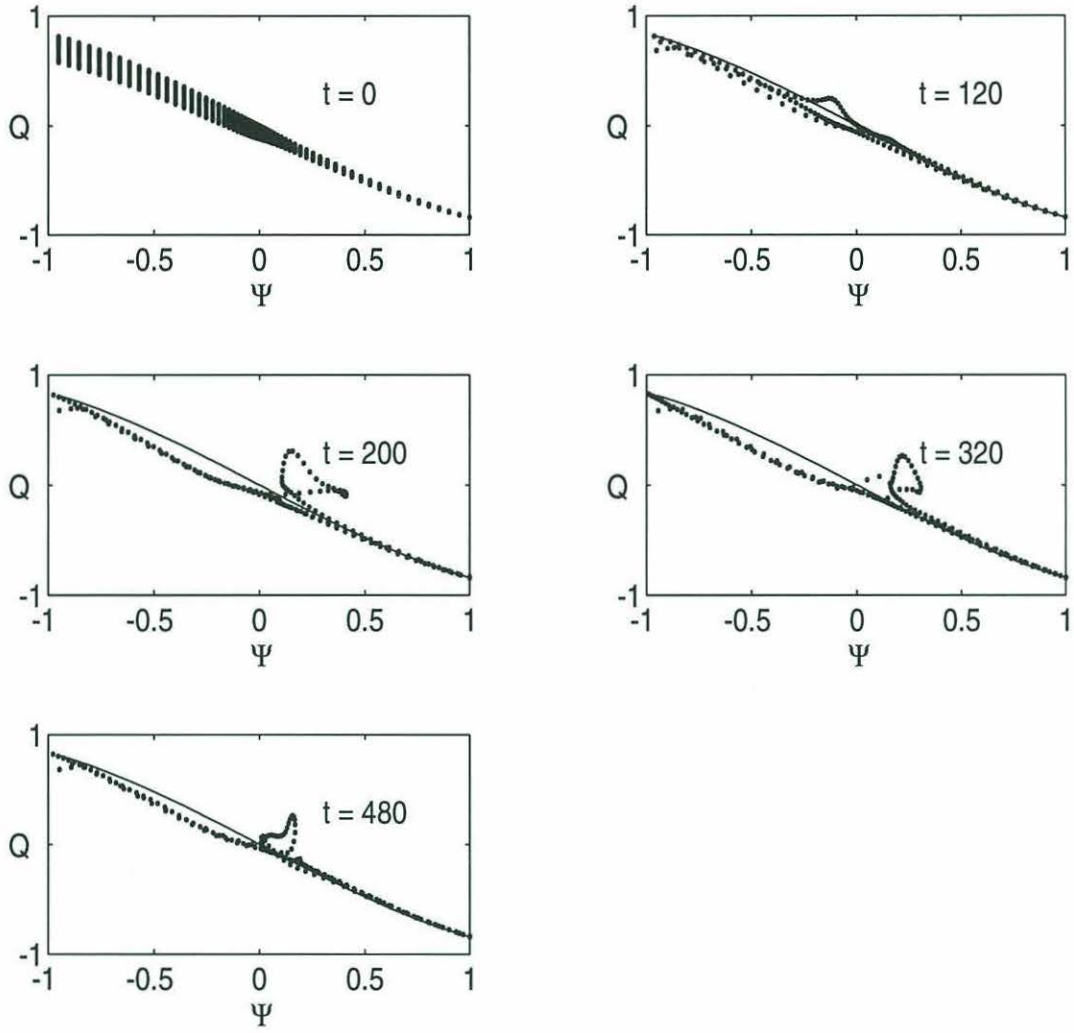

Figure 3-13: Q vs. ψ for the broad eastward flow with $\beta = 0.21$, $\beta_T = -0.03$. The $t = 0$ plot shows the entire $Q(\psi)$ field. Subsequent plots show $Q(\psi)$ only at $X = -33, 0$ and $+33$. The solid line is the original $Q = -sin\psi$.

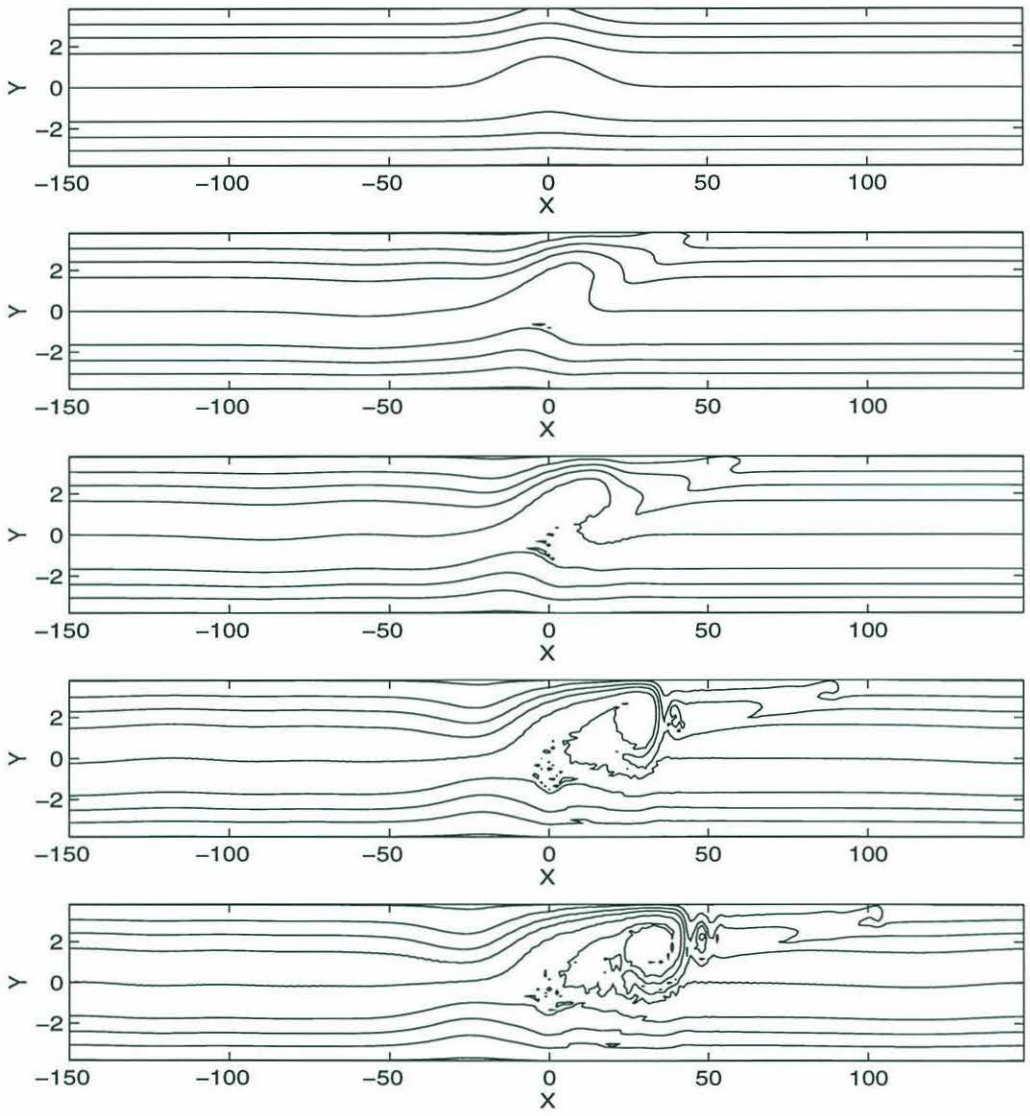

Figure 3-14: Potential vorticity contours at times 0, 80, 120, 200, 240 for the broad eastward flow with $\beta = 0.21$, $\beta_T = -0.03$ and zero viscosity. The contour interval is 0.2.

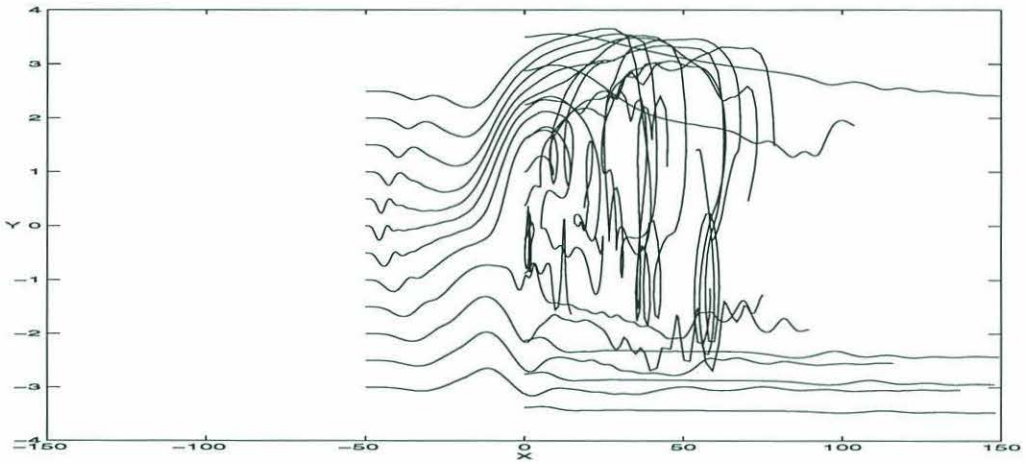

Figure 3-15: Spaghetti diagram for the Eulerian flow field shown in figure 3-11.

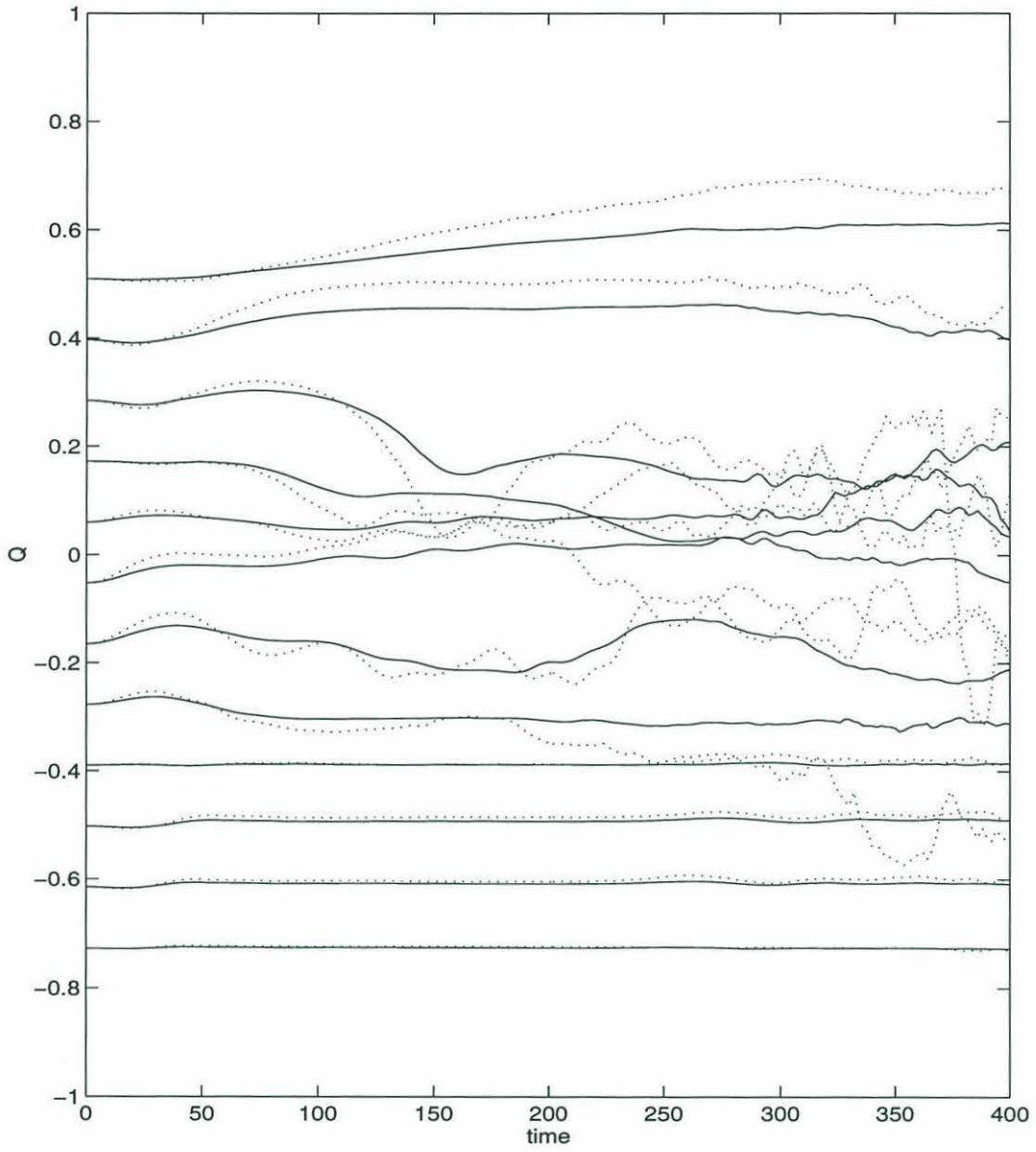

Figure 3-16: Values of potential vorticity for the twelve floats that began at $X = 0$. The dotted line indicates the run with zero viscosity; the solid line is for the run with artificial viscosity.

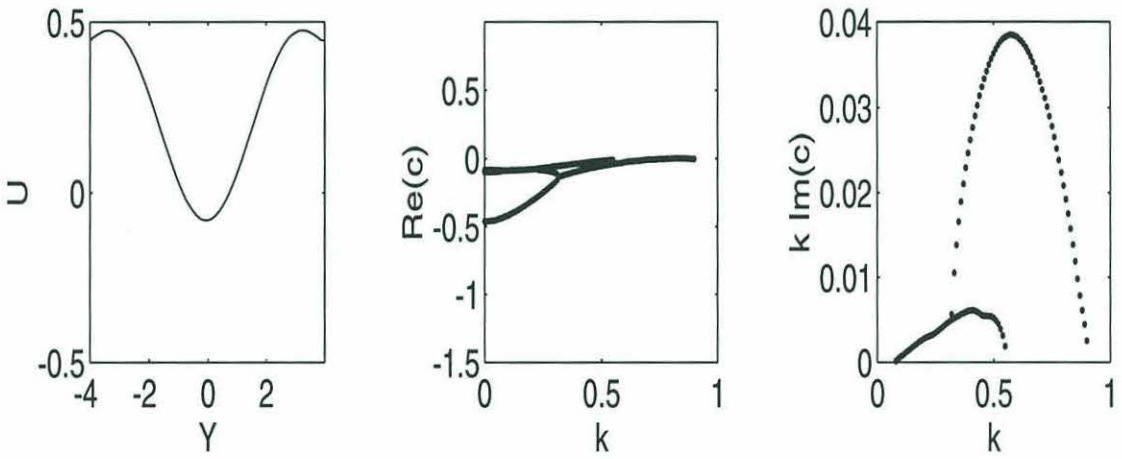

Figure 3-17: The velocity profile and dispersion characteristics when $\beta = 0.19$ and the solution lies on the center branch of the solution curve. Of the two distinct normal modes, the sinuous mode has the larger growth rate.

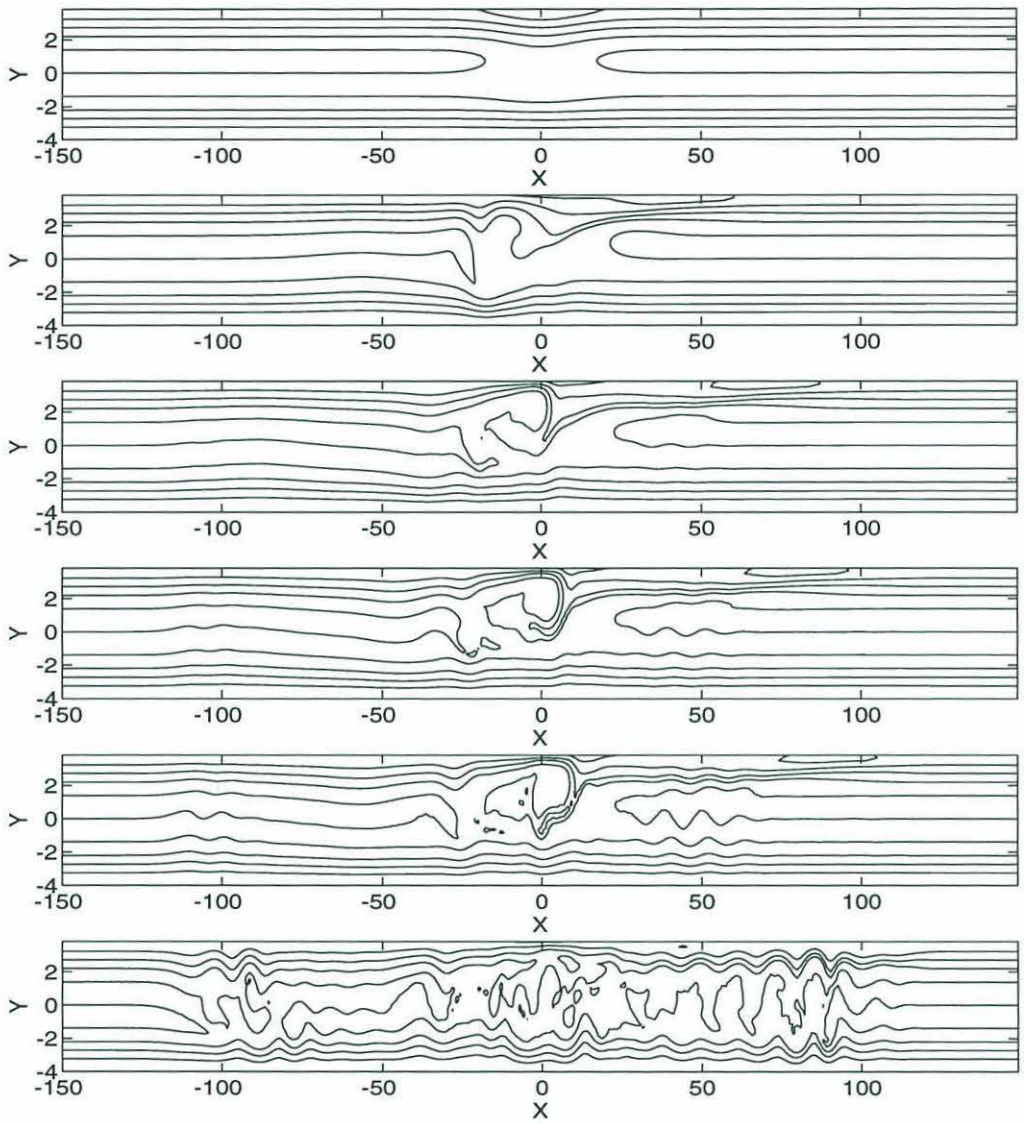

Figure 3-18: Evolution of the potential vorticity contours at times 0, 125 200 225 250 350 for the unstable "split flow" with $\beta = 0.19$, $\beta_T = 0.03$.

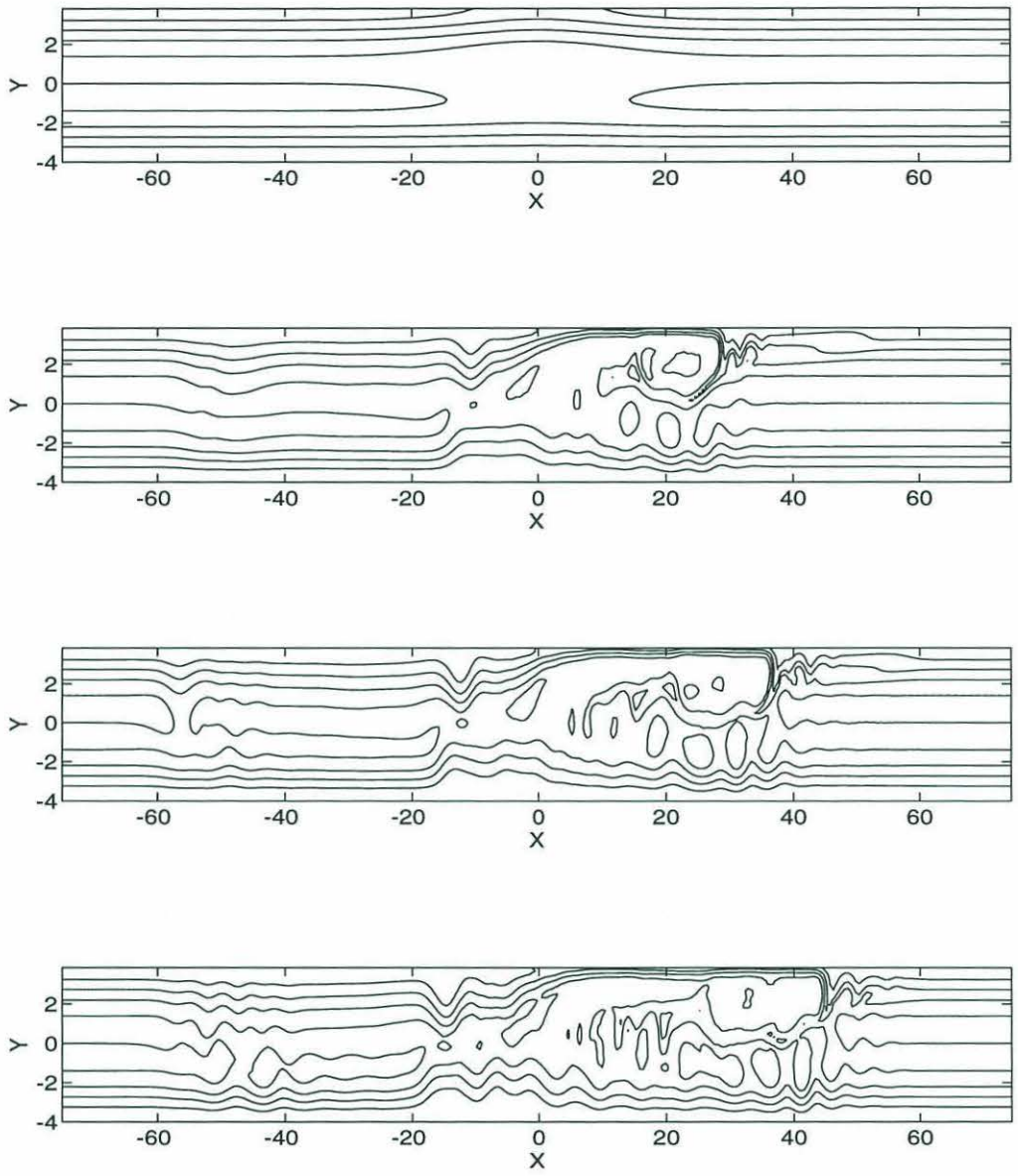

Figure 3-19: Potential vorticity contours at times 0, 160, 200, 240 for the "split flow" with $\beta = 0.19$, $\beta_T = -0.03$.

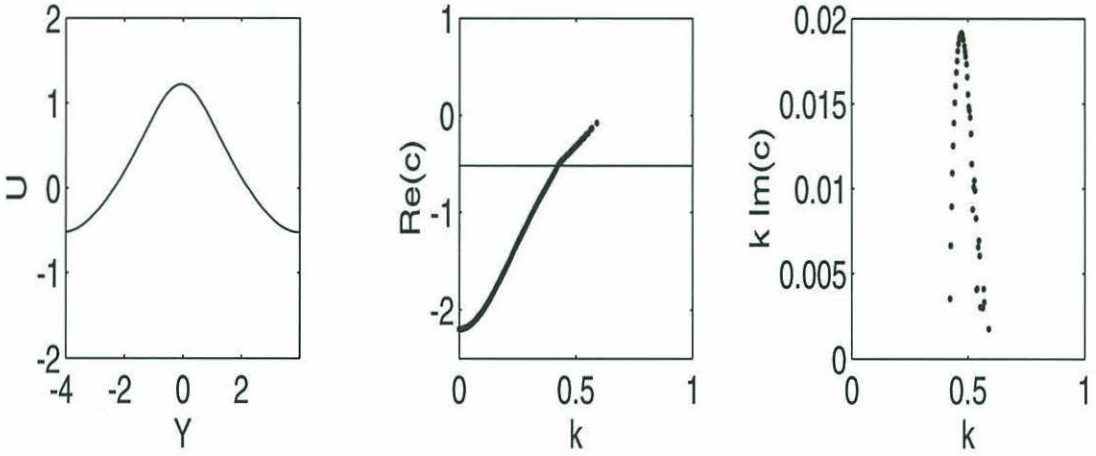

Figure 3-20: The velocity profile $u(y)$ and dispersion characteristics for section 3.5.

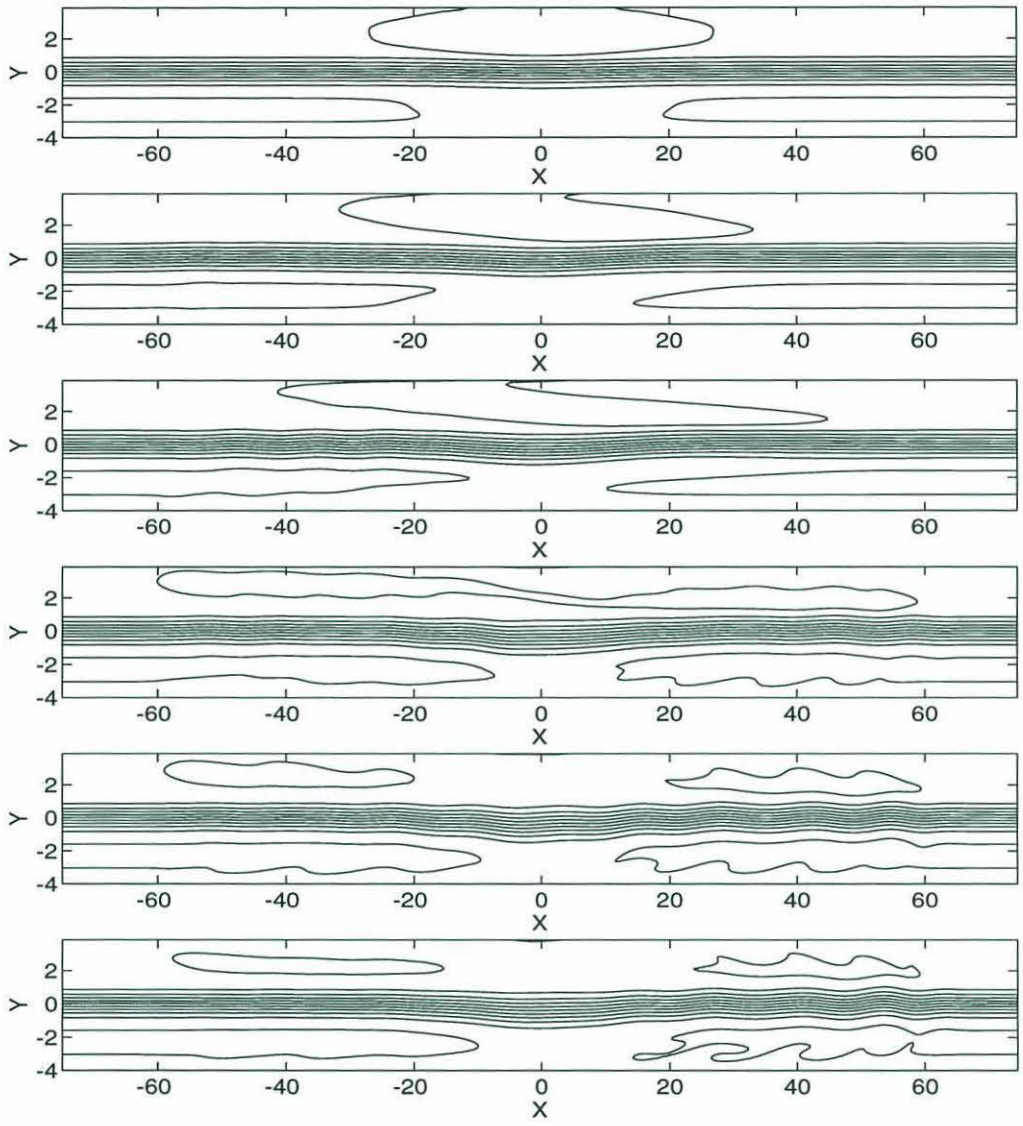

Figure 3-21: Potential vorticity contours at times 0, 25, 50, 175, 275, 350 for the narrow eastward jet with $\beta = 0.21$, $\beta_T = 0.03$. Contour interval is 0.2.

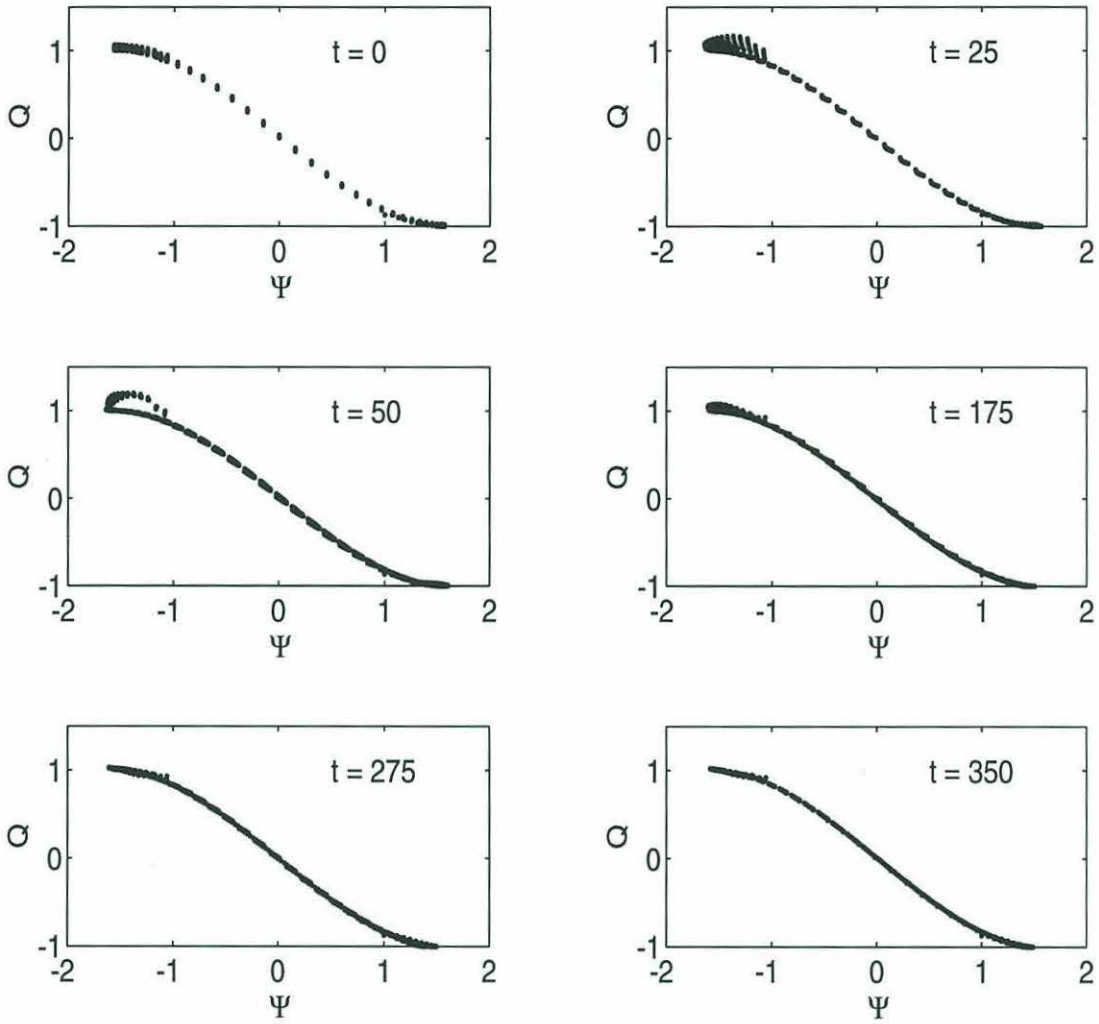

Figure 3-22: Scatter plots of Q versus ψ for the narrow eastward jet with $\beta = 0.21$, $\beta_T = 0.03$.

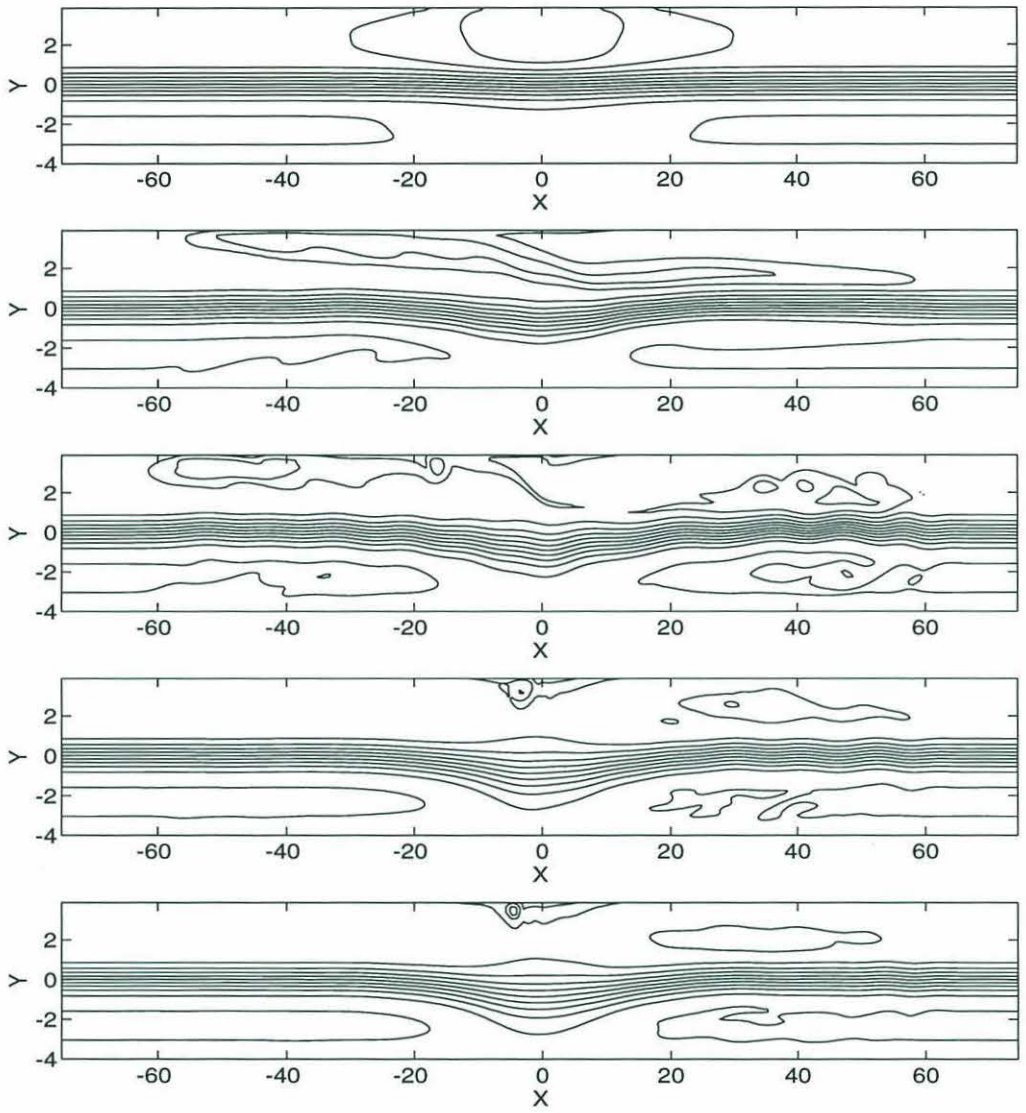

Figure 3-23: Potential vorticity contours at times 0, 75, 150, 325, 500 for the narrow, eastward jet with $\beta = 0.21$, $\beta_T = 0.06$. Contour interval is 0.2.

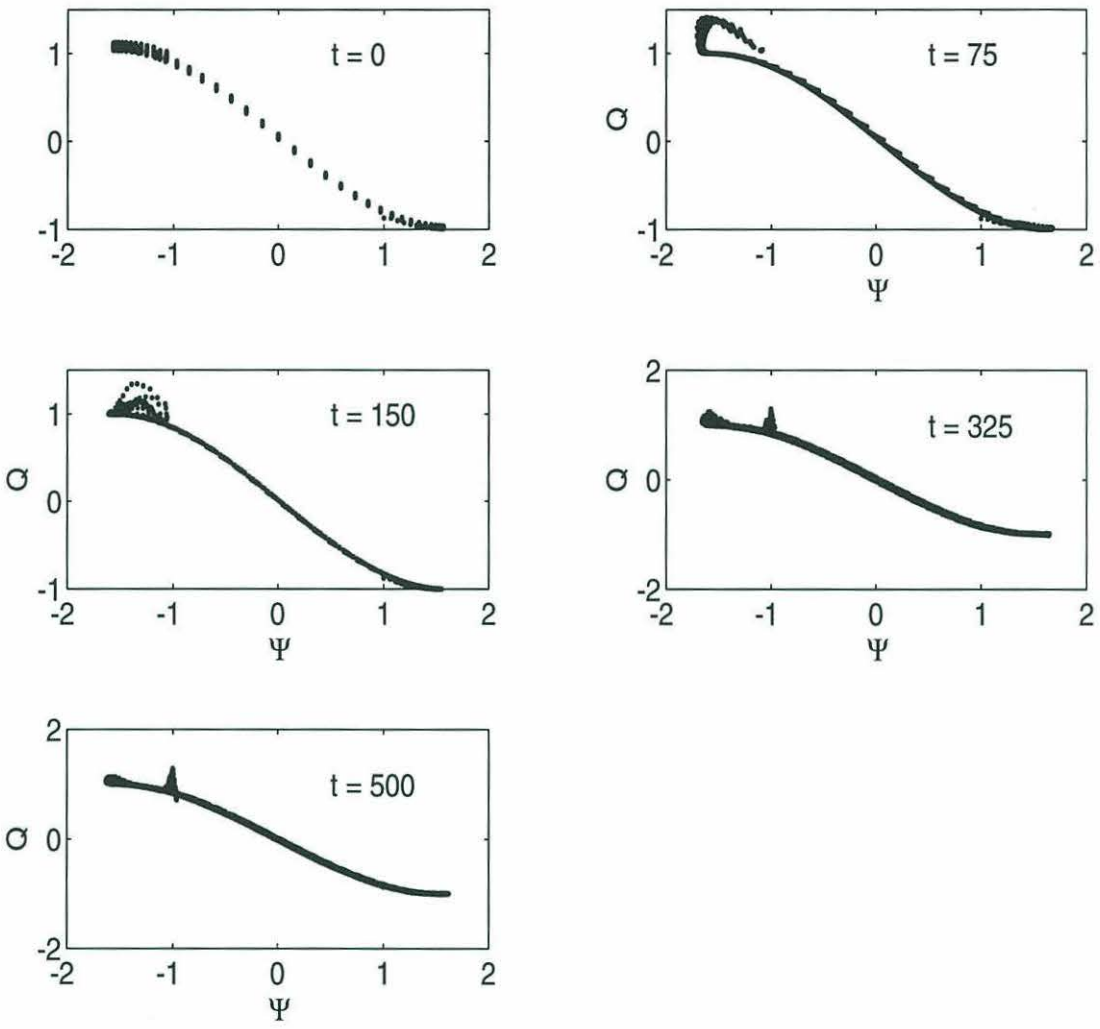

Figure 3-24: Scatter plots of Q versus ψ for the the narrow, eastward jet with $\beta = 0.21$, $\beta_T = 0.06$.

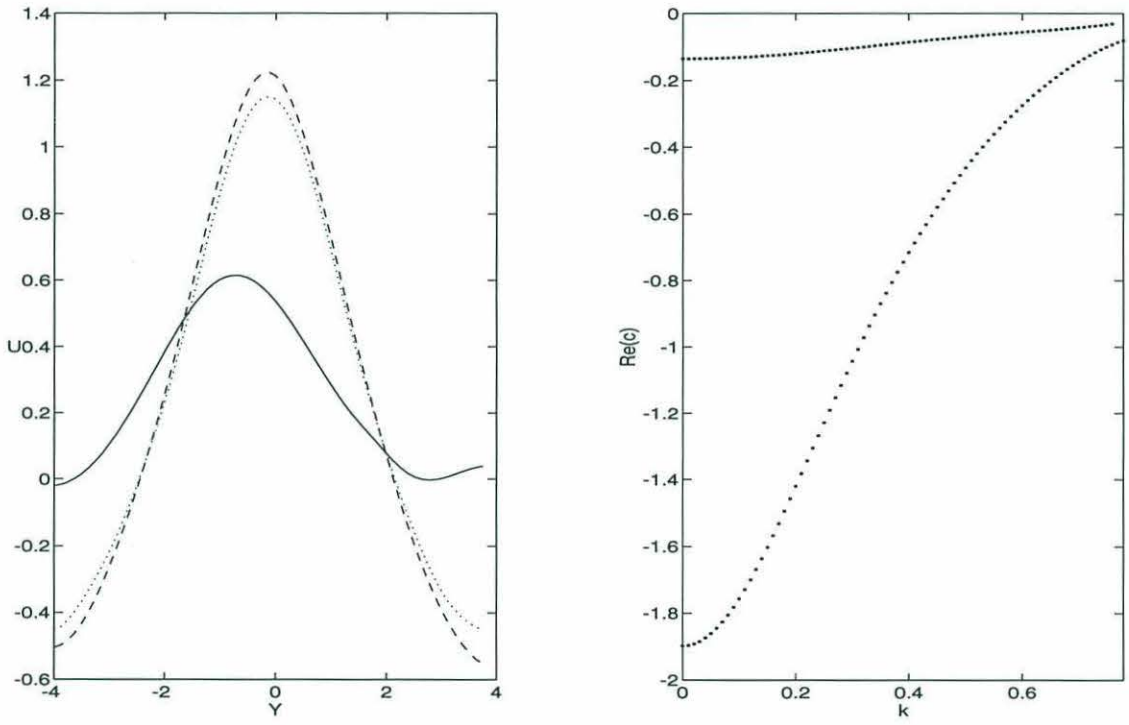

Figure 3-25: Zonal velocities at $X = -30$ (dashed line), $X = 30$ (dotted line), and $X = 0$ (solid line) at $t = 500$ for the originally narrow jet with $\beta = 0.21, \beta_T = 0.06$. Also shown (on the right) is the dispersion diagram for the zonal flow at $X = 0$.

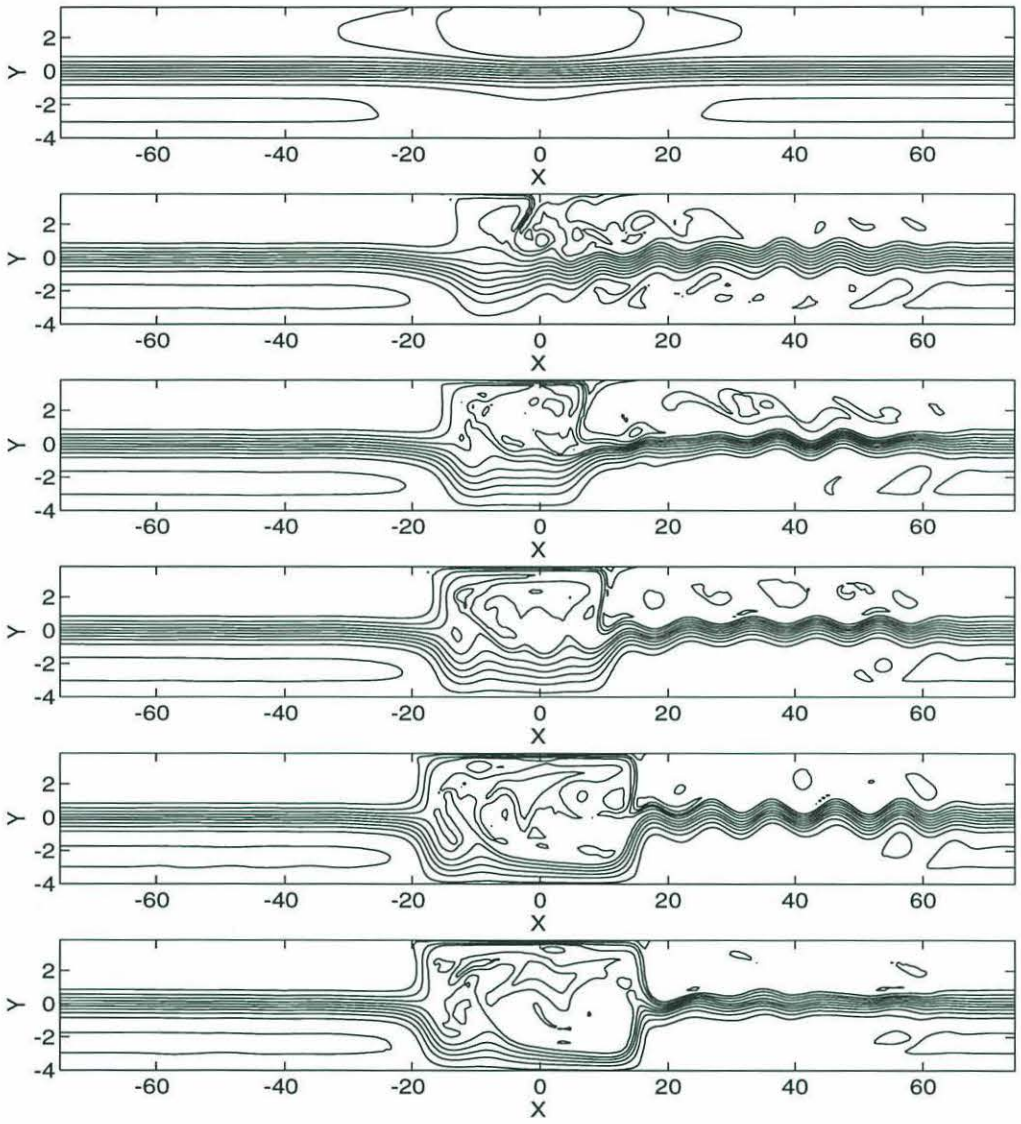

Figure 3-26: Potential vorticity contours at times 0, 360, 640, 840, 1600, 4000 for the narrow, eastward jet with $\beta = 0.21$, $\beta_T = 0.09$. Contour interval is 0.2.

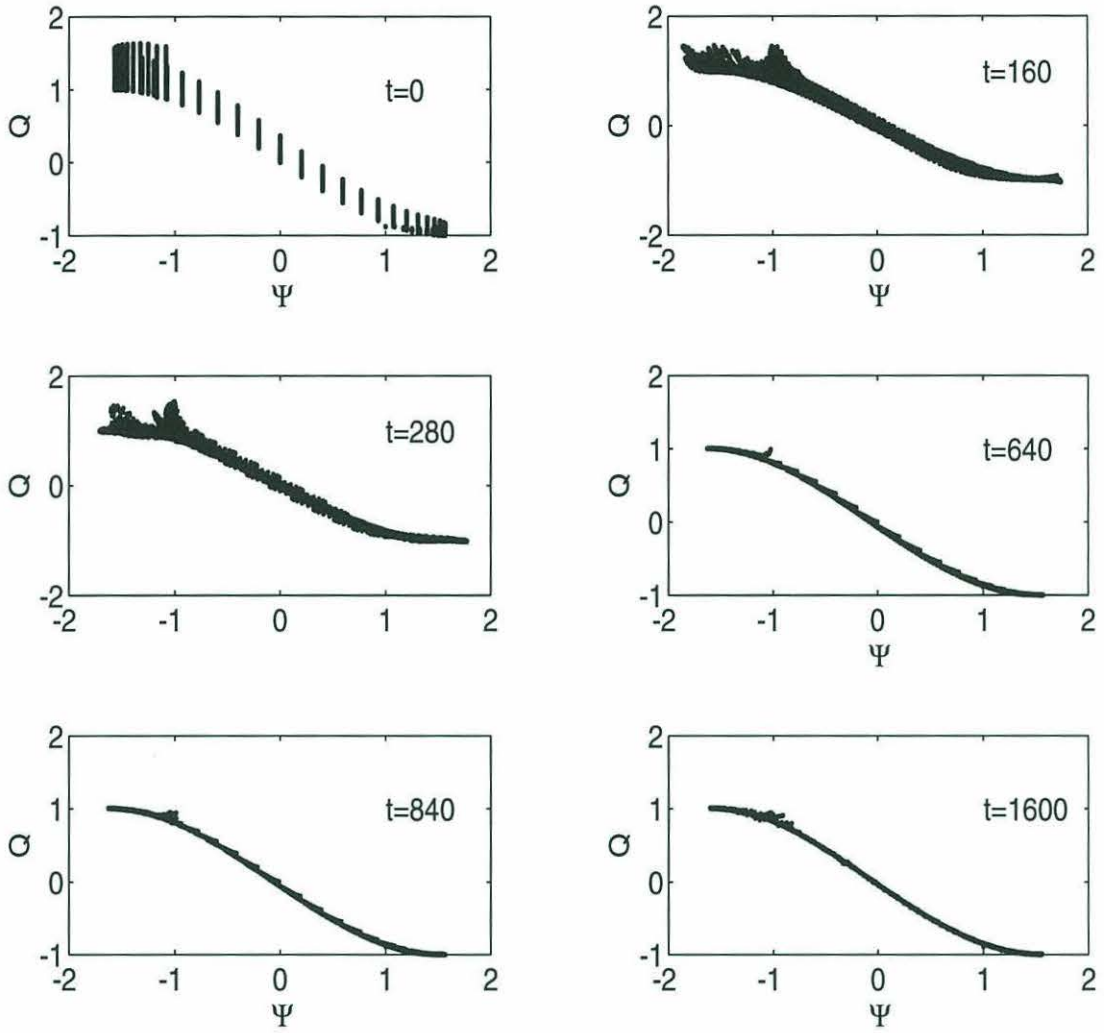

Figure 3-27: Scatter plots of Q versus ψ for the narrow eastward jet with $\beta = 0.21$, $\beta_T = 0.09$.

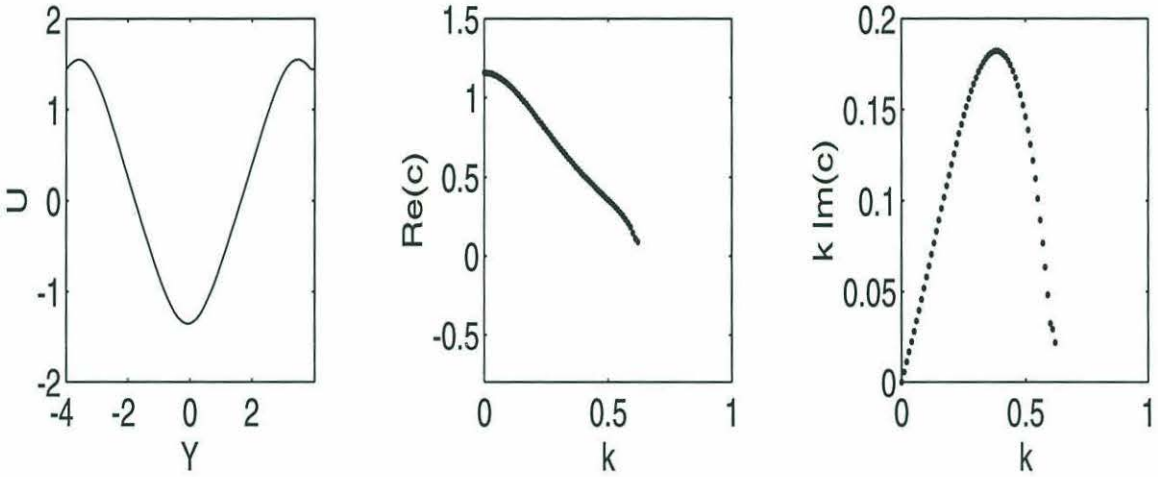

Figure 3-28: The velocity profile and dispersion characteristics for the "split flow" of §3.6 with $\beta = 0.08$.

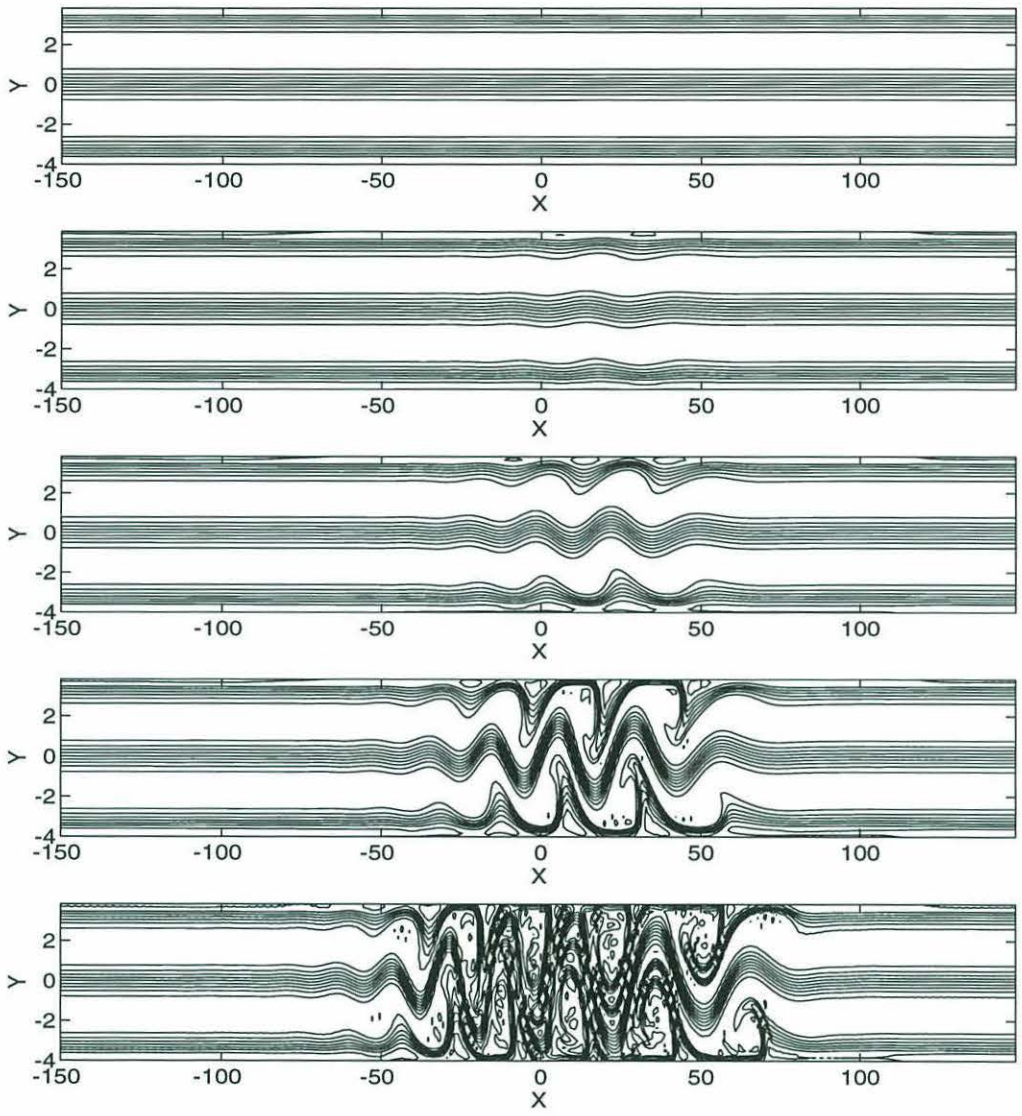

Figure 3-29: Potential vorticity contours at times 0, 50, 60, 70, 80 for the "split flow" with $\beta = 0.08$, $\beta_T = -0.001$. Contour interval is 0.2.

Chapter 4

Unbounded Domains

4.1 Introduction

In chapter 2, a necessary condition for the existence of non-unique states was found and this condition is identical to Arnol'd's second theorem which provides a necessary condition for instability. The derivative $dQ/d\psi$ provides a bound to the local meridional wavenumber of the flow, and solutions are unique if the channel width is smaller than this bound. It was also shown that the equivalence of the two theorems was not fortuitous; multiple solutions arise at a pitchfork bifurcation as a stability parameter is raised above the threshold determined by Arnol'd's theorem. However, these results depended crucially on the boundedness of the domain, and in fact, by normalizing the $Q(\psi)$ function, the channel half-width, L, was used as the stability parameter. In an unbounded domain the condition for uniqueness reduces to $dQ/d\psi > 0$, which is identical to Arnol'd's first theorem. This criterion for uniqueness was first mentioned by Carnevale and Fredricksen (1987). It is natural to ask, what happens if this condition is violated? Do multiple states exist, and do they correspond to stable and unstable equilibria as they did in the bounded domain? The purpose of this brief chapter is to make a few comments about the existence of alternate states in an unbounded domain.

At first glance, this seems like a trivial issue. Certainly there is no difference in the instability mechanism in bounded and unbounded domains. However, perhaps

the boundaries play a role in the equilibration of the instability. Certainly in the numerical calculations of chapter 3, and in Helfrich and Pedlosky (1994), the channel walls serve to confine the flow. In fact, many of the applications of catastrophe theory take place in bounded domains. For example, the elastic stability problem of a loaded beam, with fixed endpoints is often used as an example of the cusp catastrophe (Thompson and Hunt, 1973). In hydrodynamic stability, Benjamin (1978b) has applied bifurcation theory to account for qualitative experimental results regarding the Taylor experiments on Couette flow between rotating cylinders. Benjamin points out that some of the properties associated with the bifurcating system arise because the flows are bounded, and may become untrue if this assumption is relaxed.

The following two sections contain a description of two simple examples of unbounded flows. The first is based on the well-known Bickley jet which has unstable sinuous and varicose modes. The second example is a piecewise-linear $Q(\psi)$ function in two layers.

4.2 Bickley Jet

As a simple example of a symmetric jet on the infinite plane, consider the Bickley jet

$$U = sech^2 y.$$

The stability properties of this jet have been well documented, dating back to Bickley (1937) and Sato and Kuriki (1961). A symmetric, or sinuous mode is unstable in the range $k = [0, 2]$. An antisymmetric, varicose wave is unstable for $k = [0, 1]$. The short-wave cutoff for both waves have a phase speed $c = 2/3$, equal to the velocity at the critical latitude.

Since the flow is unstable we expect that $dQ/d\psi$ is negative somewhere in the flow. This may easily be verified since, on the f-plane, the $Q(\psi)$ function may be found analytically and is

$$Q(\psi) = 2\psi(\psi^2 - 1). \tag{4.1}$$

Given this $Q(\psi)$ function, a shooting method is employed to find solutions $\psi(y)$ to the potential vorticity equation. In the unbounded domain, Perov's theorem predicts an infinite number of solutions, each with its own number of turning points. However, the wave-like solutions, which have turning points at infinity are inappropriate alternate states, where we expect the structure to be undisturbed at infinity. The only solutions that decay as $y \to \pm\infty$ are the null solution and $\psi = \pm \tanh y$, and since this is on the f-plane, the latter two solutions are equivalent. Therefore, the Bickley jet is a unique solution.

Multiple solutions can be found in an unbounded domain if a shear region is bounded by fronts, across which the potential vorticity relation $Q(\psi)$ changes. These fronts separate the interior shear region of the jet (with $Q(\psi)$ given by 4.1) from an exterior flow, which decays smoothly to a uniform flow at infinity. The exterior potential vorticity is taken to be

$$Q = \alpha^2\psi \pm Q_0$$

where the sign convention will be that the constant is positive north of the fronts and negative to the south. The actual form of the exterior potential vorticity is determined by the constants α^2 and Q_0, and in particular they set the strength of the jump of potential vorticity. At the southern front

$$\Delta Q = \alpha^2\psi_0 - Q_0 - Q_{interior}(\psi_0)$$

The exterior streamfunction is

$$\psi = \left(\psi_0 + \frac{\beta}{\alpha^2}L - \frac{Q_0}{\alpha^2}\right) e^{\alpha(y-L)} + \frac{\beta}{\alpha^2}y + \frac{Q_0}{\alpha^2}, \quad y > L$$

$$\psi = \left(-\psi_0 - \frac{\beta}{\alpha^2}L + \frac{Q_0}{\alpha^2}\right) e^{-\alpha(y-L)} + \frac{\beta}{\alpha^2}y + \frac{Q_0}{\alpha^2}, \quad y > -L$$

where $\pm L$ are the unknown latitudes of the fronts and $\mp\psi_0$ are the streamlines along the fronts. The shooting method begins at $-L_g$, an estimate of the latitude of the

southern front, and integrates across the interior until $y = +L_g$. The process is iterated until the streamfunction ψ_0 and the velocity u match the exterior solution at the proper L.

A solution curve for $\psi_0 = 1$, $Q_0 = -2$ and $\alpha^2 = 1$ is shown in figure 4-1. With this value of ψ_0, the potential vorticity just on the interior side of the front is $Q = 0$. For a given β each solution is characterized by L, the latitude of the potential vorticity front. All points on the curve connecting A,P and B correspond to symmetric velocity profiles. This curve has a turning point at $\beta = 0.222$. No symmetric solutions exist for β larger than this value. The point P denotes a pitchfork bifurcation. All points on the curve connecting D, P and C are asymmetric. The upper branch of this curve has a turning point at $\beta = 0.27$. If β is larger than this value then no solution with this potential vorticity function exists.

None of these solutions look like the Bickley jet because of the discontinuity in Q. The solutions can be made more similar to the Bickley jet if the jump in Q is reduced; however multiple solutions can not be found unless $Q_0 > \alpha^2\psi_0$, i.e. $dQ/d\psi$ must be negative across the fronts.

The curve of symmetric solutions has a turning point at $\beta = 0.222$. Does this turning point separate the symmetric solutions into states that are stable and unstable with respect to a particular mode? Because the turning point separates symmetric solutions of different widths, the relevant wave mode is the varicose wave. In addition, there is a bifurcation of asymmetric solutions. Does this point separate solutions that are stable and unstable to the sinuous mode?

The two symmetric velocity profiles A and B at $\beta = 0.18$ are shown in figure 4-2 along with their dispersion characteristics. The dispersion characteristics are quite similar for these two solutions on opposite branches. Both velocity profiles have four distinct normal modes; two of which are antisymmetric and two of which are symmetric. In each of these pairs, one is stable and the other is unstable. Both of the stable modes have $c < u_{min}$, and although the phase speed of the two modes overlaps for small k, this does not represent a merger of two neutral modes to form an unstable mode, since the waves maintain their distinct symmetry. The fastest

growing unstable mode for both velocity profiles is the sinuous wave. For solution A, the sinuous wave is unstable in the range $k = [0, 2.5]$, and the varicose wave is unstable from $k = 0.3$ to $k = 1.9$. When $L = 3$, for solution B, the sinuous wave is unstable in the range $k = [0.6, 1.75]$ and the varicose is unstable from the longest waves to a short-wave cutoff at $k = 0.75$. Note, that based on the real part of the phase speed, no hydraulic interpretation is possible for these two states, since both velocity profiles have phase speeds c with the same sign for identical varicose modes.

On both sides of the turning point, the stability properties are very similar; both branches of steady, zonal flows are unstable to both the varicose mode and the sinuous mode. This is in sharp contrast to the change in stability seen in the channel model, where typically one branch was stable and the other was unstable. In the channel model unstable flows equilibrated by "jumping" to the stable branch on the other side of the turning point. Presumably, no such equilibration can take place with this potential vorticity distribution in the unbounded domain since both zonal states are unstable.

4.3 Two Layer Fluid

In the present work and previous work on the hydraulics of zonal flows, the problem was considered in a single moving layer of fluid. This is clearly an oversimplification in modeling current systems such as the Gulf Stream which have much stronger velocities in the upper portions of the water column. For instance, Hall and Fofonoff (1993) state that a minimum of three layers are necessary to capture the vertical structure of the potential vorticity dynamics. These layers include a top layer with a single front of potential vorticity, a thermocline layer with a double front of potential vorticity, containing a relative minimum between the two fronts, and a lower layer with nearly uniform potential vorticity. In addition, they conclude that the lower layer must be active, since interactions with the ocean bottom play an important role in the downstream evolution of the stream.

The purpose of this final section is to explore the effect of stratification on the

existence of multiple solutions in an unbounded domain. For simplicity, only two layers will be considered, corresponding to the lower two layers suggested by Hall and Fofonoff (1993). As in the rest of the thesis, we make use of a steady, inviscid quasi-geostrophic model on the β-plane, and as in the rest of the chapter, the domain is assumed to be unbounded. In non-dimensional units, the potential vorticity equations are

$$\nabla^2\psi_n \; + \; (-1)^n F_n\,(\psi_1 - \psi_2) \; + \; \beta y \; + \; \eta_b \delta(n-2) \; = \; Q_n(\psi_n) \qquad (4.2)$$

where $n = 1$ refers to the upper layer and $n = 2$ refers to the lower layer. The new non-dimensional parameter

$$F_n \; = \; \frac{f_0^2 L^2}{g\left(\frac{\Delta\rho}{\rho}\right) D_n}$$

is a measure of the stratification, where $\frac{\delta\rho}{\rho}, L$, and D_n are respectively, the density difference between the two layers divided by the mean density, a typical horizontal length scale in the problem, and the thickness of each layer.

It is assumed that the functional relationship between $Q_n(\psi_n)$ is determined by the equilibration of processes that occur upstream, out of the model region. To mimic the recirculations, which have much stronger barotropic components than the stream itself, it is assumed that far from the topography, and far from the core of the jet the background flow in both layers is taken to be a weak, uniform westward flow $u = -u_b$. A uniform flow on the β plane leads to a linear relationship between the potential vorticity and the streamfunction, so that far from the jet

$$Q_n(\psi_n) \; = \; (-1)^n F_n\,(\psi_1 - \psi_2) \; + \; \alpha^2 \psi_n$$

where

$$\alpha^2 \; = \; (\beta/u_b)\,.$$

In the upper layer, the choice of $Q(\psi)$ is based on the existence of steep gradients of potential vorticity that exist in the upper waters of the Gulf Stream system east of Cape Hatteras. As in many contour dynamic models of zonal jets, these gradients are modeled as discontinuities in the potential vorticity function. The potential vorticity

in the upper layer is chosen to be

$$Q_1(\psi_1) \;=\; \alpha^2\psi_1 \;- F_1\,(\psi_1 - \psi_2) \;+\; J(\psi_1)$$

where the jumps in potential vorticity are represented by

$$J = \begin{cases} \Pi_1 & y > L_1(x) \\ \Pi_2 & L_2(x) > y > L_1(x) \\ \Pi_3 & y < L_2(x) \end{cases}$$

Note that $L_1(x)$ and $L_2(x)$ are the locations of streamlines, ψ_N and ψ_S, that separate the flow into three regions, across which the potential vorticity jumps.

It is further assumed that the zonal scales of the topography and the flow are much longer than the meridional scales and the deformation radius, and that u is much larger than v. In this case, the relative vorticity $\nabla^2\psi$ may be replaced by the shear, $\partial^2\psi/\partial y^2$.

With these assumptions, the potential vorticity equation becomes a set of coupled, ordinary differential equations

$$\partial^2\psi_1/\partial y^2 \;-\; F_1\,(\psi_1 - \psi_2) \;+\; \beta y \;=\; Q_1(\psi_1) \;=\; -F_1(\psi_1 - \psi_2) \;+\; \alpha^2\psi_1 \;+\; J$$
$$\partial^2\psi_2/\partial y^2 \;-\; F_2\,(\psi_2 - \psi_1) \;+\; \beta y \;+\; \eta_B \;=\; Q_2(\psi_2) \;=\; -F_2(\psi_2 - \psi_1) \;+\; \alpha^2\psi_2.$$

Because the coupled equations are piecewise-linear, they can be "diagonalized" leading to uncoupled equations for the barotropic and baroclinic modes

$$\partial^2\psi_T/\partial y^2 \;-\; \alpha^2\psi_T \;=\; -\beta y(1 + \frac{F_2}{F_1}) - \frac{F_2}{F_1}\eta_B \;+\; J \qquad (4.3)$$
$$\partial^2\psi_C/\partial y^2 \;-\; \left(\alpha^2 \;+\; F_1 \;+\; F_2\right)\psi_C \;=\; +\eta_B \;+\; J \qquad (4.4)$$

where

$$\psi_T = \psi_1 + \frac{F_2}{F_1}\psi_2 \quad \text{and} \quad \psi_C = \psi_1 - \psi_2.$$

Solutions to these uncoupled equations are easily found by assuming that the streamfunction and the velocity field must match across the jumps in potential vorticity. In addition, the zonal velocity field must approach the constant background value, $-u_b$ as $y \to \pm\infty$. The solutions are

$$\psi_T = \alpha^{-2}\left[\beta(1+\tfrac{F_2}{F_1})y + \tfrac{F_2}{F_1}\eta_B\right] + \begin{cases} (2\alpha^2)^{-1}\left[(\Pi_2-\Pi_3)e^{-\alpha\Delta L}+(\Pi_1-\Pi_2)\right]e^{-\alpha(y-L_1)} - \alpha^{-2}\Pi_1 & y > L_1 \\ (2\alpha^2)^{-1}\left[(\Pi_2-\Pi_1)e^{-\alpha(L_1-y)}+(\Pi_2-\Pi_3)e^{-\alpha(y-L_2)}\right] - \alpha^{-2}\Pi_2 & L_2 < y < L_1 \\ (2\alpha^2)^{-1}\left[(\Pi_2-\Pi_1)e^{-\alpha\Delta L}+(\Pi_3-\Pi_2)\right]e^{-\alpha(L_2-y)} - \alpha^{-2}\Pi_3 & y < L_2 \end{cases} \tag{4.5}$$

$$\psi_C = -\gamma^{-2}\eta_B + \begin{cases} (2\gamma^2)^{-1}\left[(\Pi_2-\Pi_3)e^{-\gamma\Delta L}+(\Pi_1-\Pi_2)\right]e^{-\gamma(y-L_1)} - \gamma^{-2}\Pi_1 & y > L_1 \\ (2\gamma^2)^{-1}\left[(\Pi_2-\Pi_1)e^{-\gamma(L_1-y)}+(\Pi_2-\Pi_3)e^{-\gamma(y-L_2)}\right] - \gamma^{-2}\Pi_2 & L_2 < y < L_1 \\ (2\gamma^2)^{-1}\left[(\Pi_2-\Pi_1)e^{-\gamma\Delta L}+(\Pi_3-\Pi_2)\right]e^{-\gamma(L_2-y)} - \gamma^{-2}\Pi_3 & y < L_2 \end{cases} \tag{4.6}$$

where $\gamma^2 = \alpha^2 + F_1 + F_2$. A sketch of a sample velocity profile for zonal flow far from the topography is shown in figure 4-3. The fronts of potential vorticity form an eastward jet, primarily in the upper layer, and there is a weak background barotropic flow that is directed to the west. The non-dimensional scales used for this figure are chosen to characterize the Gulf Stream. If we take $L \approx 100km$ and $U = 1ms^{-1}$, then the non-dimensional $\beta \approx 0.15$. The scales for the layer depths are $D_1 \approx 500m$ and $D_2 \approx 4000m$, which gives $F_1/F_2 = 8$. The transport is non-dimensionalized by $UL(D_1 + D_2) = 450Sv$. Using Mann's (1967) estimate of $50Sv$ entering the branching region gives a non-dimensional transport of $T_T = 1/9$. For these non-dimensional numbers, the potential vorticity fronts are quite close together, forming a single eastward jet, primarily in the upper layer and there is a weak background barotropic flow that is directed to the west.

The whole approach of this section is similar to Pratt (1989) who considered a double front of potential vorticity in the lower layer of a two layer model in which the upper layer was quiescent. In both cases, the model is carried out on the β-plane, with slowly-varying bottom topography. Since, in the present example, the

fronts and topography are in separate layers, the Pratt model is not a limit of this two-layer model as $D_1 \rightarrow \infty$. Yet, a comparison with Pratt (1989) shows that the barotropic component of the flow (4.5) is identical in form to the 1-1/2 layer solution; the only effect of the stratification is to temper the effect of the topography. This is in sharp contrast to contour dynamics calculations which behave quite differently for 1-1/2 layer models and models which do include a barotropic component. In contour dynamics, the potential vorticity is piecewise constant and the intrinsic length scale for each mode is the radius of deformation. Thus, if a barotropic mode is present, the infinitely-long barotropic deformation radius is the relevant length scale for that mode. The dynamical equation in that case is a Laplacian, rather than Helmholtz's equation; a difference which leads to a quite different Green's function for the barotropic mode. In the present calculations, the ambient potential vorticity gradient, α^2, determines the intrinsic length scale for the barotropic mode, and a Helmholtz equation, (4.3) is recovered.

Given the piecewise-linear potential vorticity function, are multiple barotropic states with the same $Q(\psi)$ and transport possible? For these flows, a natural choice for a measure of the transport is the flux through the center portion of the jet, between the two streamlines that lie along the fronts of potential vorticity. The barotropic transport is then

$$T_T = \psi_T(y = L_1) - \psi_T(y = L_2) \tag{4.7}$$

$$= \frac{1}{2}(\Pi_1 - \Pi_3)(1 - e^{-\alpha\Delta L} - \beta(1 + \frac{F_2}{F_1})\Delta L - \frac{F_2}{F_1}\beta_T \Delta L \tag{4.8}$$

which can be rewritten as

$$(1 + \frac{F_2}{F_1})\beta + \frac{F_2}{F_1}\beta_T = \frac{1/2(\Pi_1 - \Pi_3)(1 - e^{-\alpha\Delta L}) - \alpha^2 T_T}{\Delta L} \tag{4.9}$$

The left hand side is the total ambient potential vorticity gradient. Thus, for a given $Q(\psi)$ relationship, (4.9) determines the possible values of ΔL, which can exist for a given ambient potential vorticity gradient. Figure 4-4 illustrates how ΔL depends

on the topographic slope for a particular choice of $Q(\psi)$. It is clear from (4.9), that when the total ambient potential vorticity gradient approaches zero, one of the two solutions has $\Delta L \to \infty$. Thus, two alternate states are possible only when the total ambient potential vorticity gradient is positive and less than a critical value which depends on the particular choice of $Q(\psi)$. The critical slope can be found for arbitrary piecewise linear $Q(\psi)$ by differentiating (4.9) with respect to ΔL and then using (4.9) to eliminate T_T

$$\beta_T(critical) = \frac{F_1}{F_2}\frac{\alpha}{2}(\Pi_1 - \Pi_3)e^{-\alpha\Delta L_c} - (\frac{F_1}{F_2} + 1)\beta. \tag{4.10}$$

In this particular example, the critical topographic slope is $\beta_T \approx 0.22$; in dimensional units this corresponds to a depth change of approximately $1000m$ over $100km$ in latitude, a value which is consistent with the change in depth southeast of the Grand Banks of Newfoundland. The alternate state is a split flow.

4.4 Discussion

Two different potential vorticity functions in an unbounded domain were considered in this chapter. The first had a nonlinear $Q(\psi)$ function bounded by two fronts of potential vorticity which separated the interior region from an exterior flow with a linear $Q(\psi)$. The specific functional form of the interior $Q(\psi)$ was chosen to be the same as the Bickley jet. Multiple solutions were found for β less than a critical value which depends on the specific $Q(\psi)$ function chosen. In the particular example given, two symmetric solutions exist for $\beta < 0.22$, and two branches of asymmetric solutions bifurcate off of the curve of symmetric solutions. Because of the fronts of potential vorticity, the velocity profiles do not look like the Bickley jet, or a split jet. The choice of the fronts and the exterior potential vorticity was arbitrary, and simply chosen to allow the velocity field to decay as $y \to \pm\infty$. Another choice for the potential vorticity might be to use the nonlinear Bickley $Q(\psi)$ function in the exterior with a different function in the interior, representing the split flow. However,

there is no a priori way of determining the function $Q(\psi)$ in the interior.

The second set of velocity profiles has a piecewise linear $Q(\psi)$ in two layers. This two-layer system was chosen to have transport values, layer depths and potential vorticity fronts that are consistent with Gulf Stream values. The $Q(\psi)$ function also exhibits multiple states for ambient potential vorticity gradients less than a critical value, which in this case can be determined analytically. For the Gulf Stream parameters, the value of the critical gradient is consistent with the topographic slope southeast of the Grand Banks. This system does not have any symmetry-breaking pitchfork bifurcations; the only way the piecewise linear potential vorticity can have asymmetric velocity profiles is through an asymmetry in the potential vorticity function itself.

These two examples exhibit two differences from the results for a bounded domain. In the channel geometry, at least one solution with the original $Q(\psi)$ exists for all ambient potential vorticity gradients. In the present examples, solutions do not exist if the ambient potential vorticity exceeds some critical value. If the ambient potential vorticity is raised above this critical value, then the flow must adjust to some other $Q(\psi)$ distribution, since there is no other solution branch with the original $Q(\psi)$ to which the flow can adjust. In addition, the turning points of the solution curve do not correspond to stability thresholds. In the first example of this chapter, both sets of solutions on either side of the turning point are unstable. This implies that if a zonal flow lying on one branch is perturbed, it does not equilibrate to a zonal flow on the other branch with the same $Q(\psi)$ since that solution is unstable as well. Presumably, the flow will equilibrate to some other $Q(\psi)$ distribution, or perhaps a periodic flow. To explore these issues, numerical adjustment problems similar to those in chapter 3, would have to be carried out.

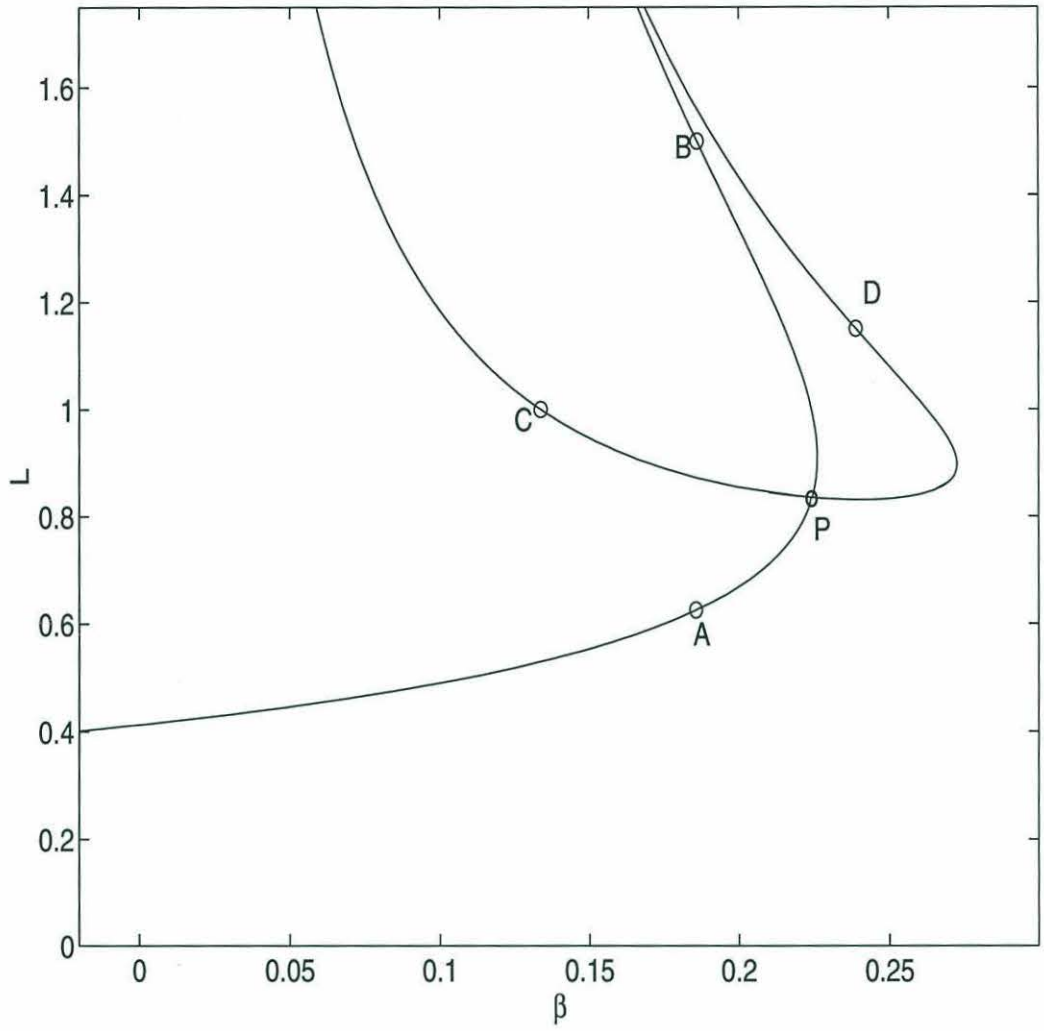

Figure 4-1: Solution curves showing L, the latitude of the jump in Q as a function of β.

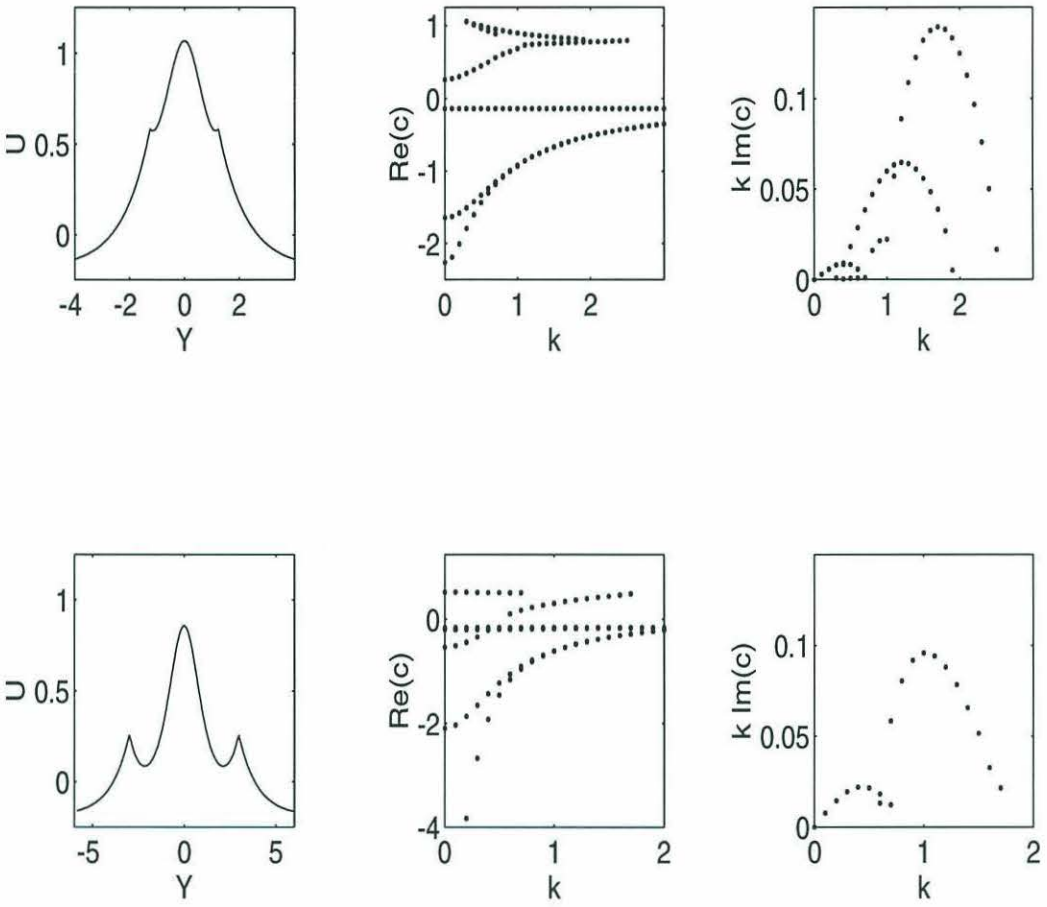

Figure 4-2: Velocity profiles and dispersion relationships for solution A (upper panels) and B (lower panels).

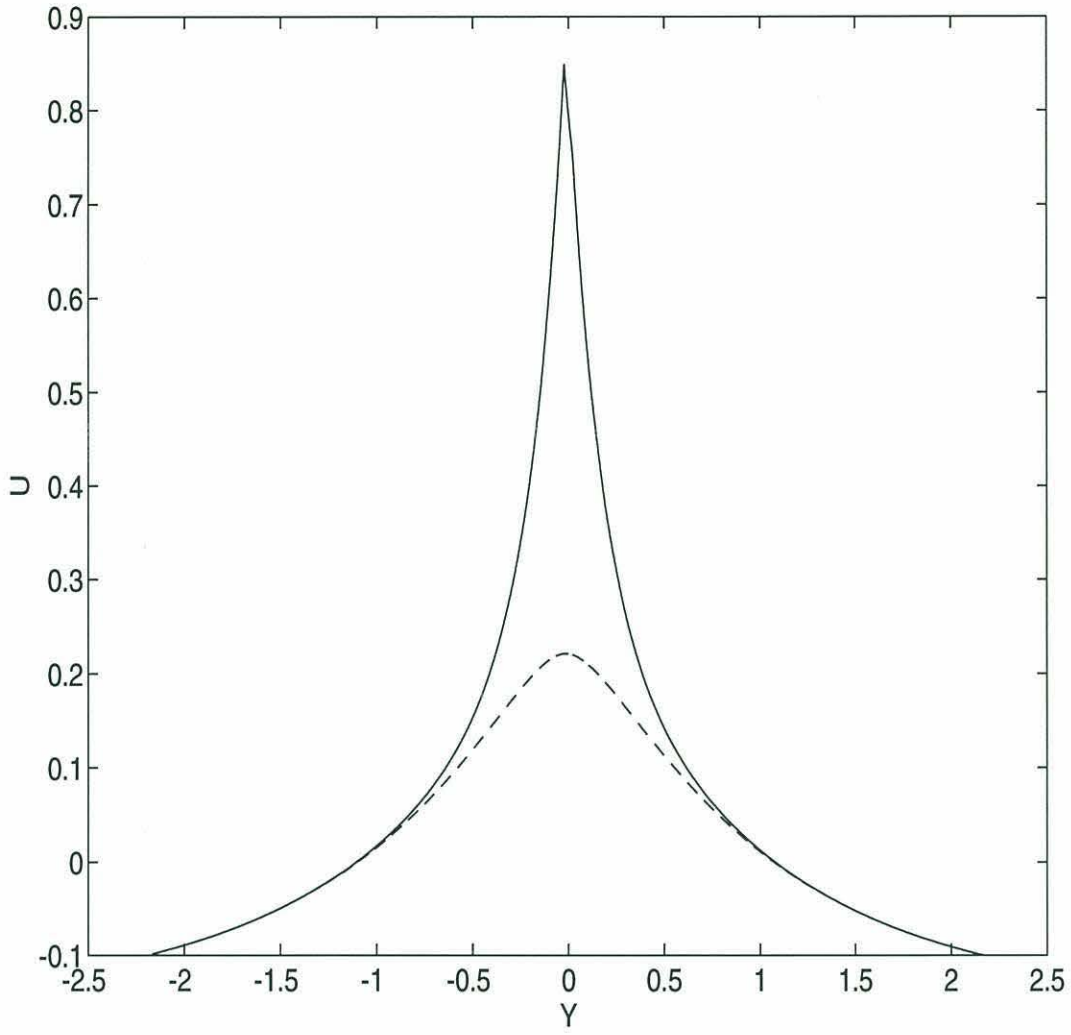

Figure 4-3: A sample velocity profile for the case $\alpha = 1$, $\beta = 0.15$, $a - b = 6.5$, $b - c = 1.5$, $\beta_T = 0$, $F_1/F_2 = 8$. The solid line shows the velocity profile in the upper layer; the dashed line shows $u(y)$ in the lower layer.

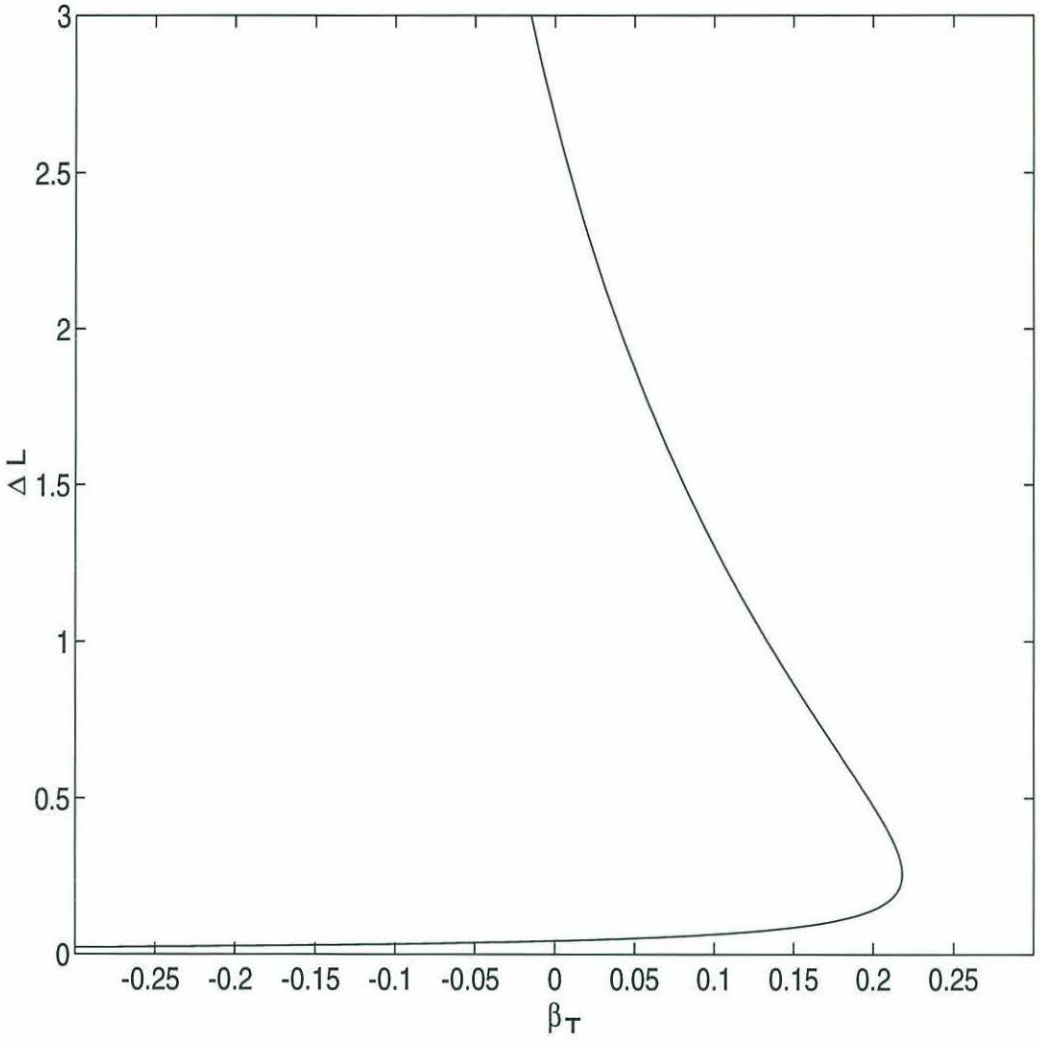

Figure 4-4: Solution curve showing ΔL as a function of β_T for the parameter values chosen in figure 4-3.

Chapter 5

Conclusions

This thesis was concerned with the dynamics behind the splitting of jets in the atmosphere and the ocean. Observations of such phenomena, discussed in chapter 1, indicate that the transitions are fairly persistent in time and that the double-jet structure is quite long in space. These observations suggest considering transitions between zonally-uniform equilibrium states. One such theory, originally suggested by Rossby (1950) to account for atmospheric blocking, is based on an analogy with open channel hydraulics. Previous authors (Pratt (1989) and Woods (1993)) have interpreted the existence of multiple flows with the same $Q(\psi)$ relationship as an indication that the flow behaves as a hydraulic system; transitions between alternate states can occur if the ambient potential vorticity gradient is varied (by, for instance, topography) along the direction of the flow. Another theory to account for local changes in a zonal flow are the theories of local instability. The work by Pierrehumbert (1984) and Samelson and Pedlosky (1990) indicate that changes in the topographic gradient could render the flow locally unstable, and the disturbance is felt downstream of the topography and not upstream. By inference, this suggests that the $Q(\psi)$ relationship is carried from the upstream flow to a different velocity structure downstream.

In an attempt to understand these transitions, several questions were addressed. The first asks, rather generally, what conditions are necessary for a given $Q(\psi)$ function to have several different velocity structures? Then, given the existence of these alternate states, it is necessary to consider the dispersion characteristics of such flows,

and the time-dependent adjustment of them to topographic perturbations to determine the extent to which the hydraulic analogy holds and also if and how the instabilities of the flow equilibrate.

By referring to the theory of two-point boundary value problems, chapter 2 established conditions on $Q(\psi)$ which cause the potential vorticity equation to have a unique solution. If $\frac{dQ}{d\psi}$ is positive everywhere in the fluid domain, then the velocity structure is unique; note that this condition is identical to Arnol'd's first stability theorem. If $\frac{dQ}{d\psi}$ is negative somewhere in the flow, but it is bounded from below by the meridional wavenumber of the finite domain, then the flow is unique. This condition is identical to Arnol'd's second theorem, which guarantees stability in the bounded domain. The violation of these conditions give a necessary condition for multiplicity, as well as the equivalent necessary condition for instability. Another important condition for alternate states is that $Q(\psi)$ is nonlinear. If $\frac{dQ}{d\psi}$ is a constant, then section 2.6 shows that either 1) there is a unique solution or 2) there can be an uncountable infinity of solutions which satisfy the potential vorticity equation, since, in that case, the amplitude of the sinusoidal wave is not specified by the boundaries. To have a discrete set of alternate states, $\frac{dQ}{d\psi}$ must not be a constant. It is interesting to note that the weakly nonlinear theories also demand that $\frac{d^2Q}{d\psi^2}$ be non-zero for the existence of solitary waves.

The onset of instability and the existence of multiple equilibria were shown to coincide for the barotropic instability problem considered in section 2.7, in which the potential vorticity varied sinusoidally with the streamfunction. On the stable side of the stability threshold, there exists a unique stable solution without normal modes. Multiple solutions arise at a pitchfork bifurcation as a stability parameter is raised above the stability threshold determined by the necessary condition for instability. The center branch of the pitchfork is unstable to the gravest mode, while the two outer branches do not even have discrete modes. Other pitchfork bifurcations occur as higher meridional modes become unstable. Again, the inner branch is unstable to the next gravest mode, while the outer branches do not support this discrete mode. These results place the barotropic instability problem into a large set of nonlinear

systems described by bifurcation theory. However, if the eastward transport across the channel is large enough, the normal modes may stabilize and these waves have a phase speed less than the minimum velocity of the flow. In this case, the flow is analogous to sub-critical hydraulic flow.

In Chapter 3 the time-dependent evolution of the jets described in §2.7.2 was examined, to consider whether transitions among alternate states take place and whether these are due to hydraulic behavior or the equilibration of localized instabilities. If the equilibrium is unstable, then the disturbance will cause the flow to equilibrate to some new, stable (although not necessarily steady) equilibrium as the instability mechanism saturates. In chapter 3, potential vorticity was altered by the introduction of a topographic feature. The meridional slope of the topography varies slowly in the zonal direction, allowing a slow change in the dispersion characteristics of vorticity waves which depend on dQ/dy. Three different types of adjustments to other zonally uniform states were observed in chapter 3, and these are described below.

For stable, subcritical flow it has been shown that the adjustment proceeds in a similar way to the hydraulic adjustment experiments of Long (1954) and Pratt (1983). A transition to a supercritical eastward jet takes place over the topography when $\beta + \beta_T$ exceeds the critical value determined by the steady state theory. Note that this change in the ambient potential vorticity enhances the stability of the flow. Upstream and downstream influence take place simultaneously, as the topography controls the flow. In this case the vorticity waves, and specifically the second cross-channel mode, play the role of gravity waves in the open channel hydraulic adjustment. However, in the quasi-geostrophic example presented here, the waves do not carry any mass, so the transition is effected by shifting potential vorticity into a new equilibrium distribution.

If the initial flow was unstable, or made unstable in a localized region by the topography, then the instability dominates the evolution. When the flow field outside of the topography is more unstable than the localized region, plane waves are excited and destroy any localized signal of the initial perturbation. On the other hand, if the

instability is localized by the topography, because the initial flow is stable or just less unstable than the local region, then the instability grows only over the topography, and then spreads eastward. The flow evolves into a split jet on the downstream face of the topography. Although the interior is westward, the streamlines are all connected to the upstream flow, and the reversed flow arises as some streamlines "wrap-around." During the adjustment a potential vorticity wave also propagates upstream, causing the $Q(\psi)$ relationship to change there. Accordingly, in the local instability problem, the topography has exerted upstream influence on the flow and the fluid can be said to be "controlled" by the topography, since a change in the local topography causes changes in the far field. By the final time step, both up- and downstream have the same $Q(\psi)$ on all streamlines originating from upstream. Because of the westward interior, the downstream state bears a qualitative resemblance to the solutions along the lower branch of figure 3-1, and it is tempting to think of this transition between two alternate zonal flows (with the same $Q(\psi)$) as a catastrophic jump from the unstable equilibrium branch to a stable branch.

When the initial flow was a strong eastward jet with no varicose mode, hydraulic transitions are not possible. Anomalous potential vorticity is trapped over the topography when β_T exceeds the critical value, yet the flow up- and downstream is virtually symmetric. Nothing resembling a hydraulic jump forms, precisely because there is no varicose mode to cause energy to converge in the fluid. Only when β_T is nearly double the critical value does an abrupt transition take place. As a result of the large disturbance, the flow reaches a new zonal equilibrium with the same $Q(\psi)$ relationship everywhere in the flow. Although the transition did not take place when β_T was at its critical value, these runs are still consistent with the notion of a catastrophic jump. In the present case, as β is increased, the flow does pass along the solution branch until it merges with another equilibrium state. However, because this equilibrium is also stable, there is no mechanism to amplify small disturbances and cause the flow to move to a new equilibrium. It is only when the disturbance itself is quite large that a new state is achieved. As in the previous run, the new zonal flow bears a qualitative resemblance to the solutions along the lower branch of the solution

curve in figure 3-1. In this case, no upstream influence is felt, precisely because no varicose mode exists to carry the signal upstream and away from the region of the topography.

This thesis has established a connection between the previous work of "hydraulics" theories and the barotropic instability of the flow. Both types of dynamics arise from adjustments among multiple equilibria. The stable, eastward flow is subject to hydraulic control and establishes a narrow eastward jet downstream of the region of topography, while exerting influence upstream. The control is established only when the topographic slope exceeds a critical value, determined by the semi-analytical theory. If the same eastward flow is made locally unstable by topography, then a "split flow" is established downstream, and upstream influence is again felt. In both cases, the topography "controls" the fluid, and the final state depends on the sign of the topographic slope. A hallmark of both of these phenomena is that $Q(\psi)$ is maintained across the transition, although it has adjusted from its original upstream form. Hydraulic behavior only appears when the flow is broad and stable. If the flow is unstable at any wavelengths, hydraulic control is not established and instead the instability dominates the evolution. The localized instability, which causes a "splitting" is probably more relevant since geophysical flows are never firmly stable, but rather only marginally so.

Several interesting questions about the equilibration of disturbed flows have been raised in this thesis. Both processes, stable hydraulic control and the local instability, produce a transition between quite different zonal flows which nevertheless share the same $Q(\psi)$ structure. However, the observations of atmospheric blocking show that the flow is not particularly zonal after the split. An area of future work involves looking for multiple states which are x-dependent, and determining whether transitions between them take place when modes with finite wavelengths are unstable. These considerations suggest that a semi-analytical model of the nonlinear equilibration of local instabilities could possibly be constructed in the future, if the change in $Q(\psi)$ from its original form was understood. Another interesting question regards the equilibration of instabilities in an unbounded domain, in which all of the alternate velocity

profiles are unstable. The thesis suggests that the flow can not equilibrate to a zonal alternate, and must find another equilibrated form. It is clear that an answer to either question can not be found by considering the multiple velocity structures that have the same $Q(\psi)$ as the original flow, since an adjustment of $Q(\psi)$ takes place during the evolution. However, perhaps by considering other constants of the motion, such a model could be constructed.

Finally, I would like to say a few words regarding the relevance of this thesis to actual flows in the atmosphere and the ocean. Clearly, the assumptions made and the velocity structures used were over-simplifications which may have made the problem tractable, but eliminated very important dynamical effects due to stratification, and external forcing. However, these simplifying assumptions, which reduced the potential vorticity equation to its simplest possible form, did suggest several processes which have hitherto gone unnoticed in the context of the instability of geophysical flows. Nevertheless, some of these assumptions should be examined to test whether their inclusion would alter the conclusions of the thesis.

One simplification was the use of a single layer to model the dynamics of geophysical systems which typically need at least two or three layers to accurately model their full dynamics. However, the principal dynamics involving topographic forcing and nonlinear interaction due the advective terms may be studied in the context of a barotropic model. Work by Helfrich and Pedlosky (1994) indicates that the baroclinic instability equilibrates to alternate $Q(\psi)$ structures as well. In the one example of this thesis with two-layers, the lower layer only served to insulate the upper layer with the jet from the topography. The existence of multiple states was unaffected by the addition of a second layer.

Another concern is the importance of the varicose wave in this work, even though, for most jets, the sinuous wave typically has a larger growth rate and dominates the observed fluctuations of the Gulf Stream. Even for the $Q = -\sin\psi$ jets considered here, the sinuous mode has a larger growth rate than the the varicose mode and the fully nonlinear adjustment calculations show large amplitude meanders (reflected from the "sponge") that are consistent with the dispersion characteristics of the basic flow.

Indeed, for the "split" initial condition (described in section 3.6), the meandering motion quickly dominated the evolution and there is no sign of a "jump" to another symmetric state. However, for the other initial conditions, the meanders do not affect the finite-amplitude equilibration of the varicose mode and the conclusion is that the "splitting" due to the finite-amplitude varicose motion is possible in the presence large amplitude meanders, although this issue needs to be examined more carefully.

Although the potential vorticity structures used in the numerical calculations are too simple to be an accurate model of the Gulf Stream, the multiple solutions arise at realistic values of the non-dimensional parameters. For instance, in the Gulf Stream, typical values of $\beta = \frac{\beta^* L^2}{U}$ range between 0.05 and 0.3, which are within the range of values for which the $Q = -\sin\psi$ system has multiple solutions. Even though the choice of $Q = -\sin\psi$ was arbitrary, the Gulf Stream and other geophysical jets are considered to be unstable and the thesis suggests that they are therefore also non-unique.

In the introductory chapter, it was stated that an objective of the thesis was to examine the theory of planetary scale hydraulics in order to explore its strengths as a conceptual model for understanding the dynamics of geophysical zonal jets, which are typically unstable. This issue will now be examined by discussing several features of the hydraulics and instability theories.

There are several features which indicate that hydraulic control has been established

- The topography exerts its influence into the far-field, "controlling" the flow.
- There is a strong asymmetry in the flow in the along-stream direction; the flow is subcritical upstream of the topography and supercritical downstream.
- A jump is established downstream, bringing the supercritical flow back to its its original, undisturbed form.

In chapter 3, a localized instability problem was examined, and this example does indeed exhibit these features. For instance, although the flow only exceeded the stability threshold in a localized region, the influence of this region was felt far down

field, as the "rolled-up" region slowly spreads downstream, filling the eastern half of the domain. Upstream influence is also felt, as a vorticity wave propagated upstream, altering the $Q(\psi)$ structure. In addition, the field shows a strong asymmetry in the along-channel direction; the flow undergoes a transition from a nearly uniform, eastward flow on the upstream side of the topography, to a "split" flow with a westward interior, on the downstream side. The transition takes place right at the crest of the ridge where there is a stagnation point. Finally, in the downstream flow, the "roll-up" region is connected to the undisturbed flow by a strong meridional jet, which propagates downstream.

At a fundamental level, a hydraulic control is a resonance phenomenon. When the flow is at or near the critical condition, large changes in the flow may be brought about by small changes in geometry of the flow (either the level of the bed, or the horizontal width of the flow). One conceptual picture of non-dissipative shear instabilies is also based on the phenomenon of resonance. For example, Lighthill (1963), Bretherton (1966b) and Hoskins *et al.* (1985), Hayashi and Young (1987) show that shear instability operates when two counter-propagating vorticity waves remain stationary relative to each other. Another example is the 'orographic' instability considered by Plumb (1981) and described by McIntyre and Shepherd (1987). The instability is suppressed if the domain is such that stationary Rossby waves can not exist, preventing the resonance, or self-tuning phenomenon from working.

The theory of hydraulics led to a consideration, in chapter 2, of multiple equilibria in an unforced, inviscid system. This is in contrast to other multiple equilibria theories, such as Charney and DeVore (1979) which are carried out for forced, dissipative systems. It is suggested that there is an internal mechanism due to localized instability, or hydraulic control, which can provide a transition among free modes.

The lack of external forcing may actually be a strength of the present model since there is evidence that observed transitions (discussed in chapter 1) are due to internal mechanism, rather than external forcing. For instance, Kelly (1991) concludes that the New England Seamount Chain is the site of an abrupt transition from a narrow supercritical jet to a jet with large amplitude meanders which have no con-

sistent propagation direction. However, this region is also a region of maximum heat flux and wind stress, so that local atmospheric forcing may also cause changes in the Gulf Stream there. Ezer (1994) addressed this issue using a primitive equation model forced by climatological wind stresses and heat fluxes. By comparing a simulation with the full bottom topography, with a control run without the New England Seamount Chain, he demonstrated that the topography has a significant influence on the variability and energetics of the Gulf Stream. In particular, the Gulf Stream broadens as it passes over the seamount chain, and several recirculation cells develop in the region; these features are consistent with Kelly's observations, and indicate that the topography, not external forcing, causes the transition. An examination of the results of similar numerical experiments by Thompson and Schmitz (1989), indicates that the splitting of the Gulf Stream is also caused by topography (the Newfoundland Rise), and not external forcing.

In addition, there is considerable evidence that atmospheric blocks may be considered as a free mode of the atmospheric system, not simply because of their longevity, but because observational studies show that their is a close coincidence of potential vorticity contours and streamlines in the atmosphere (Illari and Marshall, 1983; Butchart, *et al.,* 1989). These studies used scatter plots of Q, the quasi-geostrophic potential vorticity, versus the streamfunction and showed that the functional relationship between the two is nearly linear, with a negative slope, which is consistent with the necessary condition for multiple equilibria established here. If the block is strongly nonlinear, then the interior region is a closed patch of potential vorticity, the value of which must be determined through a balance of forcing and dissipation, as described by Pierrehumbert and Malguzzi (1984). However, the observational studies of blocking by Illari (1982) and Miyakoda *et al.* (1983) show no closed streamlines, suggesting that they are not a necessary component of blocking. In that case, the existence of unforced equilibria may be a more appropriate description of the free modes observed in the atmosphere.

References

Armi, L., Hydraulic control of zonal currents on a β-plane, *J. Fluid Mech., 201,* 357–377, 1989.

Arnol'd, V. I., On an a-priori estimate in the theory of hydrodynamical stability, *Eng. transl.: 1969, Am. Math. Soc. Transl. Ser. 2, 79,* 267–269, 1966.

Bailey, P. and P. Waltman, On the distance between consecutive zeros for second order differential equations, *J. Math. Anal. Appl., 14,* 23–30, 1966.

Bailey, P., L. Shampine, and P. Waltman, *Nonlinear Two Point Boundary Value Problems,* Academic Press, 1968.

Ball, F. K., Long waves, lee waves and gravity waves, *Q. J. R. Met. Soc., 85,* 24–30, 1954.

Batchelor, G. K., *An Introduction to Fluid Dynamics,* Cambridge University Press, Cambridge, 1985.

Bell, G. and L. Pratt, Eddy-jet interaction the potential vorticity flows, *submitted,* 1994.

Benjamin, T. B., Theory of the vortex breakdown phenomenon, *J. Fluid Mech., 12,* 593–629, 1962.

Benjamin, T. B., Internal waves of finite amplitude and permanent form, *J. Fluid Mech., 25,* 241–275, 1966.

Benjamin, T. B., Some developments in the theory of vortex breakdown, *J. Fluid Mech., 28,* 65–84, 1967.

Benjamin, T. B., Applications of Leray-Schauder degree theory to problems of hydrodynamic stability, *Math. Proc. Camb. Phil. Soc., 79,* 373–392, 1976.

Benjamin, T. B., Bifurcation phenomena in steady flows of a viscous fluid I. Theory, *Proc. R. Soc. London A, 359,* 1–26, 1978a.

Benjamin, T. B., Bifurcation phenomena in steady flows of a viscous fluid II. Experiments, *Proc. R. Soc. London A, 359,* 27–43, 1978b.

Benjamin, T. B., Steady flows drawn from a stably stratified reservoir, *J. Fluid Mech., 106,* 245–260, 1981.

Benjamin, T. B., Impulse, flow force and variational principles, *IMA Journal of Appl. Math., 32,* 3–68, 1984.

Beran, P. S. and F. E. C. Culick, The role of non-uniqueness in the development of vortex breakdown in tubes, *J. Fluid Mech., 242,* 491–527, 1992.

Berggren, R., B. Bolin, and C. G. Rossby, An aerological study of zonal motion, its perturbations and breakdown, *Tellus, 1,* 14–37, 1949.

Bernfeld and Lakshmikanthan, *An Introduction to Nonlinear Two-Point Boundary Value Problems,* Academic Press, 1974.

Bickley, W., The plane jet, *Phil. Mag., 23,* 727–731, 1937.

Binnie, A. M., The passage of a perfect fluid through a critical cross-section or 'throat', *Proc. Roy. Soc. A, 197,* 545–555, 1949.

Blandford, R. R., Inertial flow in the Gulf Stream, *Tellus, 17,* 69–76, 1965.

Bretherton, F. P., Critical layer instability in baroclinic flows, *Q. J. Royal Meteor. Soc., 92,* 325–334, 1966a.

Bretherton, F. P., Baroclinic instability and the short wavelength cut-off in terms of potential vorticity, *Q. J. Royal Meteor. Soc., 92,* 335–345, 1966b.

Butchart, N., K. Haines, and J. C. Marshall, A theoretical and diagnostic study of solitary waves and atmospheric blocking, *J. Atmos. Sci., 46,* 2063–2078, 1989.

Canuto, C., M. Y. Hussaini, A. Quarteroni, and T. A. Zang, *Spectral methods in fluid dynamics,* Spring-Verlag, New York, 1988.

Carnevale, G. and J. S. Frederiksen, Nonlinear stability and statistical mechanics of flow over topography, *J. Fluid Mech., 175,* 157–181, 1987.

Charney, J. G. and J. G. DeVore, Multiple flow equilibria in the atmosphere and blocking, *J. Atmos. Sci., 36,* 1205 –1216, 1979.

Charney, J. G., The Gulf Stream as an inertial boundary layer, *Proc. Nat. Acad. Sci., 41,* 731–740, 1955.

Clarke, R. A., H. W. Hill, R. F. Reiniger, and B. A. Warren, Current system south and east of the Grand Banks of Newfoundland, *J. Phys. Oceanogr., 10,* 26–65, 1980.

Courant, R. and D. Hilbert, *Methods of Mathematical Physics,* Interscience Publishers, New York, 1953.

Dole, R. M. and N. D. Gordon, Persistent anomalies of the extratropical Northern Hemisphere wintertime circulation: Geographical distribution and regional persistence characteristics, *Mon. Wea. Rev., 111,* 1567–1586, 1983.

Dole, R. M., *Persistent anomalies of the extratropical Northern Hemisphere wintertime circulation,* PhD thesis, MIT, 1982.

Drazin, P. G., D. N. Beaumont, and S. A. Coker, On Rossby waves modified by basic shear, and barotropic instability, *J. Fluid Mech., 124,* 439–456, 1982.

Dritschel, D. G., Nonlinear stability bounds for an inviscid, two-dimensional, parallel or circular flows with monotonic vorticity and the analogous three-dimensional quasi-geostrophic flows, *J. Fluid Mech., 191,* 575–581, 1988.

Ezer, T., On the interaction between the Gulf Stream and the New England seamount chain, *J. Phys. Oceanogr., 24,* 191–204, 1994.

Fofonoff, N. P., Steady flow in a frictionless, homogeneous ocean, *J. Mar. Res., 13,* 254–262, 1954.

Gill, A., The hydraulics of rotating channel flow, *J. Fluid Mech., 80,* 641–671, 1977.

Gordon, A. L., E. J. Malinelli, and T. N. Baker, *Southern Ocean Atlas,* Columbia University Press, 248 plates,42pp., 1986.

Green, J. S. A., The weather during July 1976: Some dynamical considerations concerning the drought, *Weather, 32,* 120–128, 1977.

Haidvogel, D. B., On the feasibility of particle tracking in Eulerian ocean models, *Ocean Modelling (Unpub. man.), 45,* 1982.

Haines, K. and P. Malanotte-Rizzoli, Isolated anomalies in westerly jet streams: A unified approach, *J. Atmos. Sci., 48,* 510–526, 1991.

Haines, K. and J. Marshall, Eddy-forced coherent structures as a prototype of atmospheric blocking, *Q. J. R. Meteorol. Soc.,* pp. 681–704, 1987.

Hall, M. M. and N. P. Fofonoff, Downstream Deviation of the Gulf Stream from 68° *W* to 55° *W*, *J. Phys. Oceanogr., 23,* 225–249, 1993.

Hansen, A. R. and T. C. Chen, A spectral energetics analysis of atmospheric blocking, *Mon. Wea. Rev., 110,* 1146–1165, 1982.

Hayashi, Y. and W. Young, Stable and unstable shear modes of rotating parallel flows in shallow water, *J. Fluid Mech., 184,* 477–504, 1987.

Haynes, P. H., E. R. Johnson, and R. G. Hurst, A simple model of Rossby-wave hydraulic behavior, *J. Fluid Mech., 253,* 359–384, 1993.

Helfrich, K. R. and J. Pedlosky, Time-dependent isolated anomalies in zonal flows, *J. Fluid Mech., 251,* 377–409, 1993.

Helfrich, K. R. and J. Pedlosky, Large-amplitude coherent anomalies in baroclinic zonal flows, *submitted,* 1994.

Helland-Hansen, B., *The Depths of the Ocean,* pp. 210–306, J. Murray, London, 1912.

Hogg, N. G., Hydraulic control and flow separation in a multi-layered fluid with applications to the Vema channel, *J. Phys. Oceanogr., 13,* 695–708, 1983.

Hoskins, B. J., M. E. McIntyre, and A. W. Robertson, On the use and significance of isentropic potential vorticity maps, *Q. J. Roy. Met. Soc., 111,* 877–946, 1985.

Howard, L. N., Note on a paper by John W. Miles, *J. Fluid Mech., 10,* 509–512, 1961.

Howard, L., The number of unstable modes in hyd. stab. problems, *J. Mecan, 3,* 433–443, 1964.

Hua, B. L., The conservation of potential vorticity along Lagrangian trajectories in simulations of eddy-driven flows, *J. Phys. Oceanogr., 24,* 498–508, 1994.

Huang, R. X., On the structure of inertial western boundary currents with two moving layers, *Tellus, 42A,* 594–604, 1990a.

Huang, R. X., Matching a ventilated thermocline model with inertial western boundary currents, *J. Phys. Oceanogr., 20,* 1599–1607, 1990b.

Hughes, R. L., Multiple criticalities in coastal flows, *Dyn. Atmos. Oceans, 9,* 321–340, 1985.

Hughes, R. L., On the rolse of criticality in coastal flows over irregular bottom topography, *Dyn. Atmos. Oceans, 10,* 129–147, 1986.

Hughes, R. L., The role of higher shelf modes in coastal hydraulics, *J. Mar. Res., 45,* 33–58, 1987.

Illari, L. and J. C. Marshall, On the interpretation of eddy fluxes during a blocking episode, *J. Atmos. Sci., 40,* 2232–2242, 1983.

Illari, L., A diagnostic study of the potential vorticity in a warm blocking anticylcone, *J. Atmos. Sci., 40,* 1595–1612, 1984.

Iselin, C., A study of the circulation of the western North Atlantic, *Papers in Physical Oceanography and Meteorology, 4,* 4–101, 1936.

Kelly, K. A., The meandering Gulf Stream as seen by the Geosat altimeter: surface transport, position and velocity variance from 73° to 46° W, *J. Geophys. Res., 96,* 16721–16738, 1991.

Koshlyakov, M. N. and T. G. Sazhina, Water circulation and a cylconic ring in the Gulf Stream splitting region in May-June 1990, *J. Geophys. Res., 99,* 14091–14100, 1994.

Krauss, W., R. H. Kase, and H. H. Hinrchsen, The branching of the Gulf Stream southeast of the Grand Banks, *J. Geophys. Res., 95,* 13089–13103, 1990.

Kuo, H. L., Dynamic instability of two-dimensional non-divergent flow in a barotropic atmosphere, *J. Met., 6,* 105–122, 1949.

Lee, T. and P. Cornillon, Propagation of Gulf Stream meanders between 74° and 70° W, *J. Phys. Oceanogr., submitted,* 1994a.

Lee, T. and P. Cornillon, Propagation and growth of Gulf Stream meanders between 75° and 45° W, *J. Phys. Oceanogr., submitted,* 1994b.

Lettenmeyer, F., Uber die von einem Punkt ausgehenden Intergalkurven einer Differentialgleichung 2. Ordung, *Deutsche Math., 7,* 56–74, 1944.

Lighthill, M. J., *Laminar boundary layers,* chapter Introduction, Oxford University Press, 1963.

Long, Some aspects of the flow of stratified fluids II. Experiments with a 2-fluid system, *Tellus, 5,* 97–115, 1954.

Lozier, M. S. and S. Rizer, Potential vorticity dynamics of boundary currents in a quasi-geostrophic ocean, *J. Phys. Oceanogr., 19,* 1373–1396, 1989.

Luyten, J. and H. Stommel, Upstream effects of the Gulf Stream, *Prog. Oceanogr., 14,* 387 – 399, 1985.

Malguzzi, P. and P. Malanotte-Rizzoli, Nonlinear stationary Rossby waves on non-uniform zonal winds and atmospheric blocking. Part I: The analytical theory, *J. Atmos. Sci., 41,* 2620–2628, 1984.

Mann, C. R., The termination of the Gulf Stream and the beginning of the North Atlantic current, *Deep Sea Research, 14,* 337–359, 1967.

Marshall, D. and J. Marshall, Zonal penetration scale of midlatitude jets, *J. Phys. Oceanogr., 22,* 1018–1032, 1992.

McIntyre, M. E. and T. G. Shepherd, An exact local conservation theorem for finite-amplitude disturbances to non-parallel shear flows, with remarks on Hamiltonian structure and on Arnol'd's stability theorems, *J. Fluid Mech., 181,* 527–565, 1987.

Miyakoda, K., T. Gordon, R. Caverly, W. Stern, J. Sirutis, and W. Bourke, Simulation of a blocking event in January 1977, *Mon. Wea. Rev., 111,* 846–949, 1983.

Mizuno, K. and W. B. White, Annual and interannual variability in the Kuroshio current system, *J. Phys. Oceanogr., 13,* 1347–1867, 1983.

Nowlin, W. D. and M. Clifford, The kinematic and thermohaline zonation of the Antarctic Circumpolar Current at Drake Passage, *J. Mar. Res. (Suppl.), 41,* 481–507, 1982.

Orszag, S. A., Numerical simulations of incompressible flows within simple boundaries: accuracy, *J. Fluid Mech., 49,* 75–112, 1971.

Pedlosky, J., The stability of currents in the atmosphere and the ocean: Part I, *J. Atmos. Sci., 21,* 201–219, 1964.

Perov, A. I., A boundary value problem for a system of two differential equations, *Dokl. Akad. Nauk. SSR,* pp. 759–762, 1962.

Picard, E., Sur l'application des méthods d'approximations successives à l'étude de certains equations différentielles ordinaires, *J. Math., 9,* 219–271, 1893.

Pierrehumbert, R. T. and P. Malguzzi, Forced coherent structures and local multiple equilibrium in a barotropic atmosphere, *J. Atmos. Sci., 41,* 246–257, 1984.

Pierrehumbert, R. T. , Local and global baroclinic instability of zonally varying flow, *J. Atmos. Sci., 41,* 2141 – 2162, 1984.

Plumb, R. A., Instability of the distorted polar night vortex: a theory of stratospheric warmings, *J. Atmos. Sci., 38,* 2514–2531, 1981.

Pratt, L. J. and L. Armi, Hydraulic control of flows with nonuniform potential vorticity, *J. Phys. Oceanogr., 17,* 2016–2029, 1987.

Pratt, L. J. and P. A. Lundberg, Hydraulics of rotating strait and sill flow, *Ann. Rev. Fluid Mech., 23,* 81–106, 1991.

Pratt, L. J., On inertial flow over topography. Part 1. Semigeostrophic adjustment to an obstacle, *J. Fluid Mech., 131,* 195–218, 1983.

Pratt, L. J., On nonlinear flows with multiple obstructions, *J. Atmos. Sci., 41,* 1214–1225, 1984a.

Pratt, L., On inertial flow over topography. Part 2. Rotating-channel flow near the critical speed, *J. Fluid Mech., 145,* 95–110, 1984b.

Pratt, L., Critical control of zonal jets by bottom topography, *J. Mar. Res., 47,* 111–130, 1989.

Rex, D. F., Blocking action in the middle troposhere and its effects upon regional climate, *Tellus, 2,* 196–211, 1950.

Rhines, P. B. and W. R. Young, How rapidly is a passive scalar mixed within closed streamlines?, *J. Fluid Mech., 133,* 133–145, 1983.

Ripa, P., Wave energy-momentum and pseudoenergy-momentum conservation for the layered quasi-geostrophic instability problem, *J. Fluid Mech., 235,* 379–398, 1992.

Rossby, C. G., Relation between variations in the intensity of the zonal circulation of the atmosphere and the displacements of the semi-permanent centers of action, *J. Mar. Res., 2,* 38–55, 1939.

Rossby, C. G., On the dynamics of certain types of blocking waves, *J. Chinese Geophy. Soc., 2,* 1–13, 1950.

Samelson, R. M. and J. Pedlosky, Local baroclinic instability of flow over variable topography, *J. Fluid Mech., 231,* 411 – 436, 1990.

Sato, H. and K. Kuriki, Mechanism of transition in the wake of a thin flat plate placed parallel to a uniform flow, *J. Fluid Mech., 11,* 321–352, 1961.

Shepherd, T. G., Rigorous bounds on the nonlinear saturation of instabilities to parallel shear flows, *J. Fluid Mech., 196,* 291–322, 1988.

Shutts, G. J., A case study of eddy forcing during an Atlantic blocking episode, *Asv. Geophys., 29,* 135–161, 1986.

Thom, R., *Structural Stability and Morphogenesis,* W. A. Benjamin, Reading, Mass., 1975.

Thompson, J. M. T. and G. W. Hunt, Towards a unified bifurcation theory, *Z. angew. Math. Phys., 26,* 581–604, 1973.

Thompson, J. D. and J. W. J. Schmitz, A limited area model of the Gulf Stream: design, interpretation and model-data intercomparison, *J. Amer. Meteor. Soc., 19,* 791–813, 1989.

Tollmien, W., Ein allgemeines Kriterium der Instabilitat Laminarer Geschwindigkeitsverteilungen, *Nachr. Ges. Wiss. Gottingen, Math.-Phys. Klasse, 50,* 79–114, 1935.

Ukhovskii, M. R. and I. V. Iudovich, On the equations of steady state convection, *J. Appl. Math. Mech., 27,* 432–440, 1963.

Warren, B. A., Topographic influences on the path of the Gulf Stream, *Tellus, 15,* 167–183, 1963.

Whitehead, J. A., A. Leetma, and R. A. Knox, Rotating hydraulics of strait and sill flow, *Geophys. Fluid Dyn., 6,* 101–125, 1974.

Woods, A. W., The topographic control of planetary-scale flow, *J. Fluid Mech., 247,* 603–621, 1993.

Worthington, L. V. , Evidence for a two gyre circulation system in the North Atlantic, *Deep Sea Research, 9,* 51–67, 1962.

Worthington, L. V. , On the North Atlantic circulation, *The Johns Hopkins Oceanogr. Stud., 6,* 110, 1976.

Yanai, M. and T. Nitta, Finite difference approximations to the barotropic instability problem, *J. Met. Soc. of Japan, 46,* 389–403, 1986.